

UNIVERSITÁ DEGLI STUDI DELL'INSUBRIA
DIPARTIMENTO DI SCIENZA E ALTA TECNOLOGIA



TESI DI DOTTORATO
MATEMATICA DEL CALCOLO: MODELLI, STRUTTURE, METODI
ED APPLICAZIONI
XXVII CICLO

**Reaction-diffusion models on a network:
stochastic and deterministic pattern
formation**

Author:
Malbor ASLLANI

Supervisor:
Prof. Duccio FANELLI

November 2014

UNIVERSITÁ DEGLI STUDI DELL'INSUBRIA

Abstract

Dipartimento di Scienza e Alta Tecnologia

Dottorato di Ricerca

**Reaction-diffusion models on a network: stochastic and deterministic
pattern formation**

by Malbor ASLLANI

This thesis deals with the study of pattern formation on complex networks, a topic of paramount importance in different fields of broad applied and fundamental interest. Starting from a prototypical reaction-diffusion model, two main directions of investigation have been explored: on the one side, we have examined the system in its deterministic limit. Partial differential equations hence govern the evolution of the concentrations of the interacting species. In the second part of the thesis, we have conversely adopted a stochastic viewpoint to the scrutinized problem. Both in the deterministic and in the stochastic settings, the species are assumed to populate a complex graph, which provides the spatial backbone to the inspected model. Diffusion is allowed between neighbouring nodes, as designated by the associated adjacency matrix.

According to the deterministic formulation, a small perturbation of a homogeneous fixed point can spontaneously amplify in a reaction-diffusion system, as follows a symmetry breaking instability and eventually yield asymptotically stable non homogeneous patterns. These are the Turing patterns. Travelling waves can also develop as follows an analogous dynamical instability. In this Thesis we have considered the peculiar setting where the spatial support is a directed network. Due to the structure of the network Laplacian, the dispersion relation has both real and imaginary parts, at variance with the conventional case for a symmetric network. The homogeneous fixed point of the system can turn unstable because of the topology of the hosting network. This observation motivates the introduction of a new class of instabilities, termed topology driven, which cannot be induced on undirected graphs. A linear stability calculation enables one to analytically trace the boundaries of the instabilities in the relevant parameters plane. Numerical simulations show that the instability can lead to travelling waves, or quasi-stationary patterns, depending on the characteristics of the underlying graph. Another scenario where topology matters is that of multi-layered networks, also known as multiplex networks. We have shown in this Thesis that the emergence of self-organized patterns on a multiplex can be instigated by a constructive interference between layers. It can be in fact proven that patterns can emerge for a reaction-diffusion system defined on a multiplex, also when the Turing-like instability is prevented to occur on each single layer taken separately. In other cases inter-layer diffusion can have a destructive influence on the process of pattern formation, as we will discuss in details in this Thesis work.

Beyond the deterministic scenario, single individual effects can also impact the process of pattern formation. Stochastic fluctuations, originating from finite size populations, can in fact significantly modify the mean-field predictions and drive the emergence of regular macroscopic patterns, in time and space, outside the region of deterministic instability. In the second part of the Thesis we have studied the dynamics of stochastic reaction-diffusion models defined on a network. A formal approach to the problem has been

developed which makes use of the Linear Noise Approximation (LNA) scheme. Simulations based on the Gillespie algorithm were performed to test the analytical results and analyzed via a generalized Fourier transform which is defined using the eigenvectors of the discrete graph Laplacian. Travelling waves as well as stationary patterns reminiscent of the Turing instability are shown to develop as mediated by the discreteness of the stochastic medium. As a final point we considered the case of a general stochastic reaction-diffusion system, where the activator is solely allowed to diffuse. Working under the LNA, we proved that stochastic Turing like pattern can develop, an observation which marks a striking difference with the conventional, customarily adopted, deterministic scenario.

Acknowledgements

Contents

Abstract	ii
Acknowledgements	v
Contents	vi
1 Pattern formation in complex networks	5
1.1 Introduction	5
1.2 Turing instability for an activator-inhibitor system	6
1.2.1 Reaction-diffusion equations	6
1.2.2 Linear stability analysis	7
1.2.3 Reaction-diffusion system with one diffusing species	11
1.2.4 Example: Brusselator model	12
1.2.5 Oscillatory instability	12
1.3 Mathematics of networks	13
1.3.1 Networks representation and centrality measures	14
1.3.2 Models of network generation	16
1.4 Reaction-diffusion equations defined on a graph	17
1.4.1 Linear stability in network-organized systems	19
2 Topology-driven instabilities: the theory of pattern formation on directed networks	23
2.1 Introduction	23
2.2 Theory of pattern formation on a directed network	25
2.3 Numerical results	28
2.3.1 Travelling waves for systems of two diffusing species.	29
2.3.2 The case of immobile inhibitors, $D_\psi = 0$	30
2.3.3 Stationary inhomogeneous patterns.	33
2.3.4 Alternative formulation of the transport operator	34
2.4 Topology induced patterns in FitzHugh-Nagumo model	36
2.5 Conclusions	37
3 Turing patterns in multiplex networks	41
3.1 Introduction	41
3.2 Reaction-diffusion equations on multiplex networks	42

3.3	Perturbative characterization of the spectrum	44
3.4	Conclusions	49
4	Stochastic pattern formation theory: the case of one-diffusing species	51
4.1	Introduction	51
4.2	The Model and its Master Equation	52
4.2.1	The Linear Noise Approximation (LNA) method	54
4.3	Equations for the mean-field and the fluctuations	55
4.4	Power Spectrum of fluctuations	57
4.5	A simple stochastic reaction–diffusion model	65
4.6	Conclusion	71
5	Stochastic patterns on a network	73
5.1	Introduction	73
5.2	Stochastic travelling waves case	75
5.2.1	Model definition and the linear noise approximation (LNA)	75
5.2.2	Pattern formation in the deterministic limit	78
5.2.3	Power spectra of fluctuations and stochastic patterns	83
5.3	Stochastic Turing-like patterns	88
5.4	Conclusions	95
A		101
A.1	Stochastic processes	101
A.1.1	Basic definitions	101
A.1.2	Markov processes	102
A.1.3	Master equation	102
A.2	Random walk graph Laplacian	104
Bibliography		107

Introduction

Pattern formation is a rich and fascinating field of investigations which aims at characterizing the fundamental processes responsible for the spontaneous emergence of self-organized collective structures in nature. This is an important domain of study which ideally embraces different fields, ranging from biology to physics, passing through chemistry [1–6]. Patterns are indeed widespread and display a rich gallery of intriguing symmetries, as e.g. trees, spirals, stripes, waves, meanders, cracks, etc.

The first attempt to tackle the problem of pattern formation dates back to 1952 when the English mathematician Alan Turing [1] put forward the brilliant idea that morphogenesis, the biological process that causes an organism to develop its shape, could have a simple and nice mathematical explanation. In this attempt he showed that macroscopic patterns could materialize as follows a symmetry breaking instability of a spatially extended nonlinear reaction-diffusion equations. Turing suggested on the basis of a rather intuitive argument that diffusion could turn unstable a system of reacting agents initialized around a stationary stable equilibrium, thus triggering the morphogenesis process. In his analysis he considered a minimal model composed by two interacting chemicals (or species): the so called activators which cause their own growth and the inhibitors which, on contrary, have a damping effect. Allowing for the elementary constituents to freely migrate within a defined domain, one observes, after a while, the formation of islands of different concentration (in terms of the respective species abundance), which further shape in time, until a final stationary stable pattern is eventually attained.

The process of pattern formation follows a linear instability mechanism, nowadays known as the Turing instability. In fact, starting from a homogeneous stable state the system goes unstable because of diffusion and the concentrations of the species grows exponentially until the nonlinearities become so strong to balance this tendency and stabilize the pattern. In his original work, however, Turing pointed out that there are some constraints for an activator-inhibitor system to get destabilized. First of all both species should diffuse, and second, the diffusion rate of the inhibitor should be larger than that

of the activator. Only this way the conditions for the Turing instability are met and the patterns can develop.

Shortly after Turing seminal paper, plenty of applications came out; from the shape of the starfish to the skin of the chameleon from the coat of the tiger to the sand dunes in deserts, all these phenomena are seen under the lens of the *Turing instability* paradigm. A new interdisciplinary discipline was born aimed at approaching life sciences questions with the quantitative tools of mathematics and physics.

In recent years, networks based applications have been recognized as central in many distinct fields [7–9]. It is indeed amazing to observe how networks pervade our everyday life. Consider for instance the human brain, which is constituted by an incredible number of neurons connected to each other and exchanging thousands of electric pulses for seconds. Nerves starting from the spinal cord end up almost in every part of our body, so permitting the brain to gather information and response to external stimuli. The complexity of nervous system, yet to be fully explored, is only one of thousands of examples where networks apply. In fact, people have to do everyday with complex networks, when they pick up the phone or google for information, chat on social networks or travel back and forth to work; in all these examples where communication or transport are involved, the underlying backbone structure is a complex graph. From human interactions to animal ecoregions, from cellular networks to traffic flow, Turing patterns could represent a formidable approach to explain the natural tendency towards self-organization. In the 70's Othmer and Scriven [10] had the foresight to extend the theory of Turing patterns to the relevant case where the spatial support of the reaction-diffusion system is heterogeneous. In doing so, they took inspiration from the observation that, in the early stages of the embryo morphogenesis, the zygotic cells represent a multi-cellular network, rather than a continuous regular structure. Just a few year ago, the studies of Othmer and Scriven were revisited and considerably expanded by Nakao and Mikhailov [11] who generalized the analysis to include systems defined on large random complex networks. As pointed out in [11], the pattern formation theory revisited in the context of networks science broaden the pictures along interesting and undexplored directions which could prove crucial for e.g. epidemics spreading, ecosystems dynamics, chemical reactors, neurosciences, traffic systems, computer networks, power grids etc. In analogy with the continuous case, patterns on a network are represented by a differentiation of the nodes in activator-rich and activator-poor groups. Moreover, patterns on networks manifest new properties inherited by the topology of the underlying spatial support, as we will show in this thesis.

So far the study of collective dynamics based on Turing instability, has been limited to undirected graphs. In this thesis, we will extend the theory of pattern formation based

on reaction-diffusion systems to the case of directed networks [12]. Most of networks, in fact, are based on directed graphs: interaction, transport or communication do not necessarily display the symmetries that often invoked in basic reference models. In practice the simplifications assumed when dealing with undirected, hence symmetric networks, can be in several cases questioned. We will here show that the directionality of the network is a key ingredient which can eventually enhance the ability of the system to self-organize both in space and in time. At variance with the conventional case of symmetric networks, the discrete Laplacians operator defined on a directed network may admits complex eigenvalues. This complication is responsible for a new type of instability of the homogeneous fixed point, which cannot be induced according to the usual scenario. Analytical results from the linear stability analysis show that the patterns can develop with no restrictions on the relative diffusivities of the interacting species, as it is instead the case for the classical Turing vision. These results, that we shall discuss in details all along the thesis, can potentially interest fields as neuroscience or information technology.

The importance of the topology of the underlying discrete support is also manifested in other context. Consider for instance, the newly introduced multiplex networks. This family of networks is represented by a set of several graphs, called layers, interconnected to each other [13–15]. By adapting to this setting the theory of patterns formation, we will here show that the interaction between adjacent layers can seed the instability of an uniform steady state, yielding self-organized collective motifs, which cannot develop in the limit of decoupled layers [16]. Patterns on individual layers can also fade away due to cross-diffusion between layers. These observations are analytically substantiated via a spectral perturbative technique that we will make use of in the following. Multiplex share indeed peculiar characteristics, which might play a pivotal role in favouring the process of self-organization, from the microscopic to the macroscopic realms.

Often real systems in nature are composed of a moderate number of individuals which are allowed to interact only on confined regions of the spatial domain. In general, this makes impossible to model the population dynamics in terms of deterministic reaction-diffusion equations. Methods such as Linear Noise Approximation (LNA), borrowed from statistical mechanics, may be employed to account for the finite size corrections to mean-field dynamics. Working in the generalized scenario of stochastic models, we will prove that *stochastic Turing patterns* [17, 18] can emerge in a region of the parameters for which spatial order is prevented to occur in the idealized deterministic picture. This phenomenon, as revealed by direct stochastic simulations, is explained analytically by mean of LNA adapted to the networks setting, and eventually traced back to the finite size effects stemming from the inherent graininess of the scrutinized medium [19, 20].

To carry out the analysis, we have introduced a generalized Fourier transform, by expanding the signal on a basis formed by the eigenvectors of the Laplacian operator. By elaborating along these line we could also prove that patterns can be found also when the activators are solely allowed to diffuse, the inhibitors being considered as static targets, at odd with the original Turing prescriptions [21].

To sum up and conclude, we briefly describe the structure of the thesis. In the first chapter we introduce a few key elements on the theory of pattern formation for both systems defined on a continuum or discrete, network-like, support. In Chapter 2 we develop the theory of reaction-diffusion systems on directed networks by introducing the new type of instability to which we have alluded above. Pattern formation in multiplex networks is then studied in Chapter 3. The case of a two-layers multiplex is tackled in some details via a perturbative method, which holds in the limit of weak inter-layer coupling. Chapter 4 is dedicated to reviewing the theory of stochastic pattern formation for systems evolving on a regular lattice. We will in particular consider the case where only one species is allowed to diffuse in space. In the last chapter, we will discuss the linear noise approximation for stochastic reaction diffusion systems defined on a graph.

Chapter 1

Pattern formation in complex networks

1.1 Introduction

In this chapter, we introduce the concept of reaction-diffusion equations and discuss their relevance in a broad perspectives. As it is widely known reaction-diffusion equations admits a rich plethora of interesting solutions, some of which will be examined all along this thesis work. Particularly interesting is the spontaneous appearance of self-organized stationary patterns, originating from a symmetry breaking instability of a homogeneous fixed point. The dynamical mechanism that seeds the aforementioned instability was illustrated by Alan Turing in his pioneering work on the chemical basis of morphogenesis, and since then has been exploited in many different contexts, ranging from physics to biology. An extended discussion on the mathematics of pattern formation and its multifaceted applications can be found the books of Murray [2] and Cross & Greenside [3]. The concept of Turing instability also applies to reaction-diffusion systems defined on a complex graph support, as recently discussed by Nakao & Mikhailov [11]. In this chapter we will briefly review the process of diffusion driven instability, both for systems embedded on a continuum space or defined on a discrete heterogeneous network. These premises will serve as a starting point for our subsequent developments. More specifically, in Section 1.2 we will provide a basic entry to the theory of pattern formation for a system made of two interacting species. Some elements of graph theory will be then covered in Section 1.3. In the last section we will introduce the theory of reaction-diffusion equations for the case when the agents are constrained to evolve on a network.

1.2 Turing instability for an activator-inhibitor system

Realistic equations describing chemical reactions in experimental geometries are complicated to formulate and difficult to investigate. The same was true in the 1940s when Alan Turing was thinking about morphogenesis. These difficulties did not stop Turing who, in the tradition of great theoretical science, set as his goal not the quantitative explanation of morphogenesis but the discovery of a clear plausible mechanism that could guide researchers in how to think about such a complex phenomenon.

We will follow Turing original paper¹ and examine analytically the linear stability analysis of the simplest possible reaction-diffusion system that forms a pattern from a uniform state. The analysis will lead to several insights, some unexpected. One insight is that at least two interacting chemicals are needed for pattern formation to occur. Second is Turing's most surprising insight, that diffusion in a reacting chemical system can actually exert a destabilizing influence. This is contrary to intuition since diffusion by itself smooths out spatial variations of a concentration field and so would be considered as a stabilizing effect. A third insight is that the instability caused by diffusion can seed the growth of structure at a particular wave length. This provides a possible mechanism for producing patterns like the segmentation patterns in the developing fly embryo, the periodic arrangement of tentacles around the mouth of the Hydra organism or zebra stripes. A fourth insight is that pattern formation in a reaction-diffusion system will not occur unless the diffusion coefficients of at least two reagents differ substantially. The difficulty of satisfying this condition for chemicals in solution partially explains why nearly 40 years passed after Turing's paper before experiments were able to demonstrate the truth of his ideas.

1.2.1 Reaction-diffusion equations

We will study the Turing model for two reacting and diffusion species u_1, u_2 of the form:

$$\begin{aligned}\frac{\partial u_1}{\partial t} &= f_1(u_1, u_2) + D_1 \frac{\partial^2 u_1}{\partial x^2} \\ \frac{\partial u_2}{\partial t} &= f_2(u_1, u_2) + D_2 \frac{\partial^2 u_2}{\partial x^2}\end{aligned}\tag{1.1}$$

or in vectorial form

$$\frac{\partial \mathbf{u}}{\partial t} = \mathbf{f}(\mathbf{u}) + \mathbf{D} \frac{\partial^2 \mathbf{u}}{\partial x^2},$$

¹Turing's paper is also interesting from a historical point of view. For example, he could only speculate about how an organism knew how to grow since the role of DNA would only be announced a year later in 1953. The last section of the paper mentions one of the first simulations on a digital computer and Turing states his belief that these new computers will be important for future research. There is a certain irony here since Turing was one of the inventors of the digital computer.

where we have introduced a diagonal 2×2 diffusion matrix \mathbf{D} defined by

$$\mathbf{D} = \begin{pmatrix} D_1 & 0 \\ 0 & D_2 \end{pmatrix}. \quad (1.2)$$

Eqs. (1.1) describes the evolution of the concentration of the two species $u_i(t, x)$, $i = 1, 2$ on the real line $x \in \mathbb{R}$. The nonlinear functions $f_1(u_1, u_2)$, $f_2(u_1, u_2)$ are the reaction terms of the two chemicals while the D_1 , D_2 are the corresponding diffusion coefficients. The simplest possible model is obtained by assuming that there is no prior spatio-temporal structure in the system so that the functions f_i and the diffusion coefficients D_i do not depend explicitly on time t or on position x . For simplicity, we further assume that the diffusion coefficients are constants and so do not depend on the field values u_i . These assumptions are quite reasonable for many experimental situations.

1.2.2 Linear stability analysis

We now perform the linear stability analysis of uniform solutions of the two-chemical reaction-diffusion model Eqs. (1.1). Turing's surprising and important discovery was that there are conditions under which the spatially uniform state is stable in the absence of diffusion but can become unstable to nonuniform perturbations due to diffusion. Further, for many conditions the instability first occurs at a finite wave length and so a cellular pattern starts to appear.

The following discussion is aimed at deriving, and then physically understanding, the sufficient conditions for which the real parts of the growth rates become negative. When these conditions are first violated and instability occurs, it is then important to think about the values of the wave numbers corresponding to the fastest growing modes. For simplicity, we will discuss the one-dimensional case. If we assume that the evolution equations have rotational symmetry in higher dimensions, the two- and three-dimensional cases are identical: the one-dimensional Laplacian $\partial^2/\partial x^2$ becomes a higher-dimensional Laplacian ∇^2 and so on.

We begin by assuming that our system admits a stationary uniform solution $\mathbf{u}^* = (u_1^*, u_2^*)$ when all partial derivatives are set to zero, leading to $\mathbf{f}(\mathbf{u}^*) = 0$. Since, in general, this is a nonlinear system, numerical methods can be very helpful. Then, linearizing about the steady state \mathbf{u}^* , one obtains that an arbitrary infinitesimal perturbation $\delta\mathbf{u}(t, x) = (\delta u_1(t, x), \delta u_2(t, x))$ of the fixed point will evolve in time according to the

following linear equations:

$$\begin{aligned}\frac{\partial \delta u_1}{\partial t} &= J_{11} \delta u_1 + J_{12} \delta u_2 + D_1 \frac{\partial^2 \delta u_1}{\partial x^2} \\ \frac{\partial \delta u_2}{\partial t} &= J_{21} \delta u_1 + J_{22} \delta u_2 + D_2 \frac{\partial^2 \delta u_2}{\partial x^2},\end{aligned}\quad (1.3)$$

where $J_{ij} = (\partial f_i / \partial u_j)|_{\mathbf{u}^*}$ are the entries of the 2×2 Jacobian matrix \mathbf{J} evaluated at the steady state \mathbf{u}^* . Again in vectorial form we have

$$\frac{\partial \delta \mathbf{u}}{\partial t} = \mathbf{J} \delta \mathbf{u} + \mathbf{D} \frac{\partial^2 \delta \mathbf{u}}{\partial x^2}.\quad (1.4)$$

Because the above partial differential equation is linear with constant coefficients and imposing periodic boundary conditions we can look for solution in the form:

$$\delta \mathbf{u} = \delta \mathbf{u}_q e^{\sigma_q t} e^{iqx},\quad (1.5)$$

where $\delta \mathbf{u}_q$ is the constant vector and σ_q the growth rate associated to wave number q . Note that both components δu_i , $i = 1, 2$ of the perturbation vector $\delta \mathbf{u}$ share the same dependence on time and space. Substituting Eq. (1.5) in (1.4) with further computational efforts one obtains the following eigenvalue problem

$$\mathbf{J}_q \delta \mathbf{u}_q = \sigma_q \delta \mathbf{u}_q,\quad (1.6)$$

where the matrix \mathbf{J}_q is defined as

$$\mathbf{J}_q = \mathbf{J} - \mathbf{D}q^2 = \begin{pmatrix} J_{11} - D_1 q^2 & J_{12} \\ J_{21} & J_{22} - D_2 q^2 \end{pmatrix}.$$

The eigenvalue problem for a given q has generally two linearly independent eigenvectors that we will denote by $\delta \mathbf{u}_{1q}$, $\delta \mathbf{u}_{2q}$ with corresponding eigenvalues σ_{1q} , σ_{2q} . The general solution of Eq. (1.4) is a superposition over all wave numbers q of particular solutions:

$$\delta \mathbf{u}(t, x) = \sum_q (c_{1q} \delta \mathbf{u}_{1q} e^{\sigma_{1q} t} + c_{2q} \delta \mathbf{u}_{2q} e^{\sigma_{2q} t}) e^{iqx},\quad (1.7)$$

where the coefficients c_{1q} , c_{2q} are complex constants, that depend on the initial perturbation. The uniform solution \mathbf{u}^* is stable if both eigenvalues σ_{1q} , σ_{2q} have negative real parts for all wave numbers q , i.e., if $\max_i \max_q \operatorname{Re}(\sigma_{iq}) < 0$ for $i = 1, 2$.

Solving the characteristic polynomial obtained from the eigenvalue problem (1.6) gives the following result (since we are looking for the largest σ_q)

$$\sigma_q = \frac{1}{2} \left(\text{tr} \mathbf{J}_q + \sqrt{(\text{tr} \mathbf{J}_q)^2 - 4 \det \mathbf{J}_q} \right), \quad (1.8)$$

known also as the *dispersion relation*. From the expression of Eq. (1.8) a simple criterion can be derived that determines when the real parts of both eigenvalues are negative [2]; namely

$$\begin{aligned} \text{tr} \mathbf{J}_q &= J_{11} + J_{22} - (D_1 + D_2) q^2 < 0 \\ \det \mathbf{J}_q &= (J_{11} - D_1 q^2)(J_{22} - D_2 q^2) - J_{12} J_{21} > 0. \end{aligned} \quad (1.9)$$

If both conditions hold for all wave numbers q , then the stationary homogeneous state \mathbf{u}^* is linearly stable².

We now discuss the physical meaning and implications of the mathematical criterion Eqs. (1.9) in the context of pattern formation. Turing's insight was that diffusion of species may somehow cause a pattern-forming instability. If so, then the starting point is to imagine that somehow the diffusion has been turned off (mathematically by setting the diffusion coefficients to zero) and then we slowly turn on the diffusion to see if instability ensues. Then we need to assume that the reacting chemicals form a stable stationary state in the absence of diffusion. Setting the diffusion constants to zero in Eqs. (1.9), we obtain the following criterion for linear stability of the homogeneous state:

$$\begin{aligned} \text{tr} \mathbf{J} &= J_{11} + J_{22} < 0 \\ \det \mathbf{J} &= J_{11} J_{22} - J_{12} J_{21} > 0. \end{aligned} \quad (1.10)$$

If these conditions are satisfied, a well-mixed two-chemical solution will remain stable and uniform. Comparing Eqs. (1.10) with Eqs. (1.9) and recalling that diffusion constants and the quantity q^2 are non-negative, we conclude that

$$\text{tr} \mathbf{J}_q = \text{tr} \mathbf{J} - (D_1 + D_2) q^2 < \text{tr} \mathbf{J} < 0,$$

so the trace of the matrix \mathbf{J}_q is always negative. Hence diffusion can destabilize the uniform state only if it yields a violation of the second of Eqs. (1.9). The determinant $\det \mathbf{J}_q$ is a convex parabola in q^2 . The linear instability sets in if the minimum of the parabola becomes negative. Setting the derivative of $\det \mathbf{J}_q$ with respect to q^2 to zero,

²If our problem instead involved N interacting species, we can still obtain some necessary and sufficient analytical criteria that all the eigenvalues of a $N \times N$ matrix have negative real parts. The Routh-Hurwitz criterion, in fact, states that a certain sequence of determinants from size 1 to N all have to be positive.

we find that the minimum occurs at the wave number q_m given by:

$$q_m^2 = \frac{D_1 J_{22} + D_2 J_{11}}{2D_1 D_2}. \quad (1.11)$$

The corresponding value of $\det \mathbf{J}_q$ at this minimum is

$$\det \mathbf{J}_{q_m} = J_{11} J_{22} - J_{12} J_{21} - \frac{(D_1 J_{22} + D_2 J_{11})^2}{4D_1 D_2}.$$

This expression is negative when the following inequality is satisfied:

$$D_1 J_{22} + D_2 J_{11} > 2\sqrt{D_1 D_2 (J_{11} J_{22} - J_{12} J_{21})}. \quad (1.12)$$

The term inside the square root is positive because of the second of Eqs. (1.10). As a consequence, it implies that

$$D_1 J_{22} + D_2 J_{11} > 0,$$

which can also be deduced directly from Eq. (1.11) since q_m^2 is a non negative real number. From this last result and the first of Eqs. (1.10), we see that one of the quantities J_{11} and J_{22} must be positive and the other negative for the instability to set in. For simplicity and without loss of generality we will assume $J_{11} > 0$ and $J_{22} < 0$ in the subsequent discussion. This implies that species “1” enhances its own production and so it is generally called *activator*. At variance species “2” inhibits its own growth and acts as an *inhibitor*. Eqs. (1.10) further implies that the quantities J_{12} and J_{21} must also have opposite signs. The above analysis can be summarized in the following theorem

Theorem 1.1. (*Turing instability*) Eq. (1.12) is a necessary and sufficient condition for linear instability of a uniform steady state that is stable in the absence of diffusion, eqs. (1.10).

By varying one parameter, the inequality Eq. (1.12) can be eventually matched and the fixed point turns unstable to perturbations. The excited modes lay in a bounded region in q , an important requisite for the pattern to eventually stabilize. In the linear regime the pattern will grow with a characteristic wave number which is close to the value q_m in Eq. (1.11). The condition Eq. (1.12) can be expressed alternatively in terms of two diffusion lengths

$$l_1 = \sqrt{\frac{D_1}{J_{11}}}, \quad l_2 = \sqrt{\frac{D_2}{J_{22}}} \quad (1.13)$$

in the form

$$q_m^2 = \frac{1}{2} \left(\frac{1}{l_1^2} - \frac{1}{l_2^2} \right) > \sqrt{\frac{J_{11} J_{22} - J_{12} J_{21}}{D_1 D_2}}.$$

This implies that the length l_2 must be sufficiently larger than the length l_1 . The necessary condition $l_2 > l_1$ for a Turing instability is also sometimes referred to as “local activation with long range inhibition”.

The condition $l_2 > l_1$, when expressed in the equivalent form $D_2/D_1 > (-J_{22}/J_{11})$ partly explains why experimentalists had such a hard time finding a laboratory example of a Turing instability. The diffusion coefficient D_2 of the inhibitor has to exceed the diffusion coefficient D_1 of the activator by a factor $(-J_{22}/J_{11})$ which can exceed 10 for some realistic models of reaction-diffusion experiments.

1.2.3 Reaction-diffusion system with one diffusing species

Let us now focus on the specific case study where just one species, specifically u , is allowed to diffuse with a diffusion coefficient D . We will prove that no Turing instability can occur, if just one species can diffuse.

Then a simple calculation yields an equivalent expression to eq. (1.8) written in explicit form:

$$\sigma_q = \frac{(\text{tr}\mathbf{J} - Dq^2) + \sqrt{(\text{tr}\mathbf{J} - Dq^2)^2 - 4(\det\mathbf{J} - Dq^2J_{22})}}{2} \quad (1.14)$$

Since we are interested in the growth of unstable perturbations, we have here selected the largest σ_q . The Turing instability occurs if one can isolate a finite domain in q for which $\sigma_q > 0$. In formulae:

$$\begin{aligned} & (\text{tr}\mathbf{J} - Dq^2) + \sqrt{(\text{tr}\mathbf{J} - Dq^2)^2 - 4(\det\mathbf{J} - Dq^2J_{22})} > 0 \\ \implies & \sqrt{(\text{tr}\mathbf{J} - Dq^2)^2 - 4(\det\mathbf{J} - Dq^2J_{22})} > -(\text{tr}\mathbf{J} - Dq^2) \\ \implies & -4(\det\mathbf{J} - Dq^2J_{22}) > 0 \\ \implies & Dq^2J_{22} > \det\mathbf{J}. \end{aligned} \quad (1.15)$$

The right hand side contribution in equation (1.15) is positive as the homogeneous fixed point is supposed to be stable. If $J_{22} < 0$, so the species v acts as inhibitor, it is clear that (1.15) does not admit solutions, the left hand side of the equation being negative. At variance, when $J_{22} > 0$, so v is the activator, we have:

$$q^2 > \frac{\det\mathbf{J}}{DJ_{22}} \implies q < -\sqrt{\frac{\det\mathbf{J}}{DJ_{22}}} \quad \text{and} \quad q > \sqrt{\frac{\det\mathbf{J}}{DJ_{22}}}. \quad (1.16)$$

Equation (1.16) implies that the relation of dispersion σ_q is positive for all values of q above a critical threshold $q_c = \sqrt{\det\mathbf{J}/(DJ_{22})}$. The quantity σ_q grows as q does, the

instability involving smaller and smaller spatial scales. It is therefore not possible to delimit a finite window in q for which σ_q is found to be positive, and, hence, the Turing instability cannot take place. In conclusion, we have here confirmed a well establish fact [22]: a two species systems where only one species can migrate, cannot undergo Turing instability.

1.2.4 Example: Brusselator model

The criteria found above for the Turing instability of a uniform state will be now applied to a simple two-variable mathematical model known as the *Brusselator* for illustration purpose. The Brusselator model involves molecules of two chemical species, u and v . More specifically, the system evolves according to the general dynamical equations (1.1) with $f(u, v) = a - (b + d)u + cu^2v$ and $g(u, v) = bu - cu^2v$, where a , b , c and d act as external, positive definite, parameters.:

$$\begin{aligned}\frac{\partial u}{\partial t} &= a - (b + d)u + cu^2v + D_u \frac{\partial^2 u}{\partial x^2} \\ \frac{\partial v}{\partial t} &= bu - cu^2v + D_v \frac{\partial^2 v}{\partial x^2}\end{aligned}\tag{1.17}$$

The Brusselator model admits a unique homogeneous fixed point $u^* = a/d$, $v^* = bd/ac$, which is stable for $b < 1 + c(a/d)^2$. We additionally require $b > d$, such that $J_{11} = -d + b > 0$, while $J_{22} = -c(a/d)^2 < 0$. Although introduced with the goal of understanding the Belousov-Zhabotinsky reaction [23], this model was intended not to describe a specific chemical experiment but to show how an invented plausible sequence of chemical reactions could reproduce qualitative features such as the Turing patterns. Let us consider the following parameter values $a = 1.5$, $c = d = 1$, $D_u = 2.8$ and $D_v = 22.4$ and change b which acts therefore as the bifurcation parameter. The onset of instability can be visually understood by plotting the dispersion relation as a function of the wave number q for values of the parameter b below, equal to, and above the critical value $b_c \approx 2.34$, Fig. 1.1. In Fig. 1.2 we show also two different patterns for the Brusselator model. The results were obtained integrating numerically the system of partial differential equations (using a finite difference method in space and a Runge-Kutta scheme in time) with periodic boundary conditions. In both cases the concentration of the first species is plotted (color bar) in the XY - plane.

1.2.5 Oscillatory instability

We end this section with an important remark. Since $\text{tr}\mathbf{J}_q < 0$, it is clear from equation (1.8), that it is not possible to satisfy the condition for the instability $\text{Re}(\sigma_q) > 0$, and

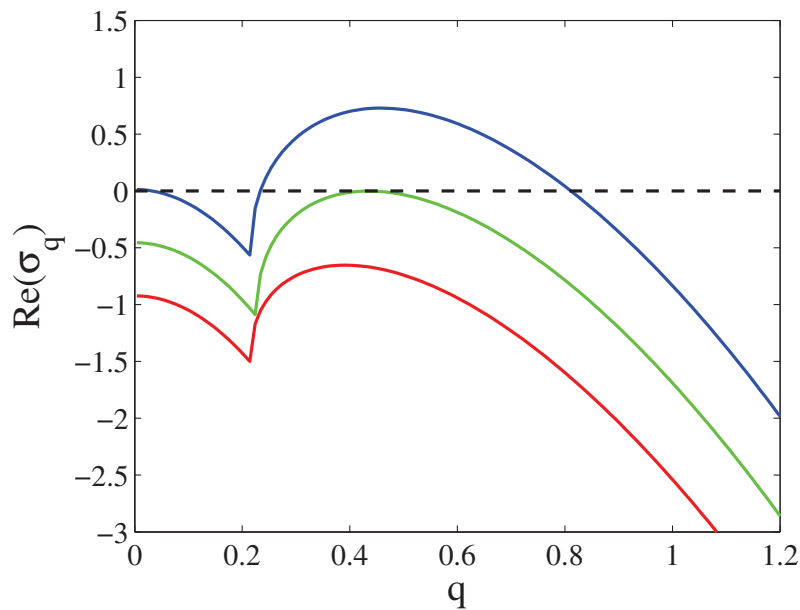


FIGURE 1.1: Plots (solid curves) of the maximum of the real part of the growth rate (dispersion relation), σ_q versus wave number q , for the Brusselator model. Three curves are plotted for different values of the bifurcation parameter ($b = 0.6b_c$ red, $b = b_c$ green and $b = 1.4b_c$ blue), which controls the instability. The critical wave number $q_c \approx 0.435$ is identified as the wave number for which the maximum real part of the growth rate first becomes zero.

have, at the same time, an imaginary component of the dispersion relation, $Im(\sigma_q)$, different from zero. This is instead possible when operating in a generalised setting which accommodates for specific long-range couplings in the reaction terms [56] or when considering at least three mutually interacting species [20, 24]. A system unstable for $q \neq 0$ and with the corresponding $Im(\sigma_q) \neq 0$ is said to undergo a *wave-instability* and the emerging patterns have the form of travelling waves [56].

So far, we have discussed the problem of pattern formation where the species diffuse in a continuous medium with general boundary conditions. Nevertheless, as anticipated in the beginning of this chapter, the analysis can be readily extended to systems defined on complex spatial supports as graphs (also called networks). Before turning to discuss this interesting generalization, we will briefly review, in the next section, some important concepts in graph theory.

1.3 Mathematics of networks

In this section, we introduce the basic theoretical tools used to describe and analyze networks, most of which come from graph theory, the branch of mathematics that deals

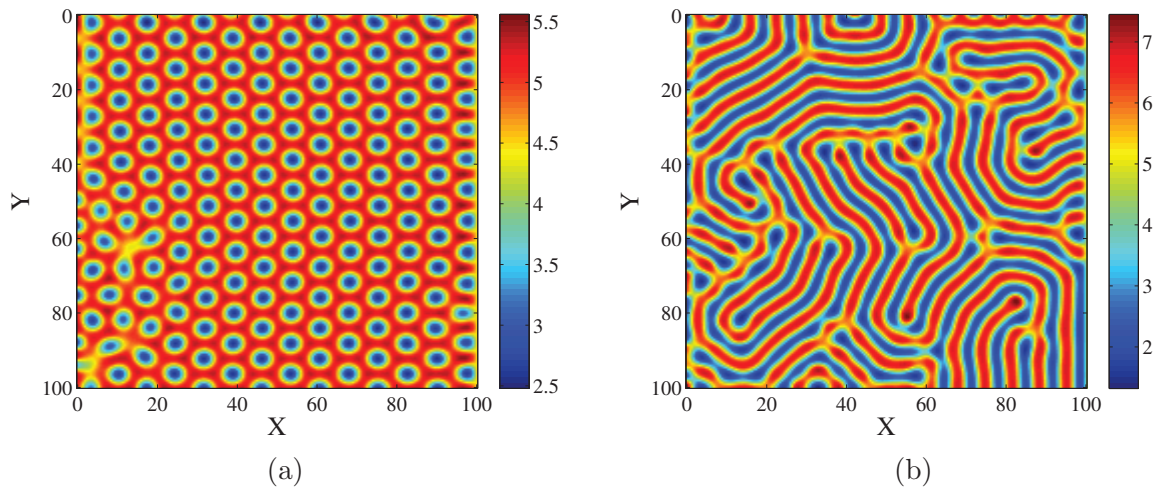


FIGURE 1.2: Turing two-dimensional patterns produced through simulating the Brusselator model. The parameters for both cases are $a = 4.5$, $c = d = 1$, $D_u = 2$, $D_v = 16$. (a) Dotted patterns, $b = 6.75$. (b) Stripes patterns, $b = 7.5$. The simulations have zero-flux boundary conditions, i.e. the boundaries are impermeable. The initial conditions are random perturbations about the homogeneous steady state.

with networks. Graph theory is a large field of investigation which branches in many directions. We will describe here only a small fraction of the results present in the literature, focusing only on those aspects that are relevant to the study of real-world applications.

1.3.1 Networks representation and centrality measures

By definition a network—also called a *graph* in the mathematical terminology—is made up of points, usually called *nodes* or *vertices*, and lines connecting them, usually called *edges*. Mathematically, a network can be represented by a matrix called the *adjacency matrix* \mathbf{A} , which, in the simplest case, is an $\Omega \times \Omega$ symmetric matrix, where Ω is the number of vertices in the network. The adjacency matrix has elements

$$A_{ij} = \begin{cases} 1, & \text{if there is an edge between } i \text{ and } j \\ 0, & \text{otherwise} \end{cases}$$

For example, the adjacency matrix of the network in Fig. 1.3 is

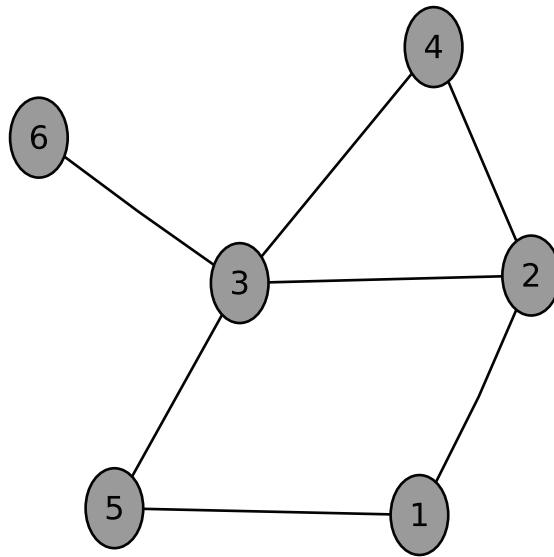


FIGURE 1.3: An example of a simple (undirected) graph.

$$A = \begin{pmatrix} 0 & 1 & 0 & 0 & 1 & 0 \\ 1 & 0 & 1 & 1 & 0 & 0 \\ 0 & 1 & 0 & 1 & 1 & 1 \\ 0 & 1 & 1 & 0 & 0 & 0 \\ 1 & 0 & 1 & 0 & 0 & 0 \\ 0 & 0 & 1 & 0 & 0 & 0 \end{pmatrix}.$$

The matrix A is symmetric since if there is an edge between i and j then clearly there is also an edge between j and i , thus $A_{ij} = A_{ji}$.

In some networks the edges are *weighted*. This means that the nonzero elements of the adjacency matrix can be generalized to values (weights w_{ij}) other than unity to represent stronger or weaker connections. In this case, we have the *coupling matrix* \mathbf{W} . Since in this thesis we will deal with unweighted networks, unless particularly specified, $\mathbf{W} = \mathbf{A}$. Another variant is the *directed* network, in which edges point in a particular direction between two vertices. It is represented by an asymmetric adjacency matrix in which $A_{ij} = 1$ implies (conventionally) the existence of an edge pointing from j to i , which will in general be independent of the existence of an edge from i to j . Networks may also have *multiedges* (repeated edges between the same pair of vertices), *self-edges* or *self-loops* (edges connecting a vertex to itself), *hyperedges* (edges that connect more than two vertices together) and many other features. We here concentrate however primarily on the simplest networks having unweighted single edges between pairs of vertices. The

only property we will be concerned with is the directionality which will prove crucial for the reaction-diffusion dynamics on networks, as we shall discuss in the next chapter.

There is still another topological approach for graphs classification, that of the *multiplex* network [13–15, 25]. In this case one is brought to consider a collections of networks interconnected with each other. Single networks are layers of a global network, the multiplex, and their dynamical interplay proves crucial, as we show in Chapter 3.

Turning to the analysis of dynamical processes that take place on networks, we start by looking at the centrality measures, which are some of the most fundamental and frequently used measures of network structure. Centrality measures quest for, who is the most important or central node of the network. There are many answers to this question, depending on what we mean by important. Perhaps the simplest of centrality measures is the *degree* centrality, also called degree. The degree of a vertex in a network is the number of edges attached to it. In mathematical terms, the degree k_i of a vertex i is

$$k_i = \sum_{j=1}^{\Omega} A_{ij}. \quad (1.18)$$

Another useful centrality measures is the *closeness* centrality, which exploits the concept of network paths. A *path* in a network is a sequence of vertices traversed by following edges from one to another across the network. A *geodesic* path is the shortest path (may not be unique), in terms of number of edges traversed, between a specified pair of vertices. The closeness centrality of vertex i is the mean geodesic distance (i.e., the mean length of a geodesic path) from vertex i to every other vertex. Closeness centrality is lower for vertices that are more central in the sense of having a shorter network distance on average to other vertices.

1.3.2 Models of network generation

In this paragraph we briefly describe the main graph generation models used along this thesis. Perhaps, the most intuitively simple is the *random graph*. In general, a random graph is a model network in which some specific set of parameters are fixed, but the network is random in all the other aspects. One of the simplest way of generation a random graph is based in the *Erdős-Rényi* [26] model $G(\Omega, m)$ in which we fix only the number of vertices Ω and the number of edges m . That is, we choose m pairs of vertices uniformly at random from all possible pairs and connect them with an edge. In order to be a simple graph, i.e., that it should have no multiedges or self-edges, the position of each edge should be chosen among only those pairs that are distinct and not already connected. Another equivalent definition which is most commonly used is that given by

Gilbert [27], denoted $G(\Omega, p)$, in which every possible edge occurs independently with probability $0 < p < 1$. Strictly speaking, the random graph model is not defined in terms of a single randomly generated network, but as an ensemble of networks, i.e., a probability distribution over possible networks.

There are other types of networks which do not arise naturally and for this reason their growth is based in generative models. Here we discuss two main kinds of such networks the *scale-free* and the *small-world* networks. The first one make use of the *preferential attachment* principle invented by Barabási and Albert [7]. According to this method if we start from an initial number of nodes Ω and edges m randomly distributed, the network grows adding at each step more links to the more connected nodes (with higher degree). A constrain which is usually imposed, is the mean degree k that the graph should have. At the end of this process according to which the “rich get richer” a network with a power-law degree distribution $P(k) \sim k^{-\gamma}$, ($2 < \gamma < 3$) is recovered.

The small-world networks on the other side are defined like graphs where most nodes can be reached from every other by a small number of steps. In fact, the typical distance L between two randomly chosen nodes grows proportionally to the logarithm of the number of nodes in the network: $L \sim \log \Omega$. Two different strategies for generating these graphs will be considered. On the one side, we will follow the *Watts-Strogatz* (WS) approach [9] that starts by constructing a k -regular ring lattice given a desired number of nodes Ω and the mean degree k . Then, for every node i , we take all edges and rewire them with a given probability $0 < p < 1$ avoiding self-loops and multiedges. At the end, the mean number of rewired links is Ωkp . Small world networks are found for intermediate values of p . We will also implement an alternative generation strategy, the so-called *Newman-Watts* (NW) algorithm [28]. It is quite similar to the previous one, with the only change that all of the original links in the regular lattice are preserved, and extra Ωkp links are added.

1.4 Reaction-diffusion equations defined on a graph

As early as 1971, Othmer and Scriven [10] pointed out that Turing instability can occur in network-organized systems and may play an important role in the early stages of biological morphogenesis, as morphogens diffuse over a network of intercellular connections. They proposed a general mathematical framework for the analysis of such network instability, which has been subsequently explored. The examples of specific applications of the theory were, however, limited to regular lattices or small networks.

Recently [11], the concept of Turing patterns was extended to large complex networks, revealing striking differences as compared to their analogues on a regular lattice. It was observed that the system initially spontaneously differentiates into activator-rich and activator-poor groups of the network nodes and the emerging patterns became furthermore strongly reshaped at the subsequent nonlinear stage. Other features observed, which go beyond the aim of this thesis, are coexistence of multiple stationary states and hysteresis effects. Here, we briefly review the general theory of reaction-diffusion dynamics on a undirected graph. The importance of the self-organizing behaviour in networks is stressed out by potential applications such like ecological metapopulations, cellular networks, traffic systems, computer networks, brain connectoma, etc.

We begin by considering a network made of Ω nodes and characterised by a general weighted $\Omega \times \Omega$ adjacency matrix \mathbf{W} : the entry W_{ij} is equal to the weight w_{ij} if nodes i and j (with $i \neq j$) are connected, and it is zero otherwise. If the network is undirected, the matrix \mathbf{W} is symmetric. Consider then two interacting species and label with (u_i, v_i) their respective concentrations on node i . A general reaction-diffusion system defined on the network takes the form:

$$\begin{aligned} \frac{du_i}{dt} &= f(u_i, v_i) + D_u \sum_{j=1}^{\Omega} \Delta_{ij} u_j \\ \frac{dv_i}{dt} &= g(u_i, v_i) + D_v \sum_{j=1}^{\Omega} \Delta_{ij} v_j \end{aligned} \quad (1.19)$$

where D_u and D_v denote the diffusion coefficients of, respectively, species u and v ; where again $f(\cdot, \cdot)$ and $g(\cdot, \cdot)$ are nonlinear functions of the concentrations and stand for the reaction terms; Δ_{ij} are the entries of the network Laplacian matrix $\mathbf{\Delta}$. This new transport operator is defined as $\mathbf{\Delta} = \mathbf{W} - \mathbf{K}$ where $\mathbf{K} = \text{diag}(k_i)$ or expressed in terms of the entries $\Delta_{ij} = W_{ij} - k_i \delta_{ij}$ where δ_{ij} is the Kronecker δ -function.

The graph Laplacian turns up in a variety of different places, including random walks on networks, resistor networks, graph partitioning, and network connectivity. As we will see in the following, its spectral properties are crucial to predict the dynamical evolution of the scrutinized system. Other formulations of the network Laplacian operator, however, exist. For more details the interested reader should refer to Appendix A and the related bibliography. (See also the study of stochastic pattern formation reported in Chapter 5).

1.4.1 Linear stability in network-organized systems

Imagine now that system (1.19) admits an homogeneous fixed point, (u^*, v^*) . This implies $f(u^*, v^*) = g(u^*, v^*) = 0$. We also require that the fixed point is stable, namely that $\text{tr}(\mathbf{J}) = f_u + g_v < 0$ and $\det(\mathbf{J}) = f_u g_v - f_v g_u > 0$, where \mathbf{J} is the Jacobian of (1.19) evaluated at (u^*, v^*) and f_u (resp. f_v) denotes the derivatives of f with respect to u (resp. v), and similarly for g_u and g_v .

Patterns arise when (u^*, v^*) becomes unstable with respect to inhomogeneous perturbations. To look for instabilities, one can introduce a small perturbation $(\delta u_i, \delta v_i)$ to the fixed point and linearise around it. In doing so, one obtains Eq. (1.20).

$$\begin{pmatrix} \delta \dot{u}_i \\ \delta \dot{v}_i \end{pmatrix} = \sum_{j=1}^{\Omega} (\mathbf{J} \delta_{ij} + \mathbf{D} \Delta_{ij}) \cdot \begin{pmatrix} \delta u_j \\ \delta v_j \end{pmatrix}, \quad (1.20)$$

where

$$\mathbf{D} = \begin{pmatrix} D_1 & 0 \\ 0 & D_2 \end{pmatrix}.$$

For regular lattices, the Fourier transform is usually employed to solve this linear system of equations, as we previously showed. When the system is instead defined on a network, a different procedure needs to be followed [11, 20]. To this end, we define the eigenvalues Λ_α and eigenvectors $\Phi^{(\alpha)} = (\Phi_1^{(\alpha)}, \dots, \Phi_\Omega^{(\alpha)})$ of the Laplacian operator:

$$\sum_{j=1}^{\Omega} \Delta_{ij} \Phi_j^{(\alpha)} = \Lambda^{(\alpha)} \Phi_i^{(\alpha)}, \quad \alpha = 1, \dots, \Omega. \quad (1.21)$$

The eigenvectors can be orthonormalized as $\sum_{i=1}^{\Omega} \Phi_i^{(\alpha)} \Phi_i^{(\beta)} = \delta_{\alpha\beta}$. In fact, when the network is undirected, the Laplacian is symmetric. Therefore the eigenvalues $\Lambda^{(\alpha)}$ are real and the eigenvectors $\Phi^{(\alpha)}$ form an orthonormal basis. This condition needs to be relaxed when dealing with the more general setting of a directed graph, which we will discuss in the next chapter. The inhomogeneous perturbations δu_i and δv_i can be expanded as:

$$\delta u_i = \sum_{\alpha=1}^{\Omega} c_\alpha e^{\lambda_\alpha t} \Phi_i^{(\alpha)}, \quad \delta v_i = \sum_{\alpha=1}^{\Omega} b_\alpha e^{\lambda_\alpha t} \Phi_i^{(\alpha)}. \quad (1.22)$$

The constants c_α and b_α depend on the initial conditions. By inserting the above expressions in Eq. (1.20) one obtains the following eigenvalue problem

$$\det \begin{pmatrix} f_u + D_u \Lambda^{(\alpha)} - \lambda_\alpha & f_v \\ g_u & g_v + D_v \Lambda^{(\alpha)} - \lambda_\alpha \end{pmatrix} = 0. \quad (1.23)$$

This is equivalent to

$$\det(\mathbf{J}_\alpha - \mathbf{I}\lambda_\alpha) = 0, \quad (1.24)$$

where $\mathbf{J}_\alpha \equiv \mathbf{J} + \mathbf{D}\Lambda^{(\alpha)}$ and \mathbf{I} stands for the identity matrix. The eigenvalue with the largest real part, $\lambda_\alpha \equiv \lambda_\alpha(\Lambda^{(\alpha)})$ defines the dispersion relation

$$\lambda_\alpha = \frac{1}{2} \left(\text{tr}\mathbf{J}_\alpha + \sqrt{(\text{tr}\mathbf{J}_\alpha)^2 - 4\det\mathbf{J}_\alpha} \right), \quad (1.25)$$

which characterises the response of the system in Eq. (1.19) to external perturbations. In Fig. 1.4 (a) is shown the dispersion relation for different choices of bifurcation parameter of the Brusselator model. The symbols stand for the discrete values of λ_α and the underlying solid curve is the continuous counterpart.

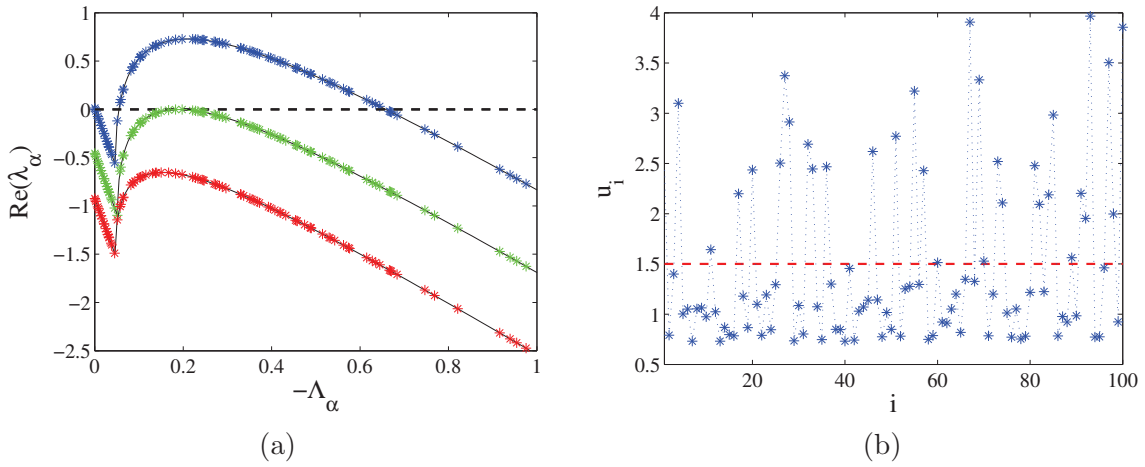


FIGURE 1.4: (a) Dispersion relation for a small-world network (weighted with $W_{ij} = 0.15$ for all links). (b) Network pattern. The dash line represent the initial steady state. The model and parameters are the same as in Fig. (1.1).

If $Re(\lambda_\alpha) > 0$, the fixed point is unstable and the system exhibits a pattern whose spatial properties are encoded in $\Lambda^{(\alpha)}$. The quantity $\Lambda^{(\alpha)}$ is the analogue of the wavelength for a spatial pattern in a system defined on a continuous regular lattice. In this case $\Lambda^{(\alpha)} \equiv -q^2$, where q labels the usual spatial Fourier frequency. From Fig. (1.4) (b) one can note that the patterns on a network (the symbols represent the concentration of the species u for each node), at variance with the continuum case, are organized in activators (inhibitors) rich and activators (inhibitors) poor nodes.

Turning on the stability problem, it can be proved that, for symmetric graphs, all the non-trivial values of $\Lambda^{(\alpha)}$ are negative. Hence, $\text{tr}\mathbf{J}_\alpha = \text{tr}\mathbf{J} + (D_u + D_v)\Lambda^{(\alpha)} < 0$. For the instability to manifest, it is therefore sufficient that $\det\mathbf{J}_\alpha = \det\mathbf{J} + (J_{11}D_v + J_{22}D_u)\Lambda^{(\alpha)} + D_v^2(\Lambda^{(\alpha)})^2 < 0$, a condition that can be met only if:

$$J_{11}D_v + J_{22}D_u > 0. \quad (1.26)$$

So, like for the continuum case, the instability can only set in if J_{11} and J_{22} have opposite signs. This means that the two involved species should constitute an activator-inhibitor system.

Working in this setting, it is instructive to consider again the limiting condition when only one of the species can diffuse. In principle if the system is defined over a discrete spatial support and at variance with the continuous domain, the instability can instead develop if the inhibitors are mobile, $D_v \neq 0$, and the activator fixed $D_u = 0$. A simple calculation shows that the dispersion relation (1.25) is positive for $|\Lambda^{(\alpha)}| > \det\mathbf{J}/D_v J_{11}$. If the spatial support is discrete, only a finite number of eigenmodes can be destabilised. The eigenmode associated to the largest eigenvalue $|\Lambda^{(\alpha)}|$ guides the instability and the patterns can develop. In this case, there is a *short wavelength instability*.

As we will show in this thesis, pattern formation in networks is an interesting domain of investigations with many important applications to real systems. Networks provide in fact the backbone for interactions of individual constituents and can remarkably contribute to the onset of the dynamical instabilities which underly the process of pattern formation.

Chapter 2

Topology-driven instabilities: the theory of pattern formation on directed networks

2.1 Introduction

For a large class of problems, including applications to neuroscience, the system under scrutiny is defined on a complex network, rather than on a regular, spatially extended lattice. The effects of the embedding graph structure on the emergence of Turing patterns in nonlinear diffusive systems were investigated in [11], paving the way for novel discoveries in an area of widespread interest. The conditions for the deterministic instability are derived following a linear stability analysis that we recalled in the preceding chapter, which requires expanding the perturbation on the complete basis formed by the eigenvectors of the discrete Laplacian. Travelling waves can also develop via a completely analogous mechanism [20]. To date, symmetric (undirected) networks have been considered in the literature. Again, the instability is driven by the non-trivial interplay between the nonlinearities, which are accounted for in the reaction parts, and the diffusion terms. The topology of the space defines the relevant directions for the spreading of the perturbation, but cannot impact on the onset of the instability. Consider for instance a reaction-diffusion system defined on a regular lattice and assume that it cannot experience a Turing-like instability: the system cannot be made unstable when placed on top of a symmetric network. In other words, the structure of the underlying graph cannot destabilise an otherwise stable scheme: the inherent ability of the model to self-organise in space and time is determined by the reaction terms.

In real applications, however, networks are not symmetric or, as they are called, undirected. It is often the case that a connection between two distinct nodes is associated with a specific direction, which means that the resulting graph is directed. Think for instance of the human mobility flow patterns with their immediate consequences for urban planning, transportation design and epidemic control. Several routes can be crossed in one direction only, so losing the symmetry between pairs of nodes. The internet and the cyberworlds, networks that we explore on a daily basis, are also characterised by an asymmetric routing of the links. Traffic symmetry typically does not hold for network locations beyond intranet and access links [29]. Furthermore, the map of the neural connection in the brain is also asymmetric, due to the physiology of neurons [30]. This can be seen in connectome models [31–33], coarse grained maps of the brain, revealed by MRI experiments, which reflects this asymmetric arrangement of connections at different scales of resolution.

Motivated by this observation, we will show that topology-driven instabilities can develop for reaction-diffusion systems on directed graphs, even when the examined system cannot experience a Turing-like or wave instability if defined on a regular lattice. This is at odds with the behaviour of symmetric networks. Therefore, the characteristics of the spatial support that hosts the interacting species play a role of paramount importance, often neglected and under appreciated in the literature. Consequently, our analysis represents a significant extension to the modelling of reaction-diffusion systems. The dynamical rules of interactions, on which the attention of the modellers has been so far solely devoted, are not the only instigators in the complex interactions that yield the rich variety of self-organised patterns seen in real-world applications. The topology of the space is also important, and significantly influences the conditions that yield the dynamical instability. This novel perspective might also hint at the causes that seem to favour an evolutionary selection of network-like structures in the organisation of living matter at different scales. For instance, the excitatory and inhibitory dynamics of neurons, and their specific spatial arrangement are two ingredients that cannot be trivially decoupled, the first being probably optimised to serve the global functioning of the brain, given the peculiar structure of the second.

This chapter is organised as follows. In Section 2.2 we will start by developing the generalised theory of patterns formation on a directed network. We will test the adequacy of the theory in Sections 2.3 and 2.4, for specific reference models, for different choices of the underlying networks and employing two plausible definitions of the Laplacian operator. Travelling waves and stationary inhomogeneous patterns will be obtained, by changing the topological characteristic of the graphs, while fixing the parameters to values for which the patterns cannot emerge when the model is defined on a symmetric spatial support. In Section 2.5 we summarise our results and draw conclusions.

2.2 Theory of pattern formation on a directed network

We will consider the pattern formation problem for a directed graph. In this case the adjacency matrix \mathbf{W} is no longer symmetric and its entries W_{ij} , if equal to one, indicate the presence of an edge directed from node i to j . Now, $k_i = \sum_{j=1}^{\Omega} W_{ij}$ refers to the *outdegree* of node i , defined as the number of exiting edges from node i . The associated Laplacian operator can be defined as $\Delta_{ij} = W_{ij} - k_i \delta_{ij}$, as it is customarily done in cooperative control applications [34], as e.g. intelligent transportation systems, routing of communications and power grid networks. The spreading of physical or chemical substances, rather than information content, requires imposing mass conservation, which results in a different formulation of the Laplacian operator [35], where W_{ij} is formally replaced by W_{ji} in the definition of Δ_{ij} , as it can be readily obtained from a simple microscopic derivation. Clearly, the two operators coincide, when defined on a symmetric network. Let denote the two interacting species on node i with (ϕ_i, ψ_i) . The reaction-diffusion equations for both cases are:

$$\begin{aligned} \frac{d\phi_i}{dt} &= f(\phi_i, \psi_i) + D_\phi \sum_{j=1}^{\Omega} \Delta_{ij} \phi_j \\ \frac{d\psi_i}{dt} &= g(\phi_i, \psi_i) + D_\psi \sum_{j=1}^{\Omega} \Delta_{ij} \psi_j, \end{aligned} \quad (2.1)$$

where D_ϕ and D_ψ are respectively the diffusion constants of the first and second species and f, g are the nonlinear reaction functions. For a directed graphs, the eigenvalues of both Laplacian operators, will in general be complex, $\Lambda^{(\alpha)} \in \mathbb{C}$. This property requires the development of a generalised theory of the instabilities, extending the analysis outlined in the previous chapter. As usual, we will assume a stable homogeneous fixed point¹, and indicate with \mathbf{J} the associated Jacobian matrix. The stability of the fixed point implies $\text{tr}(\mathbf{J}) < 0$ and $\det(\mathbf{J}) > 0$. In order to proceed with the linear stability analysis, we must ensure that the eigenvectors are linearly independent. This is not always the case when the underlying graph is directed². For this reason, the diagonalisability of the Laplacian matrix will be a minimal requirement to satisfy, in our analytical treatment of the stability problem.

¹To carry out the linear stability analysis, the homogeneous fixed point should be solution of the spatially extended system of governing equations. This prescription implies dealing with a balanced network (the outgoing connectivity equals the incoming one), when Fickian diffusion of material entities is being addressed $\Delta_{ij} = W_{ji} - k_i \delta_{ij}$, while no additional hypothesis on the structure of the spatial support are to be made when the operator $\Delta_{ij} = W_{ij} - k_i \delta_{ij}$ is assumed to hold.

²In fact, even without a complete basis, one can use the generalised eigenvectors in order to make progress. In this case however, patterns may emerge, even when the real part of the dispersion relation is negative everywhere, due to a transient growth process [36].

Introducing an inhomogeneous perturbation $(\delta\phi_i, \delta\psi_i)$ and linearising around it, one eventually obtains a dispersion relation, formally identical to equation (1.25), where now $\Lambda^{(\alpha)}$ is a complex quantity. For simplicity, and with obvious meaning of the notation, we write $\Lambda^{(\alpha)} = \Lambda_{\text{Re}}^{(\alpha)} + i\Lambda_{\text{Im}}^{(\alpha)}$, where $\Lambda_{\text{Re}}^{(\alpha)} < 0$, since the Laplacian matrix spectrum falls, according to Gerschgorin circle theorem [37], in the left half of the complex plane. A simple algebraic manipulation yields the following preliminary relations:

$$\begin{aligned}
(\text{tr}\mathbf{J}_\alpha)_{\text{Re}} &= \text{tr}\mathbf{J} + (D_\phi + D_\psi)\Lambda_{\text{Re}}^{(\alpha)} < 0 \\
(\text{tr}\mathbf{J}_\alpha)_{\text{Im}} &= (D_\phi + D_\psi)\Lambda_{\text{Im}}^{(\alpha)} \\
(\det\mathbf{J}_\alpha)_{\text{Re}} &= \det\mathbf{J} + (J_{11}D_\psi + J_{22}D_\phi)\Lambda_{\text{Re}}^{(\alpha)} \\
&\quad + D_\phi D_\psi \left[\left(\Lambda_{\text{Re}}^{(\alpha)}\right)^2 - \left(\Lambda_{\text{Im}}^{(\alpha)}\right)^2 \right] \\
(\det\mathbf{J}_\alpha)_{\text{Im}} &= (J_{11}D_\psi + J_{22}D_\phi)\Lambda_{\text{Im}}^{(\alpha)} + 2D_\phi D_\psi \Lambda_{\text{Re}}^{(\alpha)} \Lambda_{\text{Im}}^{(\alpha)},
\end{aligned} \tag{2.2}$$

where $(\cdot)_{\text{Re}}$ and $(\cdot)_{\text{Im}}$ select respectively the real and imaginary parts of the quantity in between brackets. To study the dispersion relation, we shall make use of an elementary property of the square root of a complex number $z = a + bi$, namely that

$$\sqrt{z} = \pm \left(\sqrt{\frac{a + |z|}{2}} + \text{sgn}(b) \sqrt{\frac{-a + |z|}{2}} i \right), \tag{2.3}$$

where $\text{sgn}(\cdot)$ is the standard sign function. In light of this consideration, the dispersion relation can be cast in the form:

$$\lambda_\alpha = \frac{1}{2} [(\text{tr}\mathbf{J}_\alpha)_{\text{Re}} + \gamma] + \frac{1}{2} [(\text{tr}\mathbf{J}_\alpha)_{\text{Im}} + \delta] i, \tag{2.4}$$

where:

$$\begin{aligned}
\gamma &= \sqrt{\frac{A + \sqrt{A^2 + B^2}}{2}} \\
\delta &= \text{sgn}(B) \sqrt{\frac{-A + \sqrt{A^2 + B^2}}{2}},
\end{aligned} \tag{2.5}$$

and:

$$\begin{aligned}
A &= [(\text{tr}\mathbf{J}_\alpha)_{\text{Re}}]^2 - [(\text{tr}\mathbf{J}_\alpha)_{\text{Im}}]^2 - 4(\det\mathbf{J}_\alpha)_{\text{Re}}, \\
B &= 2(\text{tr}\mathbf{J}_\alpha)_{\text{Re}}(\text{tr}\mathbf{J}_\alpha)_{\text{Im}} - 4(\det\mathbf{J}_\alpha)_{\text{Im}}.
\end{aligned} \tag{2.6}$$

The dispersion relation can now contain an imaginary contribution, which bears the signature of the imposed network topology. Travelling waves can in principle materialise for a two species reaction-diffusion model on a directed network, at variance with what happens when the system is defined on a symmetric spatial support. For the instability to occur, $(\lambda_\alpha)_{\text{Re}}$ must be greater than zero, which is equivalent to setting $|(\text{tr}\mathbf{J}_\alpha)_{\text{Re}}| \leq \gamma$, as it follows immediately from equation (2.4). A straightforward, although lengthy, calculation which involves relations (2.2), allows us to rewrite the condition for the instability in the compact form:

$$S_2(\Lambda_{\text{Re}}^{(\alpha)}) \left[\Lambda_{\text{Im}}^{(\alpha)} \right]^2 \leq -S_1(\Lambda_{\text{Re}}^{(\alpha)}), \quad (2.7)$$

where S_1 and S_2 are polynomials in $\Lambda_{\text{Re}}^{(\alpha)}$, of fourth and second degree respectively. The coefficients of the polynomials are model dependent, as specified in Eqs. (2.8), (2.9) and (2.10) below.

$$\begin{aligned} S_1(\Lambda_{\text{Re}}^{(\alpha)}) &= C_{14} \left[\Lambda_{\text{Re}}^{(\alpha)} \right]^4 + C_{13} \left[\Lambda_{\text{Re}}^{(\alpha)} \right]^3 + C_{12} \left[\Lambda_{\text{Re}}^{(\alpha)} \right]^2 + C_{11} \left[\Lambda_{\text{Re}}^{(\alpha)} \right] + C_{10} \\ S_2(\Lambda_{\text{Re}}^{(\alpha)}) &= C_{22} \left[\Lambda_{\text{Re}}^{(\alpha)} \right]^2 + C_{21} \left[\Lambda_{\text{Re}}^{(\alpha)} \right] + C_{20}, \end{aligned} \quad (2.8)$$

where

$$\begin{aligned} C_{14} &= D_\phi D_\psi (D_\phi + D_\psi)^2 \\ C_{13} &= (D_\phi + D_\psi)^2 (J_{11} D_\psi + J_{22} D_\phi) + 2 \text{tr}\mathbf{J} D_\phi D_\psi (D_\phi + D_\psi) \\ C_{12} &= \det\mathbf{J} (D_\phi + D_\psi)^2 + (\text{tr}\mathbf{J})^2 D_\phi D_\psi + 2 \text{tr}\mathbf{J} (D_\phi + D_\psi) (J_{11} D_\psi + J_{22} D_\phi) \\ C_{11} &= 2 \text{tr}\mathbf{J} (D_\phi + D_\psi) \det\mathbf{J} + (\text{tr}\mathbf{J})^2 (J_{11} D_\psi + J_{22} D_\phi) \\ C_{10} &= \det\mathbf{J} [\text{tr}\mathbf{J}]^2, \end{aligned} \quad (2.9)$$

and

$$\begin{aligned} C_{22} &= D_\phi D_\psi (D_\phi - D_\psi)^2 \\ C_{21} &= (J_{11} D_\psi + J_{22} D_\phi) (D_\phi - D_\psi)^2 \\ C_{20} &= J_{11} J_{22} (D_\phi - D_\psi)^2. \end{aligned} \quad (2.10)$$

Given the model, one can construct a class of graphs, namely those whose spectral properties match condition (2.7), for which the instability takes place. Here we are particularly interested in models that cannot develop the instability when defined on a symmetric, hence undirected, graph. In this case $\Lambda_{\text{Im}}^{(\alpha)} = 0$, by definition, and the generalised condition of instability (2.7) cannot be met. On the contrary, when the

graph is made directed, $\Lambda_{\text{Im}}^{(\alpha)} \neq 0$ and the examined models can experience a topology-driven instability, as governed by relation (2.7).

Recall that we are linearising around a stable fixed point, hence $\text{tr}\mathbf{J} = J_{11} + J_{22} < 0$ and, in addition, $\det\mathbf{J} > 0$. Because of the first inequality, the setting with both J_{11} and J_{22} positive is, as expected, ruled out a priori. Consider instead the dual scenario, where both J_{11} , J_{22} are taken to be negative. Hence, S_1 and S_2 are positive, as it can be immediately appreciated by direct inspection of Eqs. (2.9) and (2.10) defined previously³, and the instability condition (2.7) cannot be achieved. In conclusion, and in agreement with the standard theory of pattern formation on a regular symmetric lattice (network), J_{11} and J_{22} must have opposite signs, for the instability to develop.

In analogy with the discussion made in Chapter 1, we assume that the reaction-diffusion scheme is such that $J_{11} > 0$, and $J_{22} < 0$. We imagine here that the necessary condition (1.26) for the instability to set in, is not satisfied. No patterns can therefore develop, according to the classical paradigm. Under this assumptions, while S_1 is still a positive definite quantity, S_2 can take negative values, since $C_{20} < 0$ (see equation (2.10)). The instability condition (2.7) can then be satisfied and one can expect topology-driven instabilities to develop on directed graphs, as we shall demonstrate in the forthcoming section.

As an additional point, we wish to emphasise that patterns on a directed network can also emerge when the inhibitors are prevented from diffusing ($D_\psi = 0$, in our notation), at odds with the conventional vision [11]. Furthermore, travelling waves are always found for a two species model, the imaginary part of the dispersion relation λ_α being at all times different from zero, inside the instability domain. However, as we will demonstrate in the next section, when $(\lambda_\alpha)_{\text{Im}} \ll (\lambda_\alpha)_{\text{Re}}$, the system evolves towards a stationary inhomogeneous pattern, reminiscent of the Turing instability. In conclusion, a two species reaction-diffusion system on a directed graph can display a rich variety of instabilities, beyond the conventional scenario which applies to symmetric, hence undirected, spatial supports.

2.3 Numerical results

To confirm the theoretical analysis carried out in the previous section, we here focus on a specific system, the previously introduced Brusselator model and set in equations (2.1) $f(\phi_i, \psi_i) = 1 - (b + 1)\phi_i + c\phi_i^2\psi_i$ and $g(\phi_i, \psi_i) = b\phi_i - c\phi_i^2\psi_i$. It is worth stressing

³The coefficients C_{11} , C_{13} , C_{15} are negative, while C_{12} , C_{14} are positive. Recalling that $\Lambda_{\text{Re}}^{(\alpha)} < 0$, it is straightforward to conclude that S_1 and S_2 are indeed positive quantities.

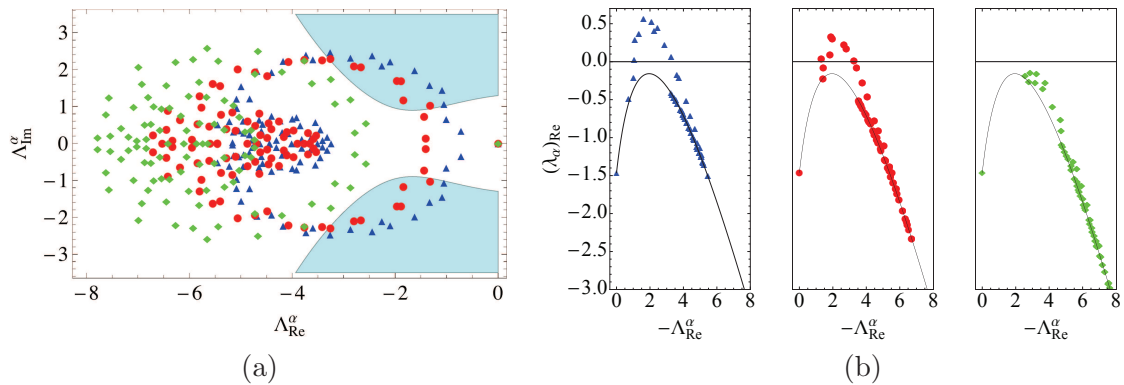


FIGURE 2.1: Panel (a): Spectral plot of three Laplacians generated from the Newman-Watts algorithm for $p = 0.27$, $p = 0.5$ and $p = 0.95$ (blue triangles, red circles and green diamonds respectively) and network size $\Omega = 100$. The shaded area indicates the instability region for the case of the Brusselator model, where the parameters are $b = 9$, $c = 30$, $D_\phi = 1$ and $D_\psi = 7$. Panel (b): The real part of the dispersion relation for the same three choices of Newman-Watts networks as in panel (a). The black line originates from the continuous theory.

that the Brusselator model has been selected for demonstrative purposes and due to its pedagogical value: the techniques here developed, and the conclusions that we shall reach, are nevertheless general and apply to a wide range of models. As an example, in the next Section we will repeat the same analysis for a version of the Fitzhugh-Nagumo scheme, that serves as a toy model for inspecting the coupled dynamics of neurons.

We will start by considering the first formulation of the Laplacian operator, $\Delta_{ij} = W_{ij} - k_i \delta_{ij}$, which, as previously mentioned, is employed in cooperative control applications [34]. To proceed, we should also specify the characteristics of the networks that define the spatial backbone for the explored systems. Two different strategies for generating the graphs will be considered. On the one side, we will follow the Watts-Strogatz (WS) approach [9], modified in order to make the network directed. We will also implement an alternative generation strategy, the Newman-Watts (NW) algorithm [28]. Both approaches are described in Chapter 1. When $\Delta_{ij} = W_{ji} - k_i \delta_{ij}$ is assumed instead, the directed networks are created with the additional prescription to balance the number of incoming and outgoing connections per node.

In the following we will report the emergence of topology-driven instabilities, defined on directed networks assembled via the two strategies mentioned here.

2.3.1 Travelling waves for systems of two diffusing species.

We commence by considering the Brusselator model in the general setting with $D_\phi \neq 0$ and $D_\psi \neq 0$. That is, both the activators and inhibitors are allowed to diffuse between connected nodes of the network. Furthermore, we set the parameters so that the system

is stable versus external perturbations of the homogeneous fixed point and no patterns can develop if the spatial support is assumed symmetric (or continuous). The generalised condition (2.7) for the instability on a directed network can be graphically illustrated in the reference plan $(\Lambda_{\text{Re}}^{(\alpha)}, \Lambda_{\text{Im}}^{(\alpha)})$. Given the parameters of the model, one can in fact determine the coefficients C_{1q} ($q = 0, \dots, 4$) and C_{2q} ($q = 0, 1, 2$) via Eqs. (2.9) and (2.10). Then, the inequality (2.7) allows one to delimit a model-dependent region of instability, which is depicted with a shaded area in Figure 2.1, panel (a). Each eigenvalue of the discrete Laplacian (defined on the directed network) appears as a point in the plane $(\Lambda_{\text{Re}}^{(\alpha)}, \Lambda_{\text{Im}}^{(\alpha)})$. If a subset of the Ω points that define the spectrum of the Laplacian fall inside the region outlined above, the instability can take place. For an undirected graph, $\Lambda_{\text{Im}}^{(\alpha)} = 0$, and the points are located on the real (horizontal) axis, thus outside the instability domain. In panel (a) of Figure 2.1 the spectral plot of three Laplacians, generated from the NW algorithm, are displayed for three choices of p . As p increases the points move to the left, away from the region of instability. The regular ring that captures the eigenvalue distribution for low p (blue triangles), becomes progressively distorted: for $p = 0.95$ the points (green diamonds) partially fill a circular patch in $(\Lambda_{\text{Re}}^{(\alpha)}, \Lambda_{\text{Im}}^{(\alpha)})$. In panel (b) of Figure 2.1 the real part $(\lambda_\alpha)_{\text{Re}}$ of the dispersion relation is plotted as a function of $-\Lambda_{\text{Re}}^{(\alpha)}$. The black solid line refers to the continuous theory: no instability can develop in the limit of continuum space, since $(\lambda_\alpha)_{\text{Re}}$ is always negative. However, when the Brusselator model evolves on a discrete support, the continuous line is replaced by a collection of Ω points. When the instability condition (2.7) is fulfilled, the points are lifted above the solid curve and cross the horizontal axis. The figure shows that $(\lambda_\alpha)_{\text{Re}}$ is positive over a finite domain in $-\Lambda_{\text{Re}}^{(\alpha)}$ and the system becomes unstable due to the topology of the underlying directed network. The travelling waves that stem from this instability are displayed in Figure 2.2. As we shall prove in the following, inhomogeneous stationary patterns are another possible outcome of the topology-driven instability.

A similar analysis can be performed when the directed network is generated using the WS method. In panel (a) of Figure 2.3, the region of instability, outlined by the shaded area, is identical to the one depicted in Figure 2.1, since the parameters of the reaction-diffusion scheme are unchanged. Here the topology-driven instability occurs for relatively large values of the parameter p , when the random nature of the network takes over its small world character. The travelling waves for this system are displayed in Figure 2.4.

2.3.2 The case of immobile inhibitors, $D_\psi = 0$.

As mentioned earlier, patterns can also emerge on a directed network when the inhibitors are prevented from diffusing ($D_\psi = 0$). This is a marginal condition for which classical

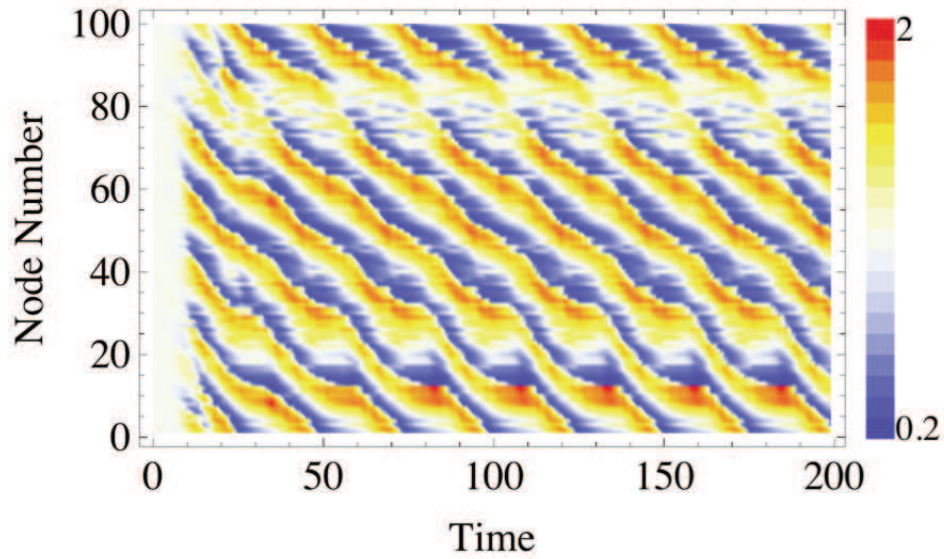


FIGURE 2.2: Time series for the case of the Brusselator model on a Newman-Watts network, generated with $p = 0.27$. The nodes are ordered as per the original lattice. Details of the network's spectra and the system's instability are displayed by the blue, triangular symbols in Figure 2.1. The caption of that figure also contains the values of the reaction parameters.

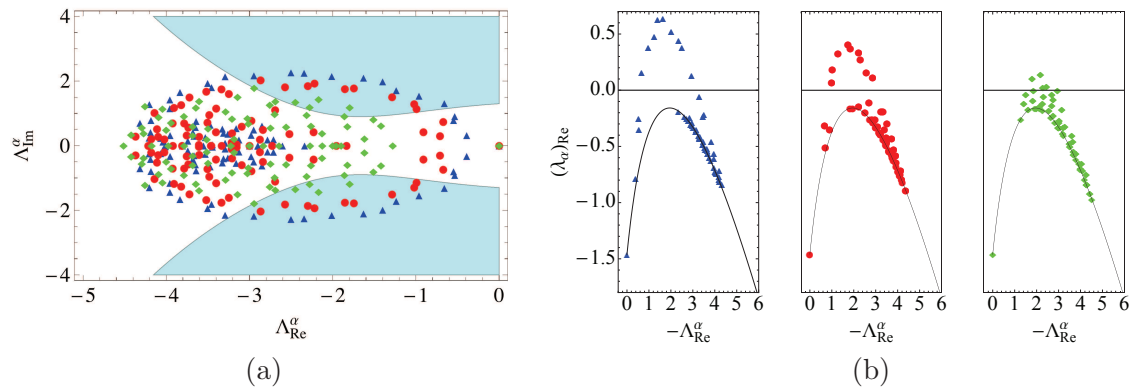


FIGURE 2.3: Panel (a): Spectral plot of three Laplacians generated from the Watts-Strogatz method for $p = 0.1$, $p = 0.2$ and $p = 0.8$ (blue triangles, red circles and green diamonds respectively). In all cases the network size is $\Omega = 100$. The coloured area indicates the instability region for the Brusselator model. Panel (b): The real part of the dispersion relation for three choices of Watt-Strogatz networks for $p = 0.1$, $p = 0.2$ and $p = 0.8$ (blue triangles, red circles and green diamonds respectively) and network size $\Omega = 100$. The parameters are as in Figure 2.1.

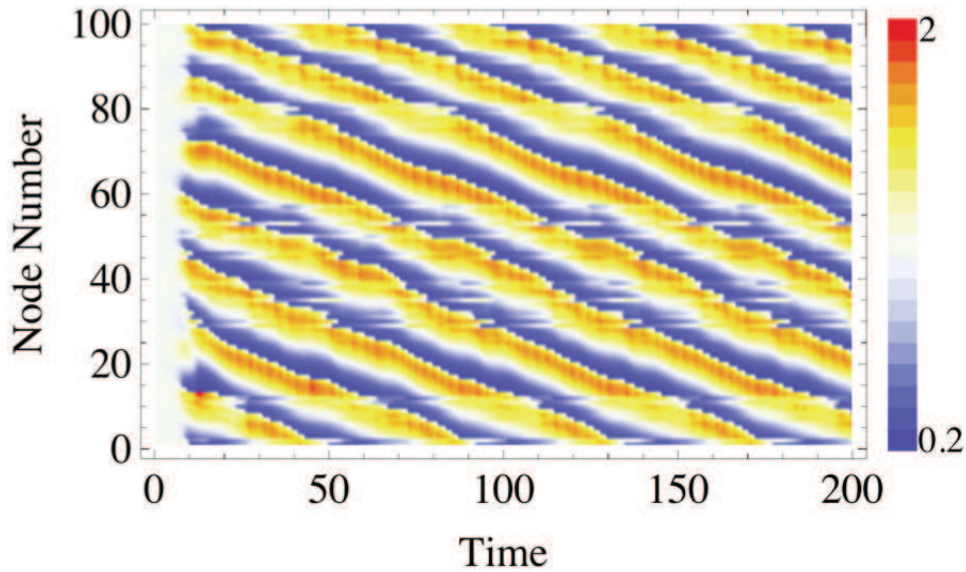


FIGURE 2.4: Time series for the case of the Brusselator model on a Watts-Strogatz network, generated with $p = 0.1$. The nodes are ordered as per the original lattice. Details of the network's spectra and the system's instability are displayed by the blue, triangular symbols in Figure 2.3. The reaction parameters are as in Figure 2.1.

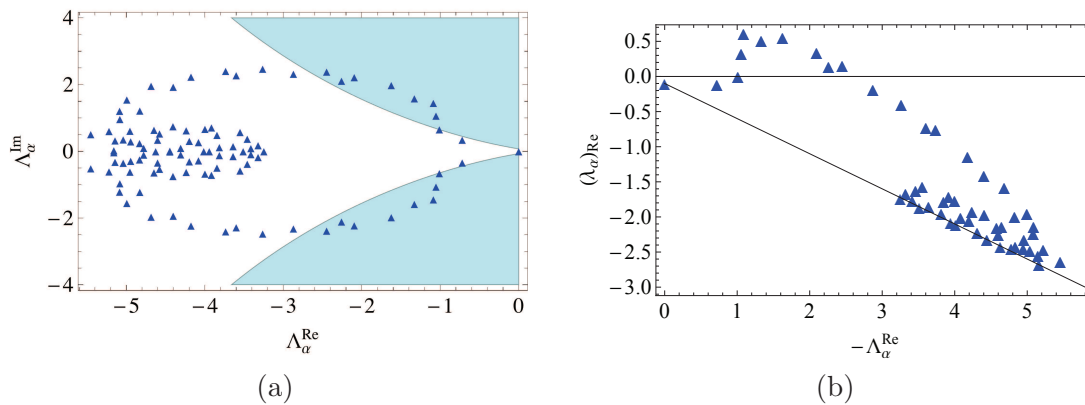


FIGURE 2.5: Panel (a): Spectral plot for a Newman-Watts network with $p = 0.27$ and $\Omega = 100$. The instability region is plotted for the choice of the Brusselator model, where the diffusion D_ψ has been set to zero. Panel (b): The real part of the dispersion relation for a Newman-Watts network with $\Omega = 100$, generated with $p = 0.27$. The black line is found from the continuous theory. The full parameter set is: $b = 9$, $c = 8.2$, $D_\phi = 1$ and $D_\psi = 0$.

patterns (both in the continuum limit or on an undirected network support) are not found. In panel (a) of Figure 2.5 the condition of instability is represented. The symbols (blue triangles) refer to a NW graph with $p = 0.27$ and fall inside the shaded domain, signalling the existence of a topology-driven instability. The same conclusion can be reached upon inspection of panel (b), where the real part of the dispersion relation is plotted and shown to be positive over finite window in $\Lambda_{\text{Re}}^{(\alpha)}$. The travelling waves found in this case are shown in Figure 2.6.

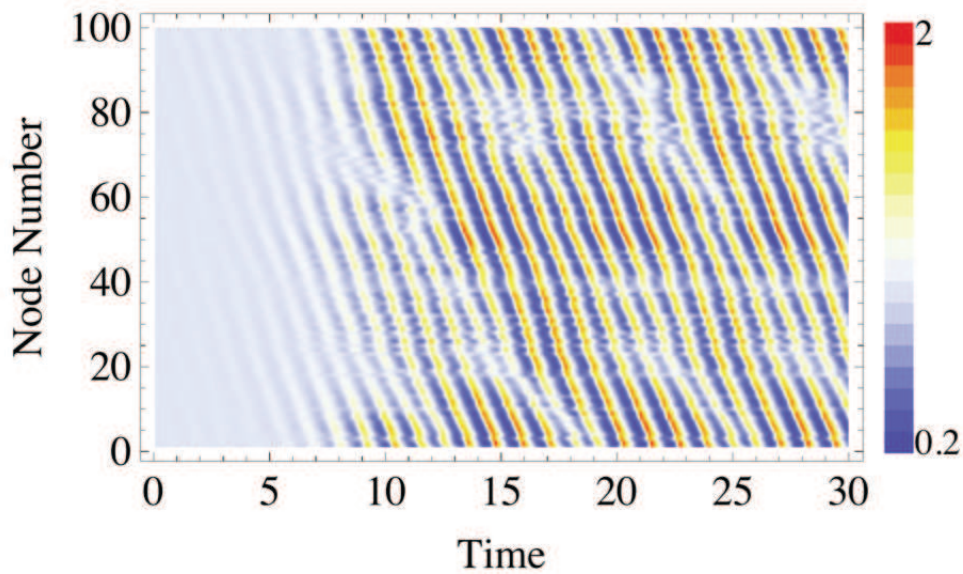


FIGURE 2.6: Time series obtained from the Brusselator model on a Newman-Watts network, in the case where $D_\psi = 0$. The network was constructed using $p = 0.27$. Details of the network's spectra and the system's instability are displayed by the blue, triangular symbols in Figure 2.5. The caption of that figure also contains the values of the reaction parameters.

2.3.3 Stationary inhomogeneous patterns.

The instability mechanism that we have here discussed results in travelling waves, which spread over the directed network. This is due to the fact that the imaginary part of the dispersion relation λ_α is always different from zero, inside the instability domain. Hence, Turing-like instabilities, which require imposing $(\lambda_\alpha)_{\text{Im}} = 0$, cannot formally develop. On the other hand, as we argued earlier, stationary inhomogeneous patterns reminiscent of the Turing instability, could be observed, provided $(\lambda_\alpha)_{\text{Im}} \ll (\lambda_\alpha)_{\text{Re}}$. This is the case considered here, as shown in Figure 2.7, for a directed network generated via the WS recipe. The parameters of the Brusselator model are instead set as in Figure 2.1. This is to stress again that different types of patterns can emerge because of the distinct characteristics of the networks: the patterns are not just selected by the imposed dynamical rules. The most unstable mode is located at around $\Lambda_{\text{Re}}^{(\alpha)} = -2$ (left panel of Figure 2.7), and its corresponding value of $(\lambda_\alpha)_{\text{Im}}$ is relatively small (right panel of Figure 2.7). The patterns found in this situation are shown in the two panels of Figure 2.8. By comparing Figures 2.4 (WS with $p = 0.1$) and 2.8 (WS with $p = 0.2$), it is immediately clear that a transitions take place, from travelling waves to asymptotically stationary stable, by tuning the rewiring probability p in the WS graph generation scheme.

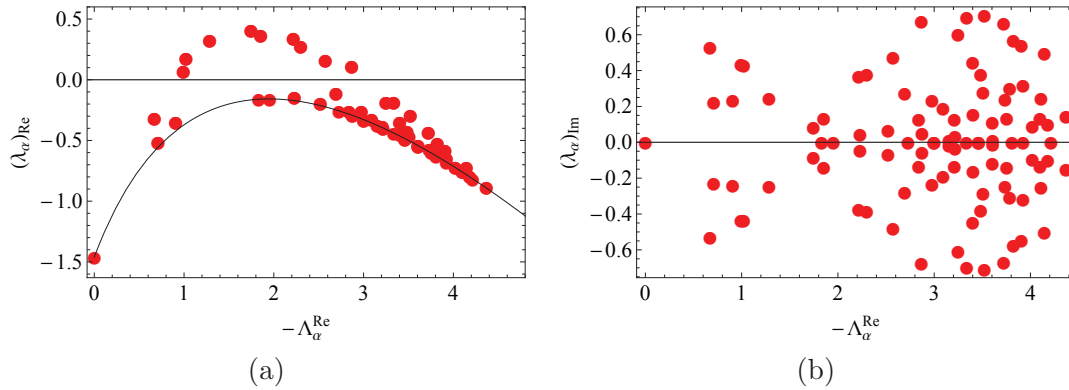


FIGURE 2.7: Panel (a): The real part of the dispersion relation for a Watts-Strogatz network with a Brusselator dynamic. The network is of size $\Omega = 100$, generated with $p = 0.2$. Panel (b): The imaginary part of the dispersion relation for a Watts-Strogatz network with a Brusselator dynamic. The network is of size $\Omega = 100$, generated with $p = 0.2$. The parameters are set as in Figure 2.1.

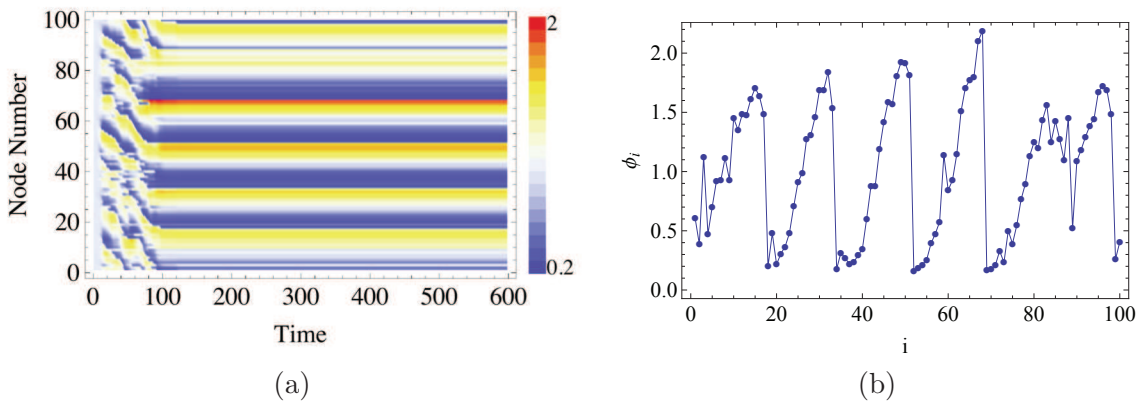


FIGURE 2.8: Panel (a): Time series showing quasi-Turing patterns on a Watts-Strogatz network with a Brusselator dynamic. The network was generated using $p = 0.2$. The system evolves from a homogeneous fixed point towards a static pattern. Panel (b); The long-time behaviour of the network, showing the concentration of each node. The dispersion relation for this system is presented in Figure 2.7.

2.3.4 Alternative formulation of the transport operator

Consider now the Laplacian operator defined as $\Delta_{ij} = W_{ji} - k_i\delta_{ij}$. As anticipated, this is the operator to be used when interested in modelling the diffusive spreading of material entities (molecules, animals) on a network. To match the assumptions of the analysis, the underlying network has to be balanced: the number of incoming connections ($\sum_j W_{ji}$) needs to be equal to the number of outgoing links (k_i). The homogeneous fixed point (ϕ^*, ψ^*) is hence solution of the spatially extended system (2.1), since $\sum_j \Delta_{ij}\phi^* = \sum_j \Delta_{ij}\psi^* = 0$, and the linear stability analysis, as discussed above, still holds⁴. In

⁴The case of unbalanced networks could be also addressed, provided one linearizes the equations (2.1) around a non homogeneous state [38]. Such generalization will be discussed elsewhere, as we here aim to a pedagogical introduction to the novel class of topology driven instabilities.

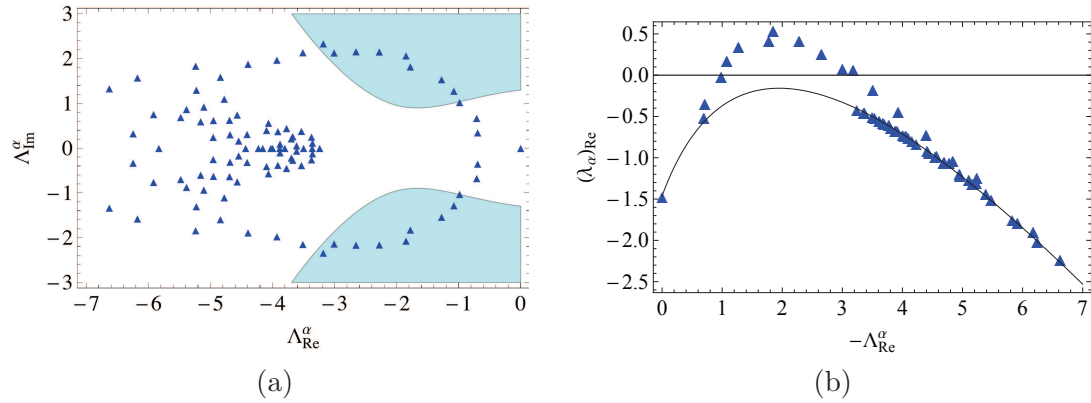


FIGURE 2.9: Panel (a): Spectral plot for a Newman-Watts network with $p = 0.27$ and $\Omega = 100$. The instability region is plotted for the Brusselator model. Panel (b): The real part of the dispersion relation for a balanced Newman-Watts network with $\Omega = 100$, generated with $p = 0.27$. Here, $\Delta_{ij} = W_{ji} - k_i \delta_{ij}$. The black line is found from the continuous theory. The full parameter set is: $b = 9$, $c = 30$, $D_{\phi} = 1$ and $D_{\psi} = 7$.

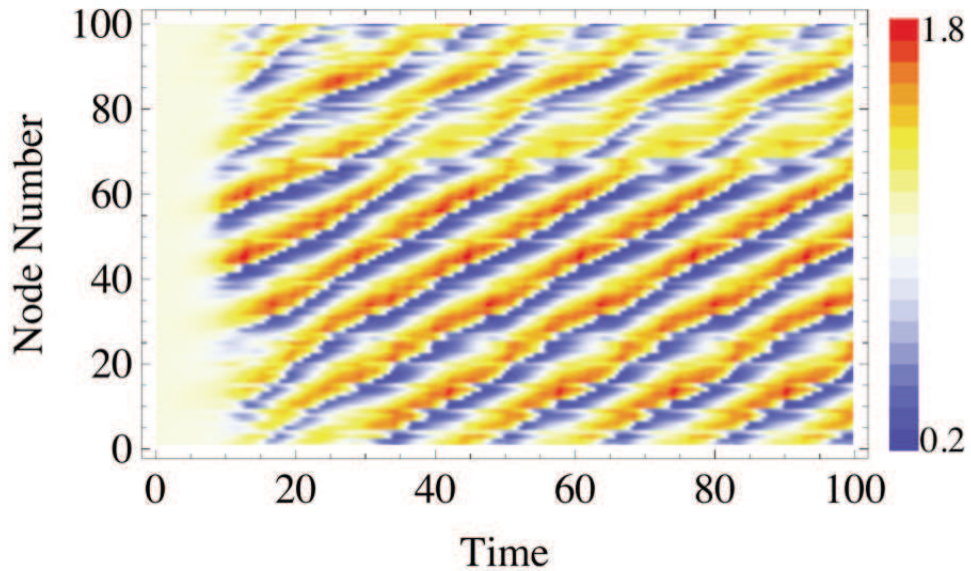


FIGURE 2.10: Time series obtained from the Brusselator model on a balanced Newman-Watts network, constructed using $p = 0.27$. Details of the network's spectra and the system's instability are displayed by the blue, triangular symbols in Figure 2.9. The caption of that figure also contains the values of the reaction parameters.

Figure 2.9, the condition of instability are displayed for a balanced NW network, while the emerging travelling waves can be clearly appreciated in Figure 2.10.

2.4 Topology induced patterns in FitzHugh-Nagumo model

As mentioned in the first part of this chapter, pattern formation in directed networks could represent an important step forward in the understanding of the complex behaviour in neuroscience where the spatial support is a neural network. Recently, substantial progress has been made in acquiring the architectural structure of the cerebral cortical areas in mammalian brains [39]. In all cases the topology of the neural networks can be approximately mimicked by a directed small-world graph [39, 40]. It is therefore quite reasonable to investigate neural dynamics based on the description that we have just introduced. To this end we consider the FitzHugh-Nagumo model [41–43],

$$\begin{aligned}\frac{du_i}{dt} &= u_i - u_i^3 - v_i + D_u \sum_{j=1}^{\Omega} \Delta_{ij} u_j \\ \frac{dv_i}{dt} &= c(u_i - av_i - b) + D_v \sum_{j=1}^{\Omega} \Delta_{ij} v_j\end{aligned}\quad (2.11)$$

which is a very simplified model that mimics to some extent the neurons dynamics. In fact, here u is the membrane potential and v the recovery variable. The model parameters are $a = 0.5$, $b = 0.04$, $c = 26$, $D_u = 0.2$ and $D_v = 15$ with a fixed point $(u^*, v^*) = (0.0795, 0.079)$. For this choice of the parameters the homogeneous fixed point is stable to inhomogenous perturbations, when the system is defined on a spatial symmetric support.

Below we discuss the network driven instability for the FitzHugh-Nagumo model, by employing both possible choices of the Laplacian operator. Fig. 2.11 shows the spectral plot of the same unbalanced NW small-world with 100 nodes with $p = 0.27$, used previously in Fig. 2.2. The instability region (shaded domain) has been redrawn for the FitzHugh-Nagumo model. Fig. 2.12 shows the real and imaginary parts of the dispersion relation, for the same parameter choice. The solid line in the left panel of Fig. 2.12 stands for the continuous linear instability theory, confirming that no instability can develop for the model defined on a symmetric support, given the choice of the parameters made. We conclude by presenting the wave pattern for this system in Fig. 2.13. Now, the values taken by the first species can be negative also, as it corresponds to the membrane potential. In Figs. 2.14, 2.15 and 2.16, the condition of instabilities, dispersion relation and the emerging wave are respectively displayed for a balanced NW network, and assuming a purely diffusive transport operator.

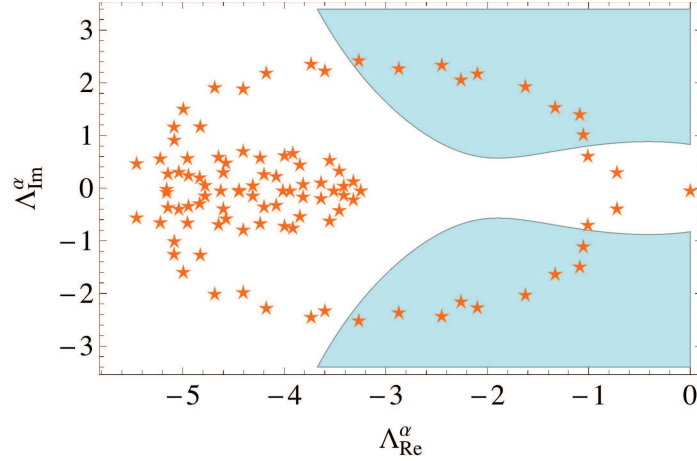


FIGURE 2.11: Spectral plot of the Laplacians $\Delta_{ij} = W_{ij} - k_i \delta_{ij}$ generated from the Newman-Watts algorithm for $p = 0.27$ and network size $\Omega = 100$. The shaded area indicates the instability region for the case of the FitzHugh-Nagumo model, where the parameters are $a = 0.5$, $b = 0.04$, $c = 26$, $D_u = 0.2$ and $D_v = 15$.

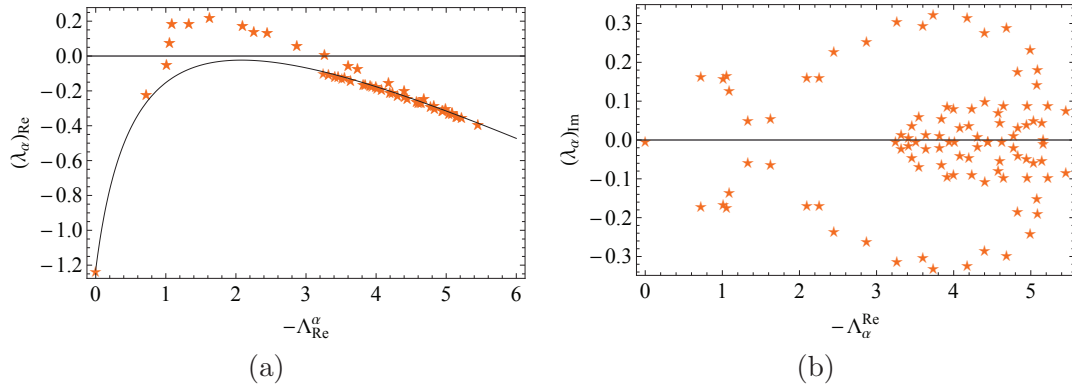


FIGURE 2.12: Panel (a): The real part of the dispersion relation for a Newman-Watts network with a Brusselator dynamic. The network is of size $\Omega = 100$, generated with $p = 0.27$. Panel (b): The imaginary part of the dispersion relation. The reaction parameter values are given in the caption of Fig. 2.11.

2.5 Conclusions

Patterns can spontaneously develop in reaction-diffusion systems following a linear instability mechanism, first discussed by Turing in his seminal paper [1]. Turing patterns are spontaneously emerging, stationary inhomogeneous motifs and represent a characteristic form of ecological self-organisation. Travelling waves can also develop in reaction-diffusion systems, following a similar instability mechanism. Alongside the clear theoretical interest, these concepts connect with many fields of application, from life science to chemistry and physics, transcending the boundaries of ecology. In general, the inspected model is assumed to be defined on a continuous spatial support or on a regular lattice.

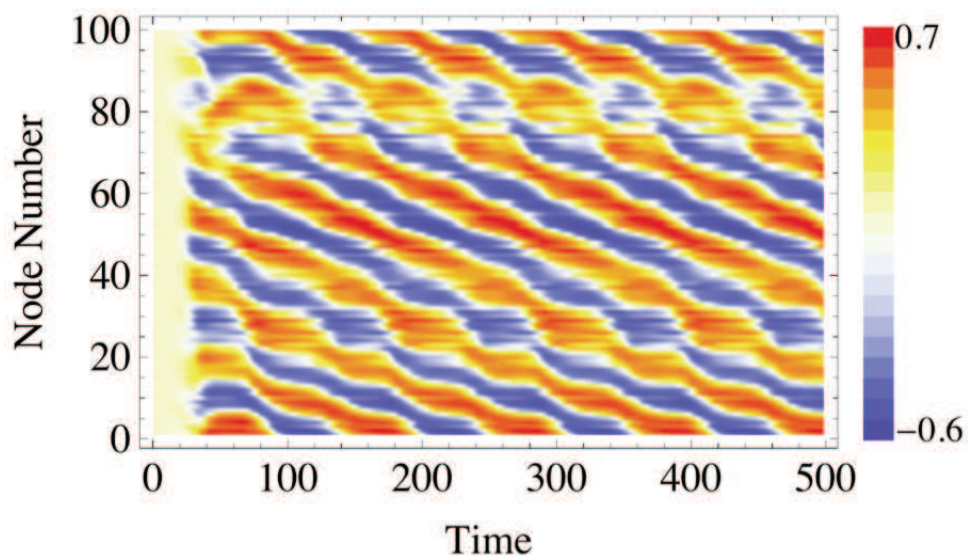


FIGURE 2.13: Time series for the case of the FitzHugh-Nagumo model on a Newman-Watts network, generated with $p = 0.27$. The nodes are ordered as per the original lattice and the reaction parameter values are given in the caption of Fig. 2.11.

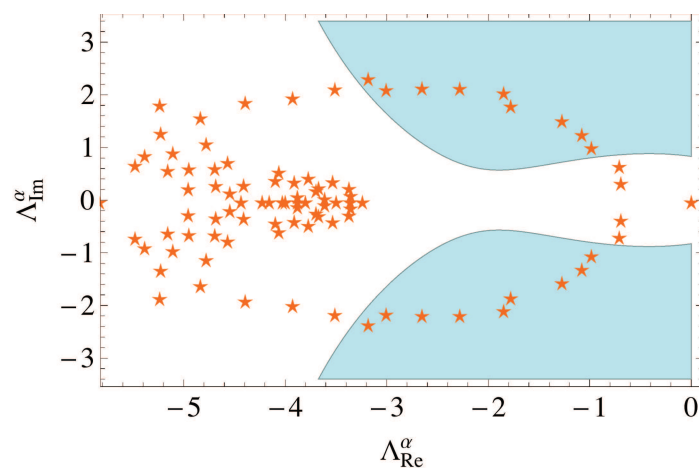


FIGURE 2.14: Spectral plot of the network Laplacians $\Delta_{ij} = W_{ji} - k_i \delta_{ij}$ generated from the balanced Newman-Watts algorithm for $p = 0.27$ and network size $\Omega = 100$. The shaded area indicates the instability region for the case of the FitzHugh-Nagumo model, where the parameters are $a = 0.5$, $b = 0.04$, $c = 26$, $D_u = 0.2$ and $D_v = 15$.

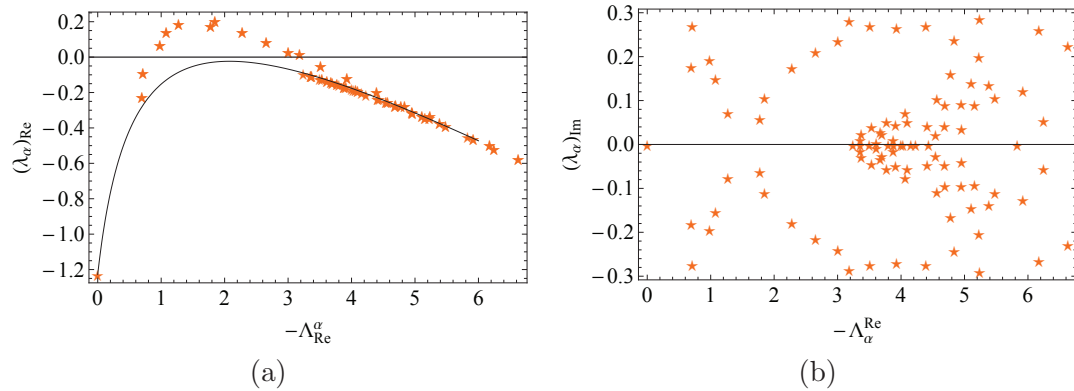


FIGURE 2.15: Panel (a): The real part of the dispersion relation for a balanced Newman-Watts network with a Brusselator dynamic. The network is of size $\Omega = 100$, generated with $p = 0.27$. Here, $\Delta_{ij} = W_{ji} - k_i \delta_{ij}$. Panel (b): The imaginary part of the dispersion relation. The reaction parameter values are given in the caption of Fig. 2.14.

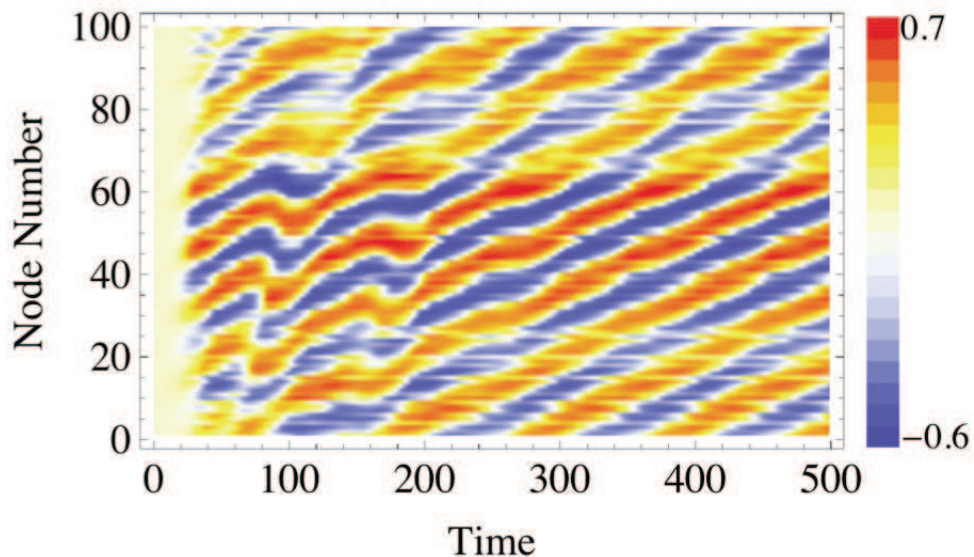


FIGURE 2.16: Time series for the case of the FitzHugh-Nagumo model on a balanced Newman-Watts network, generated with $p = 0.27$. The nodes are ordered as per the original lattice and the reaction parameter values are given in the caption of Fig. 2.14.

In many cases, it is instead more natural to establish the system on a complex network. With reference to ecology, the nodes of the networks define localised habitat patches, and the dispersal connection among habitats result in the diffusive coupling between adjacent nodes. Broadening the discussion, the brain is a network of neuronal connections, which provide the backbone for the propagation of the cortical activity. The internet and the cyberworld in general are other, quite obvious examples of applications that require invoking the concept of network. In a recent paper [11], Nakao and Mikhailov developed the theory of Turing pattern formation on random symmetric networks, highlighting the peculiarities that stem from the embedding graph structure. Travelling waves can also

set in following an analogous mechanism [20].

Starting from this context, and to reach a number of potential applications, we have here considered the extension of the analysis in [11] to the case of directed, hence non-symmetric, networks. It is often the case that links joining two distant nodes are defined with an associated direction: the reactants can move from one node to another, but the reverse action is formally impeded. In this chapter, we have shown that a novel class of instability, here termed ‘topology driven’, can develop for reaction-diffusion systems on directed graphs, also when the examined system cannot experience a Turing-like or wave instability when defined on a regular lattice or, equivalently, on a continuous spatial support. This is at variance with the case of symmetric networks, that cannot possess the intrinsic ability of turning unstable an otherwise stable homogenous fixed point. We have shown here that different patterns can be generated depending on the characteristics of the spatial support on which the reaction-diffusion system is defined. In particular, transitions from travelling waves to asymptotically stationary stable patterns, reminiscent of the Turing instability, are obtained when tuning the rewiring probability p in a WS network. The condition for the instability results in a rather compact mathematical criterion, which accounts for the spectral properties of the underlying network and whose predictive adequacy has been validated with reference to selected case studies.

The existence of a generalised class of instabilities, seeded by the topological characteristics of the embedding support, suggests a shift in the conventional approach to modelling of dynamical systems. Mutual rules of interactions, that define the reactions among constituents, are certainly important, although not decisive in determining the asymptotic fate of the system. The topology of the space, when assumed to be a directed random network, also matters and plays an equally crucial role in the onset of the dynamical instability. This is a general conclusion that we have cast in rigorous terms, which can potentially inspire novel avenues of research in all those domains, from neuroscience to social related applications, where networks prove essential.

Chapter 3

Turing patterns in multiplex networks

3.1 Introduction

Building on the pioneering work of Othmer and Scriven [10], Nakao and Mikhailov [11] developed the theory of Turing patterns formation on random undirected (symmetric) network that we have illustrated in Chapter 1. In the previous chapter, the case of directed, hence non symmetric, networks has been addressed [12]. When the reactants can only diffuse along specific directions, the tracks that correspond to the reversal moves being formally impeded, topology driven instabilities can develop also when the system under scrutiny cannot experience a Turing like (or wave instability) if defined on a regular lattice or, equivalently, on a continuous spatial support.

However, the conventional approach to network theory is not general enough to ascertain the complexity that hides behind real world applications. Self-organization may proceed across multiple, inter-linked networks, by exploiting the multifaceted nature of resources and organizational skills. For this reason, multiplex, networks in layers whose mutual connections are between twin nodes, see Figure 3.1, have been introduced as a necessary leap forward in the modeling effort [14, 15, 25, 44, 45]. These concepts are particularly relevant to transportation systems [46, 47], the learning organization in the brain [48] and to understanding the emergent dynamics in social communities [49]. In [13] the process of single species diffusion on a multiplex network has been investigated, and the spectrum of the associated Laplacian matrix characterized in term of its intra- and interlayer structure.

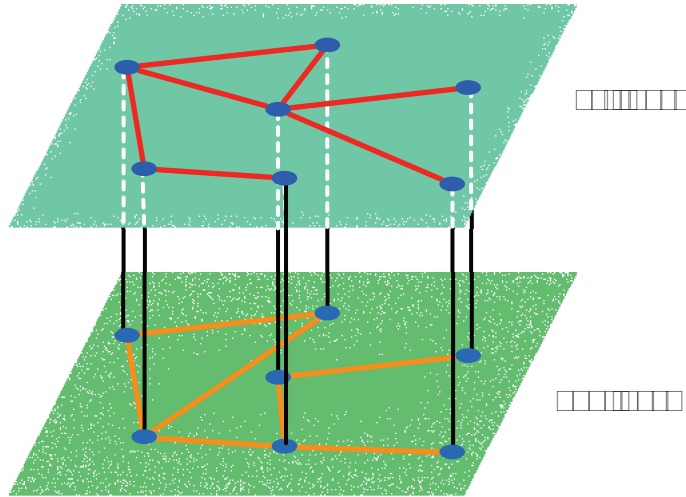


FIGURE 3.1: A schematic illustration of a two layers multiplex network.

In this chapter we build on these premises to derive a general theory of patterns formation for multispecies reaction-diffusion systems on a multiplex. Cooperative interference between adjacent layers manifests, yielding stratified patterns also when the Turing like instability on each individual layer is impeded. Conversely, patterns can dissolve as a consequence of the inter-layer overlap. The analysis is carried out analytically via a perturbative scheme which enables to derive closed analytical expressions for the critical coupling that determines the aforementioned transitions. The adequacy of the analytical predictions is confirmed by direct numerical simulations.

In the next section we will introduce the reaction-diffusion system defined on a multiplex network. In Section 5.3 a perturbative technique will be employed to approximately calculate the conditions for the Turing instability of a weakly coupled multilayer network. In the last section we sum up our results and present our conclusions.

3.2 Reaction-diffusion equations on multiplex networks

Let us consider the reaction-diffusion dynamics on a multiplex composed by two distinct layers. The analysis readily extends to an arbitrary number of independent layers. For the sake of simplicity we will here assume each layer to be characterized by an identical set of Ω nodes; the associated connectivity can however differ on each layer, as specified by the corresponding adjacency matrix W_{ij}^K , with $i, j = 1, \dots, \Omega$ and $K = 1, 2$. In principle the adjacency matrix can be weighted. The species concentrations are denoted by u_i^K and v_i^K where the index K identifies the layer to which the individuals belong. Species are allowed to diffuse on each layer, moving towards adjacent nodes with diffusion

constants respectively given by D_u^K and D_v^K . Inter-layer diffusion is also accommodated for, via Fickian contributions which scale as the local concentration gradient, D_u^{12} and D_v^{12} being the associated diffusion constants. We hypothesize that reactions take place between individuals sharing the same node i and layer K , and are formally coded via the non linear functions $f(u_i^K, v_i^K)$ and $g(u_i^K, v_i^K)$. Mathematically, the reaction-diffusion scheme generalizes to:

$$\begin{cases} \dot{u}_i^K &= f(u_i^K, v_i^K) + D_u^K \sum_{j=1}^{\Omega} L_{ij}^K u_j^K + D_u^{12} (u_i^{K+1} - u_i^K) \\ \dot{v}_i^K &= g(u_i^K, v_i^K) + D_v^K \sum_{j=1}^{\Omega} L_{ij}^K v_j^K + D_v^{12} (v_i^{K+1} - v_i^K) \end{cases} \quad (3.1)$$

with $K = 1, 2$ and assuming $K + 1$ to be 1 for $K = 2$. Here $L_{ij}^K = W_{ij}^K - k_i^K \delta_{ij}$ stands for the Laplacian matrix on the layer K . If the inter-layer diffusion is silenced, which implies setting $D_u^{12} = D_v^{12} = 0$, the layers are decoupled. Working in this limit, one recovers hence two independent pairs of coupled reaction-diffusion equations for, respectively, (u_i^1, v_i^1) and (u_i^2, v_i^2) . Turing patterns can eventually set in for each of the considered limiting reaction-diffusion system as dictated by their associated dispersion relations $\lambda_{\alpha}^K \equiv \lambda(\Lambda^{(\alpha K)})$ with $K = 1, 2$, derived following the procedure outlined above. We are here instead interested in the general setting where the inter-layered diffusion is accounted for. Can the system develop self-organized patterns which result from a positive interference between adjacent layers, when the instability is prevented to occur on each isolated level? Conversely, can patterns fade away when the diffusion between layers is switched on?

To answer to these questions we adapt the above linear stability analysis to the present context. Linearizing around the stable homogeneous fixed point (\hat{u}, \hat{v}) returns:

$$\begin{pmatrix} \delta \dot{\mathbf{u}} \\ \delta \dot{\mathbf{v}} \end{pmatrix} = \tilde{\mathcal{J}} \begin{pmatrix} \delta \mathbf{u} \\ \delta \mathbf{v} \end{pmatrix} \quad (3.2)$$

with

$$\tilde{\mathcal{J}} = \begin{pmatrix} f_u \mathbf{I}_{2\Omega} + \mathcal{L}_u + D_u^{12} \mathcal{I} & f_v \mathbf{I}_{2\Omega} \\ g_u \mathbf{I}_{2\Omega} & g_v \mathbf{I}_{2\Omega} + \mathcal{L}_v + D_v^{12} \mathcal{I} \end{pmatrix}$$

and where we have introduced the compact vector notation $\mathbf{x} = (x_1^1, \dots, x_{\Omega}^1, x_1^2, \dots, x_{\Omega}^2)^T$, for $x = u, v$. Also, $\mathcal{I} = \begin{pmatrix} -\mathbf{I}_{\Omega} & \mathbf{I}_{\Omega} \\ \mathbf{I}_{\Omega} & -\mathbf{I}_{\Omega} \end{pmatrix}$, where \mathbf{I}_{Ω} denotes the $\Omega \times \Omega$ -identity matrix. The multiplex Laplacian for the species u reads: $\mathcal{L}_u = \begin{pmatrix} D_u^1 \mathbf{L}^1 & \mathbf{0} \\ \mathbf{0} & D_u^2 \mathbf{L}^2 \end{pmatrix}$. A similar operator, \mathcal{L}_v , is associated to species v . Notice that $\mathcal{L}_u + D_u^{12} \mathcal{I}$ is the supra-Laplacian introduced in [13]. Analogous consideration holds for the term that controls the migration of v across the multiplex. Studying the 4Ω eigenvalues λ of matrix $\tilde{\mathcal{J}}$ ultimately returns the condition for the dynamical instability which anticipates the emergence of Turing

like patterns. If the real part of at least one of the λ_i , with $i = 1, \dots, 4\Omega$ is positive, the initial perturbation grows exponentially in the linear regime of the evolution. Non linear effects become then important and the system eventually attains a non homogenous stationary configuration. Unfortunately, in the multiplex version of the linear calculation, and for a generic choice of the diffusion constants, one cannot introduce a basis to expand the perturbations which diagonalizes the supra-Laplacian operators. In practice, one cannot project the full $4\Omega \times 4\Omega$ eigenvalue problem into a subspace of reduced dimensionality, as it is instead the case when the problem is defined on a single layer. Moreover, it is not possible to exactly relate the spectrum of the multiplex matrix $\tilde{\mathcal{J}}$ to those obtained when the layers are decoupled. Analytical insight can be gained through an apt perturbative algorithm which enables us to trace the modifications on the dispersion relation, as due to the diffusive coupling among layers. To this end we work in the limit of a weakly coupled multiplex, the intra-diffusion constants being instead assumed order one. Without losing generality we set $\epsilon \equiv D_v^{12} \ll 1$, and assume D_u^{12} to be at most $O(\epsilon)$. We hence write $\tilde{\mathcal{J}} = \tilde{\mathcal{J}}_0 + \epsilon \mathcal{D}_0$ where $\tilde{\mathcal{J}}_0 = \begin{pmatrix} f_u \mathbf{I}_{2\Omega} + \mathcal{L}_u & f_v \mathbf{I}_{2\Omega} \\ g_u \mathbf{I}_{2\Omega} & g_v \mathbf{I}_{2\Omega} + \mathcal{L}_v \end{pmatrix}$ and $\mathcal{D}_0 = \begin{pmatrix} \frac{D_u^{12}}{D_v^{12}} \mathbf{L}^1 & \mathbf{0} \\ \mathbf{0} & \mathbf{L}^2 \end{pmatrix}$.

3.3 Perturbative characterization of the spectrum

The spectrum of $\tilde{\mathcal{J}}_0$ is obtained as the union of the spectra of the two sub-matrices which define the condition for the instability on each of the layers taken independently. To study the deformation of the spectra produced by a small positive perturbation ϵ , we refer to a straightforward extension of the Bauer-Fike theorem [50]. We here give a general derivation of the result which will be then exploited with reference to the specific problem under investigation. Consider a matrix A_0 under the assumption that the eigenvalues of A_0 , $(\lambda_m^{(0)})_m$, have all multiplicity one ¹. The associated eigenvectors, $(\mathbf{v}_m^{(0)})_m$ are thus linearly independent and form a basis for the underlying vector space \mathbb{R}^Ω (or \mathbb{C}^Ω). Introduce now $A = A_0 + \epsilon A_1$, A_1 representing the perturbation rescaled by ϵ . We will denote with $\lambda(\epsilon)$ and $(\mathbf{v}_m(\epsilon))_m$ the eigenvalues and eigenvectors of matrix A . Let us introduce the matrices $\Lambda(\epsilon) = \text{diag}(\lambda_1(\epsilon), \lambda_2(\epsilon), \dots, \lambda_\Omega(\epsilon))$ and $V(\epsilon) = \begin{pmatrix} \mathbf{v}_1(\epsilon) & \mathbf{v}_2(\epsilon) & \dots & \mathbf{v}_\Omega(\epsilon) \end{pmatrix}$ and expand them into power of ϵ as:

$$\Lambda(\epsilon) = \sum_{l \geq 0} \Lambda_l \epsilon^l \quad \text{and} \quad V(\epsilon) = \sum_{l \geq 0} V_l \epsilon^l, \quad (3.3)$$

¹The discussion can be extended to the case where the eigenvalues are repeated, at the price of some additional complications in the calculations [51–53].

where Λ_0 stands for the eigenvalues of the unperturbed matrix; V_0 (resp. U_0 , to be used later) stands for the matrix whose columns (resp. rows) are the right (resp. left) eigenvectors of $\tilde{\mathcal{J}}_0$. Inserting formulae (3.3) into the perturbed system $(A_0 + \epsilon A_1)V = V\Lambda$ and collecting together the terms of same order in ϵ beyond the trivial zero-th order contribution, we get $A_0 V_l + A_1 V_{l-1} = \sum_{k=0}^l V_{l-k} \Lambda_k \quad \forall l \geq 1$. Left multiplying the previous equation by U_0 and setting $C_l = U_0 V_l$ yields:

$$\Lambda_0 C_l - C_l \Lambda_0 = -U_0 A_1 V_{l-1} + C_0 \Lambda_l + \sum_{k=1}^{l-1} C_{l-k} \Lambda_k. \quad (3.4)$$

which can be solved as follows.

Eq. (3.4) contains two unknowns, namely C_l and Λ_l . To obtain a close analytical solution, we observe that Eq. (3.4) can be cast in the compact form

$$[\Lambda_0, X] = Y, \quad (3.5)$$

where X and Y are $\Omega \times \Omega$ matrices and $[\cdot, \cdot]$ stands for the matrix commutator. In practice, given $Y \in \mathbb{R}^{\Omega \times \Omega}$, one needs to find $X \in \mathbb{R}^{\Omega \times \Omega}$ solution of (3.5). Since Λ_0 is a diagonal matrix, the codomain of the operator $[\Lambda_0, \cdot]$ is formed by all the matrices with zero diagonal. To self-consistently solve (3.5) it is therefore necessary to impose that Y has zero diagonal elements. Hence, matrix X will have its diagonal elements undetermined.

Because of the above remark one can solve Eq. (3.4) by setting Λ_l so to cancel the diagonal terms on its right hand side, that is:

$$(\Lambda_l)_{ij} = \begin{cases} (U_0 A_1 V_{l-1})_{ii} - \sum_{k=1}^{l-1} (C_{l-k} \Lambda_k)_{ii} & \text{if } i = j \\ 0 & \text{otherwise.} \end{cases} \quad (3.6)$$

Then C_l is readily found to match:

$$(C_l)_{ij} = \begin{cases} \frac{(-U_0 A_1 V_{l-1})_{ij} + \sum_{k=1}^{l-1} (C_{l-k} \Lambda_k)_{ij}}{\lambda_i^{(0)} - \lambda_j^{(0)}} & \text{if } i \neq j \\ 0 & \text{otherwise.} \end{cases} \quad (3.7)$$

This latter expression allows us to simplify (3.6). In fact:

$$(C_{l-k} \Lambda_k)_{ii} = \sum_h (C_{l-k})_{ih} (\Lambda_k)_{hi} = 0,$$

and thus the approximated eigenvalues are given by

$$(\Lambda_l)_{ij} = \begin{cases} (U_0 A_1 V_{l-1})_{ii} & \text{if } i = j \\ 0 & \text{otherwise,} \end{cases} \quad (3.8)$$

Observe that the previous formulae take a simpler form for $l = 1$ when they reduce to:

$$\lambda_i^{(1)} = (U_0 A_1 V_0)_{ii} \quad \text{and} \quad (C_1)_{ij} = -\frac{(U_0 A_1 V_0)_{ij}}{\lambda_i^{(0)} - \lambda_j^{(0)}} \quad \text{for } i \neq j. \quad (3.9)$$

The above expressions allows us to assess the effect of the inter-layer coupling on the stability of the system. Select the eigenvalue with the largest real part λ_0^{max} of the unperturbed matrices $\tilde{\mathcal{J}}_0$. For sufficiently small ϵ , such that the relative ranking of the eigenvalues is preserved, we have at the leading order correction:

$$\lambda^{max}(\epsilon) = \lambda_0^{max} + \epsilon(U_0 \mathcal{D}_0 V_0)_{kk} + \mathcal{O}(\epsilon^2), \quad (3.10)$$

where k is the index which refer to the largest unperturbed eigenvalue λ_0^{max} . Higher order corrections can be also computed as follows the general procedure outlined above. To illustrate how inter-layers couplings interfere with the ability of the system to self-organize in collective patterns, we apply the above analysis to a specific case study, the Brusselator model whose local reaction terms are given by $f(u, v) = 1 - (b + 1)u + cu^2v$ and $g(u, v) = bu - cu^2v$, where b and c act as constant parameters.

Suppose now that for $\epsilon = 0$ the system is stable, namely that $\lambda_0^{max} < 0$, as depicted in the main panel of Figure 3.2. No patterns can hence develop on any of the networks that define the layers of the multiplex ². For an appropriate choice of the parameters of the model, λ^{max} grows as function of the inter-layer diffusion D_v^{12} ($= \epsilon$) and becomes eventually positive, signaling the presence of an instability which is specifically sensitive to the multiplex topology. The circles in Figure 3.2 are computed by numerically calculating the eigenvalues of the matrix $\tilde{\mathcal{J}}$ for different choices of the diffusion constant D_v^{12} . The dashed line refer to the linear approximation (3.10) and returns a quite reasonable estimate for the critical value of the inter-layer diffusion $D_{v,crit}^{12}$ for which the multiplex instability sets in, $D_{v,crit}^{12} \simeq -\lambda_0^{max}/(U_0 \mathcal{D}_0 V_0)_{kk}$. The solid line is obtained by accounting for the next-to-leading corrections in the perturbative calculation. In the upper inset of Figure 3.2 the dispersion relation is plotted versus Λ_α^K , the eigenvalues of the Laplacian operators L^1 and L^2 , for two choices of the inter-layer diffusion. When $D_v^{12} = 0$ the two dispersion relations (circles, respectively red and blue), each associated

²Numerical tests have been also performed for different choices of p or employing alternative strategies to generate the networks that define the layers, reaching always qualitatively similar conclusions. The same holds for the results depicted in Figure 3.3.

to one of the independent layers, are negative as they both fall below the horizontal dashed line. For $D_v^{12} = 0.5$ the curves lift, while preserving almost unaltered their characteristic profile (square, green). In particular, the upper branch of the multiplex dispersion relation takes positive values within a bounded domain in Λ_α , so implying the instability. To confirm the validity of the theoretical predictions we integrated numerically the reaction-diffusion system (3.1), assuming the Brusselator reaction terms, and for a choice of the parameters that yield the multiplex instability exemplified in the main plot of Figure 3.2. As expected, the homogeneous fixed point (dashed line) gets destabilized: the external perturbation imposed at time zero, is self-consistently amplified and yields the asymptotic patterns displayed in lower inset of Figure 3.2.

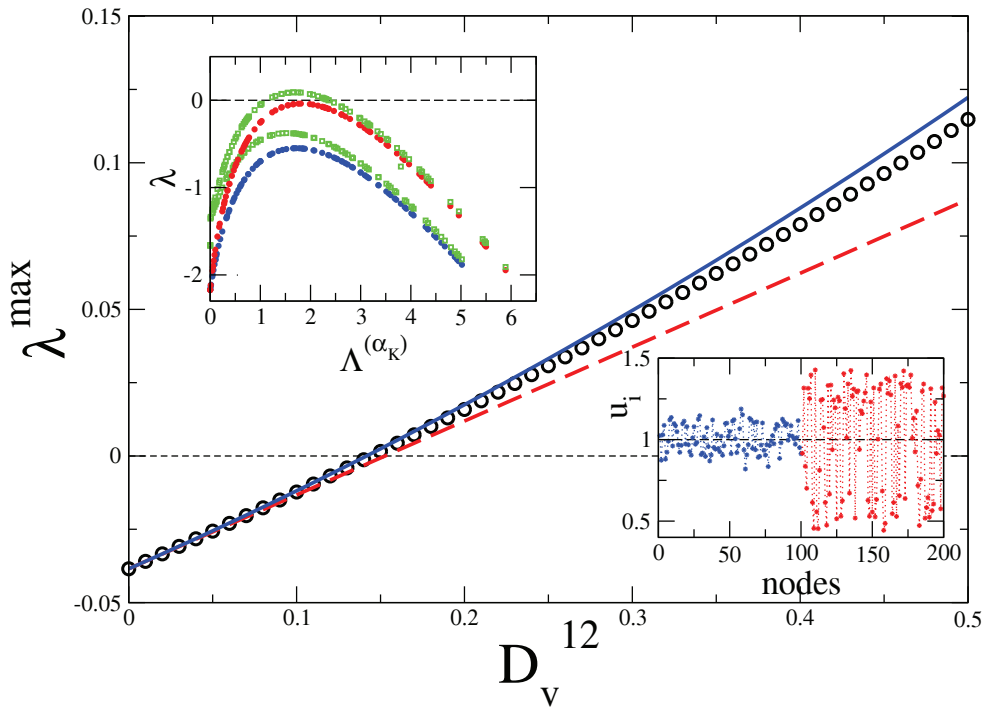


FIGURE 3.2: Main: λ^{max} is plotted versus D_v^{12} , starting from a condition for which the instability cannot occur when $D_v^{12} = 0$. Circles refer to a direct numerical computation of λ^{max} . The dashed (resp. solid) line represents the analytical solution as obtained at the first (resp. second) perturbative order. Upper inset: the dispersion relation λ is plotted versus the eigenvalues of the (single layer) Laplacian operators, L^1 and L^2 . The circles (resp. red and blue) stand for $D_u^{12} = D_v^{12} = 0$, while the squares (green) are analytically calculated from (3.3), at the second order, for $D_u^{12} = 0$ and $D_v^{12} = 0.5$. The two layers of the multiplex have been generated as Watts-Strogatz (WS) [9] networks with probability of rewiring p respectively equal to 0.4 and 0.6. The parameters are $b = 8, c = 17, D_u^1 = D_u^2 = 1, D_v^1 = 4, D_v^2 = 5$. Lower inset: asymptotic concentration of species u as function of the nodes index i . The first (blue) $\Omega = 100$ nodes refer to the network with $p = 0.4$, the other Ω (red) to $p = 0.6$.

Interestingly, the dual scenario is also possible. Assign the parameters so that the system is unstable (on at least one of the layers), in the decoupled setting $D_v^{12} = 0$. Hence, $\lambda_0^{max} > 0$, as displayed in the main panel of Figure 3.3. Patterns can therefore develop on one of the networks that define the multiplex (see unperturbed dispersion relation as plotted in the inset of Figure 3.3). The instability is eventually lost for a sufficiently large value of the inter-layer diffusion constant $D^{12} = D_u^{12} = D_v^{12}$. In other words, the interference between layers can dissolve the patterns. The perturbative calculation that we have developed provides, also in this case, accurate estimates of λ^{max} as function of D^{12} . The two branches of the dispersion relation shift downward as shown in the inset of Figure 3.3.

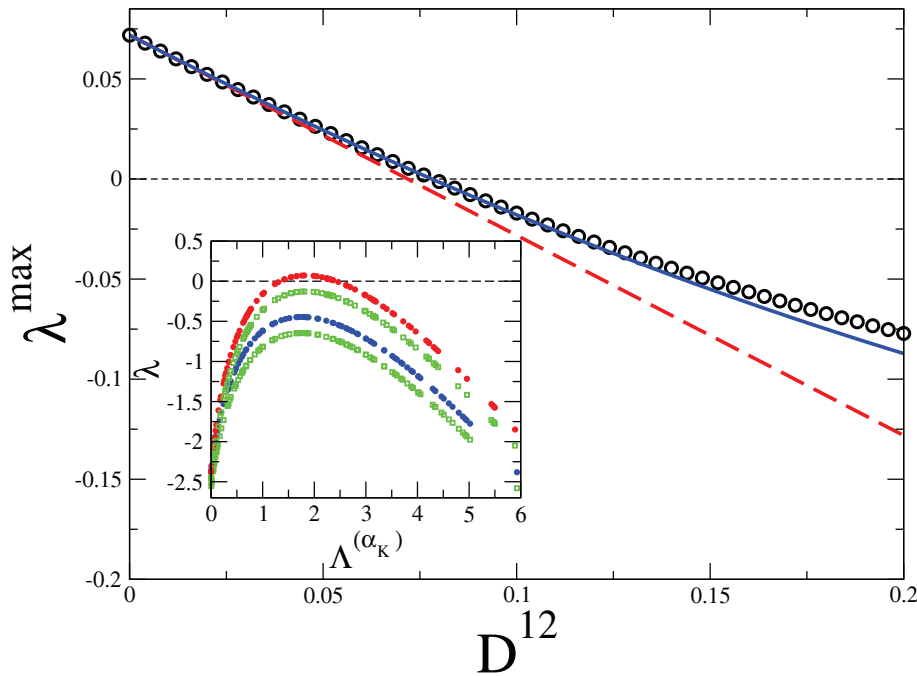


FIGURE 3.3: Main: λ^{max} is plotted versus $D^{12} \equiv D_v^{12} = D_u^{12}$, starting from the value $D^{12} = 0$ for which the instability can occur. Circles refer to a direct numerical computation of λ^{max} . The dashed (resp. solid) line represents the analytical solution as obtained at the first (resp. second) perturbative order. Inset: the dispersion relation λ is plotted versus the eigenvalues of the (single layer) Laplacian operators, L^1 and L^2 . The circles (resp. red and blue) stand for $D_u^{12} = D_v^{12} = 0$, while the squares (green) are analytically calculated from (3.3), at the second order, for $D_u^{12} = D_v^{12} = 0.2$. The two layers of the multiplex have been generated as Watts-Strogatz (WS) networks with probability of rewiring p respectively equal to 0.4 and 0.6. The parameters are $b = 8, c = 16.2, D_u^1 = D_u^2 = 1, D_v^1 = 4, D_v^2 = 5$.

3.4 Conclusions

Summing up we have developed a consistent theory of patterns formation for a reaction-diffusion system defined upon a stratified multiplex network. The analysis has been here carried out for a two species model, defined on a two layers multiplex. The methodology employed, as well as our main conclusions, readily extend to the general framework where s species are mutually interacting, while diffusing across a K levels multiplex whose layers can have arbitrary network topologies. The interference among layers can instigate collective patterns, which are instead lacking in the corresponding uncoupled scenario. Patterns can also evaporate due to the couplings among distinct levels. Conditions for the critical strength of the coupling constant are given and tested by direct numerical inspection. The hierarchical organization of the embedding space plays therefore a role of paramount importance, so far unappreciated, in seeding the patterns that we see in nature. It is also worth emphasising that novel control strategies could be in principle devised which exploit the mechanisms here characterized. These potentially interest a large plethora of key applications, which range from the control of the epidemic spreading, to the prevention of the failure of electric networks, passing through wildlife habitat restorations.

Chapter 4

Stochastic pattern formation theory: the case of one-diffusing species

4.1 Introduction

Reaction-diffusion systems are generally studied by resorting to deterministic mathematical models. The continuum concentrations of the interacting species is hence monitored over space and in time. As opposed to this strategy, one can develop an individual based description of the scrutinized dynamics, which effectively accounts for the inherent discreteness of the system. Stochastic contributions, stemming from finite size corrections, can thus modify the idealized mean-field picture and occasionally return alternative scenarios to interpret available data.

In a series of recent publications, the effect of the intrinsic noise was indeed shown to create stochastic patterns, in a region of the parameters for which macroscopically ordered structures do not occur. When the deterministic dynamics predicts a stable homogeneous state, the stochastic component can amplify via a resonant mechanism, giving birth to spatially organized patterns, also termed stochastic Turing patterns [17, 18, 54–56]. The effect of finite size fluctuations can be characterized with numerical simulations, but also analytically with Linear Noise Approximation (LNA) techniques, such as van Kampen system size expansion. This allows to expand the governing master equation, which accounts for the role of demographic fluctuations. At the first order of the expansion, the deterministic mean-field model is obtained, while the second order contributions form an equation for the stochastic fluctuations.

As previously discussed, the majority of studies devoted to the Turing instability consider two, mutually interacting, species. More specifically, and following the customarily accepted paradigm, one species activates the production of the other, this latter acting through an inhibitor feedback. Systems of three [57] simultaneously diffusing species have been also considered and shown to display a rich zoology of possible patterns and instabilities. Patterns can also develop if only one species is allowed to diffuse in the embedding medium, provided the system is composed of at least three coupled species [22]. In contrast, it is well known [22] that two species systems where only one species can migrate, cannot undergo Turing instability. This observation was made quantitatively in Chapter 1, where we did prove that, over a continuum support, the Turing instability cannot take place for reaction-diffusion models with two interacting species of which only one is allowed to diffuse [22]. If space is instead discrete, Turing like pattern can in principle take place, but only if the non diffusing species acts as a self-activator. As we shall here demonstrate, accounting for the intrinsic finite size fluctuations allows one to obtain a more complex landscape of possible instabilities. This chapter aims at elaborating along these lines, by considering the generalized concept of stochastically driven patterns.

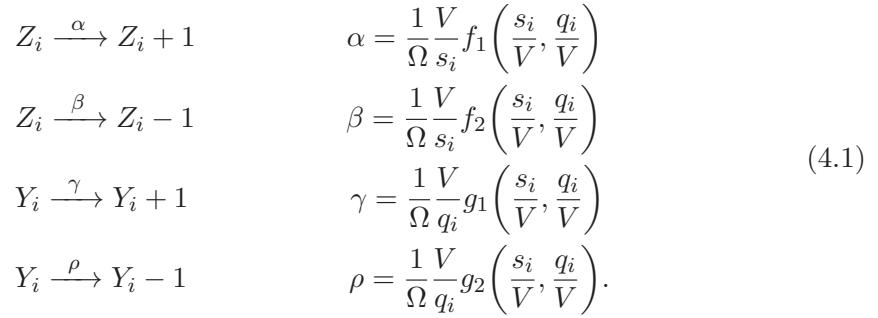
The chapter is organized as follows. In the next section we introduce the stochastic birth and death model that we shall use as a reference case study. The model is completely general and the reaction rates are assumed to depend on the species concentration, via generic non linear functions. Then, in Section 4.3, we first derive the mean-field deterministic limit: the only request that we shall put forward has to do with the existence of a stable fixed point for the aspatial mean-field system. We then proceed to derive the Fokker-Planck equation that describes the fluctuations. From this, in Section 4.4, we calculate the power spectrum of fluctuations, and find the mathematical conditions for the emergence of stochastically driven patterns. In Section 4.5 we turn to considering a particular non-linear model, so to verify the correctness of our predictions. Finally, in Section 4.6 we sum up and conclude. A synthetic discussion on the theory of stochastic processes is presented in the annexed Appendix A.

4.2 The Model and its Master Equation

The system that we are going to study is a general two species birth-death model, in which one of the species diffuses. As already mentioned, we assume the physical space to be partitioned in Ω patches of linear size a , and label with V their carrying capacity ¹. The integer index i runs from 1 to Ω and identifies the cell to which the species belong.

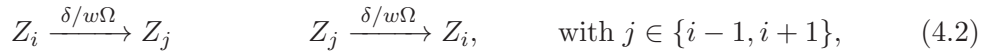
¹For the sake of simplicity, and without losing generality we will set $a = 1$ in the following.

Label the two species Z and Y and assume the following chemical reaction scheme:



We indicated as s_i the number of elements of species Z and with q_i the number of elements of species Y in the cell i . Moreover, we require that f_1, f_2, g_1, g_2 are sufficiently regular functions of the discrete number concentrations s_i/V and q_i/V .

We assume that only Z diffuses with a diffusion coefficient δ , and therefore write



where, in general, w is the number of neighboring cells of a given cell i and, therefore, $w = 2$ in the present one-dimensional case. A state of the system is characterized by two vectors, respectively $\vec{s} = (s_1, s_2, \dots, s_\Omega)$ and $\vec{q} = (q_1, q_2, \dots, q_\Omega)$. It is worth emphasizing that the model is completely general: virtually any system composed by two species, one of each diffusing, can be cast in the form introduced above, upon a proper choice of the functions f_1, f_2, g_1, g_2 .

We then turn to write down the master equation that governs the dynamics of the system. The reader can refer to the Appendix A for an introduction on the stochastic modeling techniques here employed. To this end we need to calculate the transition probability associated with each reaction:

$$\begin{aligned}
 T(s_i + 1, q_i | s_i, q_i) &= \alpha \frac{s_i}{V} \\
 T(s_i - 1, q_i | s_i, q_i) &= \beta \frac{s_i}{V} \\
 T(s_i, q_i + 1 | s_i, q_i) &= \gamma \frac{q_i}{V} \\
 T(s_i, q_i - 1 | s_i, q_i) &= \rho \frac{q_i}{V} \\
 T(s_i + 1, s_j - 1 | s_i, s_j) &= \frac{\delta}{\Omega} \frac{s_j}{wV} \\
 T(s_i - 1, s_j + 1 | s_i, s_j) &= \frac{\delta}{\Omega} \frac{s_i}{wV}.
 \end{aligned}$$

By introducing the following ‘‘step operators’’:

$$\varepsilon_{s_i}^\pm f(\vec{s}, \vec{q}) = f(\dots, s_i \pm 1, \dots, \vec{q}), \quad \varepsilon_{q_i}^\pm f(\vec{s}, \vec{q}) = f(\vec{s}, \dots, q_i \pm 1, \dots),$$

the master equation reads:

$$\begin{aligned}
\frac{d}{dt}P(\vec{s}, \vec{q}, t) &= \sum_{i=1}^{\Omega} \left[(\varepsilon_{s_i}^+ - 1) T(s_i - 1, q_i | s_i, q_i) + (\varepsilon_{s_i}^- - 1) T(s_i + 1, q_i | s_i, q_i) \right. \\
&\quad \left. + (\varepsilon_{q_i}^+ - 1) T(s_i, q_i - 1 | s_i, q_i) + (\varepsilon_{q_i}^- - 1) T(s_i, q_i + 1 | s_i, q_i) \right] P(\vec{s}, \vec{q}, t) \\
&\quad + \sum_{i=1}^{\Omega} \sum_{j \in \{i-1, i+1\}} \left[(\varepsilon_{s_i}^+ \varepsilon_{s_j}^- - 1) T(s_i - 1, s_j + 1 | s_i, s_j) \right. \\
&\quad \left. + (\varepsilon_{s_i}^- \varepsilon_{s_j}^+ - 1) T(s_i + 1, s_j - 1 | s_i, s_j) \right] P(\vec{s}, \vec{q}, t)
\end{aligned} \tag{4.3}$$

where, in accordance with our assumption of periodic boundary conditions, we adopt a periodic convention for the indices out of the set $\{1, \dots, \Omega\}$.

4.2.1 The Linear Noise Approximation (LNA) method

The master equation is difficult to handle analytically. To progress with the analysis we perform a Linear Noise Approximation (LNA) technique which is based in the van Kampen system size expansion, a perturbative calculation that introduces, by an ansatz, the following change of variables in the master equation:

$$\frac{s_i}{V} = \phi_i + \frac{\xi_i}{\sqrt{V}}, \quad \frac{q_i}{V} = \psi_i + \frac{\eta_i}{\sqrt{V}}. \tag{4.4}$$

The number density s_i/V splits into two independent contributions: ϕ_i stands for the deterministic (mean-field) concentration as measured in correspondence of the site i , and ξ_i is a stochastic variable that quantifies the fluctuation that perturbs the mean-field solution ϕ_i . Similar considerations apply to q_i/V . The factor $1/\sqrt{V}$ takes into account the finite volume of the system. In the limit for infinite systems size, the fluctuations can be neglected and the stochastic system as formulated above converges to its deterministic analogue. When working at finite V , stochastic fluctuations are important. The role of fluctuations can be quantitatively studied by implementing the aforementioned perturbative analysis, the van Kampen expansion [58], which assumes the amplitude factor $1/\sqrt{V}$ to act as a small parameter. To this end we introduce the van Kampen hypothesis into the master equation and split the contributions of order $1/\sqrt{V}$ and $1/V$, to respectively obtain the mean-field equation and Fokker-Planck equation. To carry out the calculation explicitly one needs to expand the functions f_1, f_2, g_1, g_2 with respect to the small parameter $1/\sqrt{V}$. As a representative example, we consider f_1 and obtain:

$$f_1 \left(\phi_i + \frac{\xi_i}{\sqrt{V}}, \psi_i + \frac{\eta_i}{\sqrt{V}} \right) \approx f_1(\phi_i, \psi_i) + \frac{1}{\sqrt{V}} \frac{\partial f_1}{\partial \phi_i}(\phi_i, \psi_i) \xi_i + \frac{1}{\sqrt{V}} \frac{\partial f_1}{\partial \psi_i}(\phi_i, \psi_i) \eta_i + \dots \tag{4.5}$$

where the derivatives are evaluated at $\xi_i = 0, \eta_i = 0$. Similar results hold for f_2, g_1 and g_2 .

Let us introduce the new distribution

$$\Pi(\xi_i, \eta_i, t) = P(s_i(\phi_i(t), \xi_i), q_i(\psi_i(t), \eta_i), t), \quad (4.6)$$

where $s_i(\phi_i(t), \xi_i)$ and $q_i(\psi_i(t), \eta_i)$ are given by (4.4). Inserting into the master equation, and expanding the step operators to second order, one eventually obtains

$$\sum_{i=1}^{\Omega} \frac{\partial \Pi}{\partial t} - \frac{\partial \Pi}{\partial \xi_i} \sqrt{V} \phi_i - \frac{\partial \Pi}{\partial \eta_i} \sqrt{V} \psi_i = [A + B + C] \Pi \quad (4.7)$$

where the contributions A, B, C take the following form:

$$A = \frac{1}{\Omega} \sum_{i=1}^{\Omega} \left\{ \frac{1}{\sqrt{V}} \left[(f_2 - f_1) \frac{\partial}{\partial \xi_i} \right] + \frac{1}{V} \left[\frac{\partial}{\partial \xi_i} \left(\frac{\partial f_2}{\partial \phi_i} - \frac{\partial f_1}{\partial \phi_i} \right) \xi_i + \frac{\partial}{\partial \xi_i} \left(\frac{\partial f_2}{\partial \psi_i} - \frac{\partial f_1}{\partial \psi_i} \right) \eta_i + \frac{1}{2} (f_1 + f_2) \frac{\partial^2}{\partial \xi_i^2} \right] \right\},$$

$$B = \frac{1}{\Omega} \sum_{i=1}^{\Omega} \left\{ \frac{1}{\sqrt{V}} \left[(g_2 - g_1) \frac{\partial}{\partial \eta_i} \right] + \frac{1}{V} \left[\frac{\partial}{\partial \eta_i} \left(\frac{\partial g_2}{\partial \phi_i} - \frac{\partial g_1}{\partial \phi_i} \right) \xi_i + \frac{\partial}{\partial \eta_i} \left(\frac{\partial g_2}{\partial \psi_i} - \frac{\partial g_1}{\partial \psi_i} \right) \eta_i + \frac{1}{2} (g_1 + g_2) \frac{\partial^2}{\partial \eta_i^2} \right] \right\},$$

$$C = \frac{\delta}{w\Omega} \sum_{i=1}^{\Omega} \sum_{j \in \{i-1, i+1\}} \left\{ \frac{1}{\sqrt{V}} \left[\left(\frac{\partial}{\partial \xi_i} - \frac{\partial}{\partial \xi_j} \right) \phi_i + \left(\frac{\partial}{\partial \xi_j} - \frac{\partial}{\partial \xi_i} \right) \phi_j \right] + \frac{1}{V} \left[\left(\frac{\partial}{\partial \xi_i} - \frac{\partial}{\partial \xi_j} \right) \xi_i + \left(\frac{\partial}{\partial \xi_j} - \frac{\partial}{\partial \xi_i} \right) \xi_j + \frac{1}{2} \left(\frac{\partial^2}{\partial \xi_i^2} + \frac{\partial^2}{\partial \xi_j^2} - 2 \frac{\partial}{\partial \xi_i} \frac{\partial}{\partial \xi_j} \right) (\phi_i + \phi_j) \right] \right\}.$$

4.3 Equations for the mean-field and the fluctuations

Introducing the rescaled time variable $\tau \rightarrow t/\Omega V$, we obtain from (4.7) at the order $1/\sqrt{V}$ the following system of ordinary differential equations for the mean-field concentrations ϕ_i and ψ_i :

$$\begin{cases} \dot{\phi}_i = f_1(\phi_i, \psi_i) - f_2(\phi_i, \psi_i) + \delta \Delta \phi_i \\ \dot{\psi}_i = g_1(\phi_i, \psi_i) - g_2(\phi_i, \psi_i) \end{cases} \quad (4.8)$$

where $\Delta = (\phi_{i+1} - 2\phi_i + \phi_{i-1})$, the discrete Laplacian. To proceed in the analysis we suppose that the homogeneous system:

$$\begin{cases} \dot{\phi}_i = f_1(\phi_i, \psi_i) - f_2(\phi_i, \psi_i) \equiv f(\phi_i, \psi_i) \\ \dot{\psi}_i = g_1(\phi_i, \psi_i) - g_2(\phi_i, \psi_i) \equiv g(\phi_i, \psi_i) \end{cases} \quad (4.9)$$

admits a fixed stable point $(\hat{\phi}, \hat{\psi})$. Notice that system (4.8), derived from a microscopic stochastic formulation, coincides with the general mean-field model considered in Chapter 1.

The Fokker Planck equation that describes the dynamics of the fluctuations is obtained by considering the terms proportional to $1/V$ in the master equation and reads as follows:

$$\frac{\partial}{\partial \tau} \Pi = \sum_{i=1}^{\Omega} \left(- \sum_{r=1}^2 \frac{\partial}{\partial \zeta_{r,i}} \left(\sum_{m=1}^2 \mathcal{J}_{rm,i} \zeta_{m,i} \Pi \right) + \frac{1}{2} \sum_{r,l=1}^2 \sum_{j=i-1}^{i+1} \frac{\partial}{\partial \zeta_{l,i}} \frac{\partial}{\partial \zeta_{r,j}} \left(\mathcal{B}_{rl,j}^{(i)} \Pi \right) \right). \quad (4.10)$$

Let us indicate as $\vec{\zeta}_i = (\zeta_{1,i}, \zeta_{2,i})$ the vector (ξ_i, η_i) in (4.10). The 2×2 matrices $\mathcal{J}_i = \mathcal{J}_{rm,i}$ are given by

$$\mathcal{J}_i = \begin{pmatrix} \frac{\partial f_1}{\partial \phi_i} - \frac{\partial f_2}{\partial \phi_i} + \delta \Delta & \frac{\partial f_1}{\partial \psi_i} - \frac{\partial f_2}{\partial \psi_i} \\ \frac{\partial g_1}{\partial \phi_i} - \frac{\partial g_2}{\partial \phi_i} & \frac{\partial g_1}{\partial \psi_i} - \frac{\partial g_2}{\partial \psi_i} \end{pmatrix} \quad (4.11)$$

and the three-vectors $\mathcal{B}_{rl}^{(i)}$ are given by

$$\begin{aligned} \mathcal{B}_{11}^{(i)} &= (-\delta(\phi_i + \phi_{i-1}), \delta(\phi_{i-1} + 2\phi_i + \phi_{i+1}) + f_1(\phi_i, \psi_i) + f_2(\phi_i, \psi_i), -\delta(\phi_i + \phi_{i+1})) \\ \mathcal{B}_{12}^{(i)} &= \mathcal{B}_{21}^{(i)} = (0, 0, 0), \quad \mathcal{B}_{22}^{(i)} = (0, g_1(\phi_i, \psi_i) + g_2(\phi_i, \psi_i), 0). \end{aligned} \quad (4.12)$$

Note that, in the above expressions, the indices r and l label the species while the indices i and j refer to the cells. The matrix \mathcal{J}_i is the Jacobian matrix of $(\phi_i, \psi_i) \mapsto (f_1 - f_2, g_1 - g_2)$, modified with the inclusion of the spatial contribution represented by the discrete Laplacian.

Matrix \mathcal{B} can be cast in the more compact form:

$$\mathcal{B}_{rl,j}^{(i)} = (b_{rl}^{(0)} \delta_{i-j,0} + b_{rl}^{(1)} \delta_{|i-j|,1}) + b_{rl}^{(1)} \Delta \quad (4.13)$$

where:

$$b^{(0)} = \begin{pmatrix} 2\delta\hat{\phi} + f_1(\phi_i, \psi_i) + f_2(\phi_i, \psi_i) & 0 \\ 0 & g_1(\phi_i, \psi_i) + g_2(\phi_i, \psi_i) \end{pmatrix}$$

$$b^{(1)} = \begin{pmatrix} -\delta\phi_i & 0 \\ 0 & 0 \end{pmatrix}.$$

We are interested in studying the fluctuations around the fixed point, when the deterministic system is in a steady state, i.e. when $(\phi_i, \psi_i) \equiv (\hat{\phi}, \hat{\psi}), \forall i$. A powerful mean of investigation is the power spectrum of fluctuations, that allows us to resolve the typical spatio-temporal frequencies that are represented in the recorded signal. The analysis of the power spectrum is carried out in the next section.

4.4 Power Spectrum of fluctuations

The above Fokker-Planck equation is equivalent [58] to the Langevin equation:

$$\frac{d}{dt}\zeta_{r,i}(t) = \sum_{l=1}^2 \mathcal{J}_{rl,i}\zeta_{l,i}(t) + \lambda_{r,i}(t) \quad (4.14)$$

where $\lambda_{r,i}(t)$ is a stochastic contribution which satisfies the following relations:

$$\langle \lambda_{l,i}(t), \lambda_{r,i'}(t') \rangle = \mathcal{B}_{lr,|i-i'|} \delta(t-t'), \quad (4.15)$$

$$\langle \lambda_{l,i}(t) \rangle = 0. \quad (4.16)$$

and $\langle \cdot \rangle$ denotes expectation. Upon Fourier transform one gets:

$$-i\omega\tilde{\zeta}_{r,k}(\omega) = \sum_{l=1}^2 \tilde{\mathcal{J}}_{rl,k}\tilde{\zeta}_{l,k}(\omega) + \tilde{\lambda}_{r,k}(\omega) \quad (4.17)$$

where $(\tilde{\cdot})$ stands for the Fourier transform both in space and time. Notice that matrix $\tilde{\mathcal{J}}_i$ coincides with the matrix \mathcal{J}_i given in (4.11) where the discrete Laplacian Δ , is replaced by its Fourier transform $\tilde{\Delta}_k$. As previously remarked one gets:

$$\tilde{\Delta}_k = 2(\cos(k) - 1). \quad (4.18)$$

Define

$$\Phi_{rl,k}(\omega) = -i\omega\delta_{rl} - \tilde{\mathcal{J}}_{rl,k},$$

then the solution of (4.17) reads:

$$\tilde{\zeta}_{r,k}(\omega) = \sum_{l=1}^2 \Phi_{rl,k}^{-1}(\omega) \tilde{\lambda}_{r,k}(\omega). \quad (4.19)$$

The power spectrum of the stochastic variable $\zeta_{r,i}(t)$ is defined as:

$$P_r(k, \omega) = \langle |\tilde{\zeta}_{r,k}(\omega)|^2 \rangle. \quad (4.20)$$

Making use of condition (4.15) one gets:

$$P_r(k, \omega) = \langle |\tilde{\zeta}_{r,k}(\omega)|^2 \rangle = \sum_{l,p=1}^2 \Phi_{rl,k}^{-1}(\omega) \tilde{\mathcal{B}}_{lp,k} (\Phi^\dagger)_{rp,k}^{-1}(\omega). \quad (4.21)$$

By recalling expression (4.13) one gets:

$$\tilde{\mathcal{B}}_{lp,k} = (b_{lp}^{(0)} + 2b_{lp}^{(1)}) + b_{lp}^{(1)} \tilde{\Delta}_k, \quad (4.22)$$

which allows us to rewrite the power spectra in the form $P_r(k, \omega)$ [59, 60]:

$$P_Z(k, \omega) \equiv P_1(k, \omega) = \frac{C_{Z,k} + \tilde{\mathcal{B}}_{11,k} \omega^2}{(\omega^2 - \Omega_0^2)^2 + \Gamma^2 \omega^2}, \quad (4.23)$$

$$P_Y(k, \omega) \equiv P_2(k, \omega) = \frac{C_{Y,k} + \tilde{\mathcal{B}}_{22,k} \omega^2}{(\omega^2 - \Omega_0^2)^2 + \Gamma^2 \omega^2} \quad (4.24)$$

where the functions $C_{Z,k}$ and $C_{Y,k}$ are respectively defined:

$$C_{Z,k} = \tilde{\mathcal{B}}_{11,k} (\tilde{\mathcal{J}}_{22,k})^2 + \tilde{\mathcal{B}}_{22,k} (\tilde{\mathcal{J}}_{12,k})^2 - 2\tilde{\mathcal{B}}_{12,k} \tilde{\mathcal{J}}_{12,k} \tilde{\mathcal{J}}_{22,k}, \quad (4.25)$$

$$C_{Y,k} = \tilde{\mathcal{B}}_{22,k} (\tilde{\mathcal{J}}_{11,k})^2 + \tilde{\mathcal{B}}_{11,k} (\tilde{\mathcal{J}}_{21,k})^2 - 2\tilde{\mathcal{B}}_{12,k} \tilde{\mathcal{J}}_{21,k} \tilde{\mathcal{J}}_{11,k}$$

and

$$\Omega_0 = \sqrt{\det \hat{\mathcal{J}}_{rl,k}} \quad (4.26)$$

$$\Gamma = -\text{tr} \hat{\mathcal{J}}_{rl,k}. \quad (4.27)$$

In the above expression, the symbol $(\hat{\cdot})$ indicates that from hereon the matrices are evaluated at the fixed point $(\hat{\phi}, \hat{\psi})$; $(\tilde{\cdot})$ stands instead for the spatial Fourier transform.

As anticipated, we are interested in studying the presence of stochastic stationary patterns. We remember that stochastic Turing patterns [17, 18] are signaled by the presence of at least a peak for the power spectrum in the direction of k , the spatial wavenumber, for $\omega = 0$, where ω stands for the time frequency. We are therefore going to analyze the functions $P_Z(k, 0) \equiv P_1(k, 0)$ and $P_Y(k, 0) \equiv P_2(k, 0)$, which respectively reads:

$$P_Z(k, 0) = \frac{C_{Z,k}}{\Omega_0^4} = \frac{b_{22}(\mathcal{J}_{11} + \delta\tilde{\Delta})^2 + (b_{11} - 2\hat{\phi}\delta\tilde{\Delta})\mathcal{J}_{21}^2}{(\det \mathcal{J} + \mathcal{J}_{22}\delta\tilde{\Delta})^2} \quad (4.28)$$

$$P_Y(k, 0) = \frac{C_{Y,k}}{\Omega_0^4} = \frac{(b_{11} - 2\hat{\phi}\delta\tilde{\Delta})\mathcal{J}_{22}^2 + b_{22}\mathcal{J}_{12}^2}{(\det \mathcal{J} + \mathcal{J}_{22}\delta\tilde{\Delta})^2}, \quad (4.29)$$

where we have introduced:

$$b_{11} = f_1(\hat{\phi}, \hat{\psi}) + f_2(\hat{\phi}, \hat{\psi}), \quad (4.30)$$

$$b_{22} = g_1(\hat{\phi}, \hat{\psi}) + g_2(\hat{\phi}, \hat{\psi}). \quad (4.31)$$

To study the conditions that yield to one or more peaks, we need to calculate the power spectrum derivative. We make use of the notation $g(k) \equiv \delta\tilde{\Delta} = 2\delta(\cos k - 1)$ and obtain the following general expression:

$$\frac{dP_j(k, 0)}{dk} = \frac{g'(k)}{(\det \mathcal{J} + \mathcal{J}_{22}g(k))^3} \{B_j g(k) + C_j\} \quad \text{for } j \in \{Z, Y\}, \quad (4.32)$$

where B_j and C_j are defined as:

$$B_Z = 2\hat{\phi}\mathcal{J}_{22}^3 \quad (4.33)$$

$$C_Z = -2\mathcal{J}_{22} \left(b_{11}\mathcal{J}_{22}^2 + b_{22}\mathcal{J}_{12}^2 + \hat{\phi}\mathcal{J}_{22} \det \mathcal{J} \right) \quad (4.34)$$

$$B_Y = 2\mathcal{J}_{21}(-b_{22}\mathcal{J}_{12} + \hat{\phi}\mathcal{J}_{21}\mathcal{J}_{22}) \quad (4.35)$$

$$C_Y = -2\mathcal{J}_{21}(b_{22}\mathcal{J}_{11}\mathcal{J}_{12} + \hat{\phi}\mathcal{J}_{21} \det \mathcal{J} + b_{11}\mathcal{J}_{22}\mathcal{J}_{21}). \quad (4.36)$$

Recall that \mathcal{J}_{ij} are the entries of the Jacobian matrix of system $(\phi_i, \psi_i) \mapsto (f_1 - f_2, g_1 - g_2)$ and b_{ij} are given by eqs. (4.31).

We observe that $k = 0$ and $k = \pi$ are always stationary points of P_j . In fact $g'(k) = -2\delta \sin(k)$ is null if $k = 0, \pi$. To have additional stationary points of P_j , one should require the quantity $B_j g(k) + C_j$ to vanish. This implies:

$$\cos(k) = 1 - \frac{C_j}{2\delta B_j}.$$

As $\cos(k) \in [-1, 1]$, it is necessarily the case that:

$$0 \leq \frac{C_j}{2\delta B_j} \leq 2. \quad (4.37)$$

Then, the derivative of P_j can be zero in k if B_j and C_j have the same sign. We indicate as k_1 and k_2 , the stationary wavenumbers different from π .

There are only two possible cases for the existence of k_1 and k_2 :

(i) Existence condition of k_1, k_2

(a) $B_j, C_j > 0$ and $\delta \geq \frac{C_j}{4B_j}$,

(b) $B_j, C_j < 0$ and $\delta \geq \frac{|C_j|}{4|B_j|}$.

We are interested to know whether k_1 and k_2 correspond to maxima or minima of $P_j(k, 0)$. To achieve this goal we calculate the second derivative of $P_j(k, 0)$:

$$\frac{d^2}{dk^2} P_j(k, 0) = \frac{g''(k) (B_j g(k) + C_j) + B_j g'(k)^2}{(\det \mathcal{J} + \mathcal{J}_{22} g(k))^3} - \frac{3\mathcal{J}_{22} g'(k)^2 (B_j g(k) + C_j)}{(\det \mathcal{J} + \mathcal{J}_{22} g(k))^4}. \quad (4.38)$$

Remember that k_1 and k_2 are solution of $B_j g(k) + C_j = 0$. The expression of the second order derivative is therefore cast into the form:

$$\left. \frac{d^2}{dk^2} P_j(k, 0) \right|_{k=k_1, k_2} = \frac{B_j g'(k)^2}{(\det \mathcal{J} + \mathcal{J}_{22} g(k))^3}. \quad (4.39)$$

The nature of the stationary points k_1 and k_2 depends on the sign of both the denominator and B_j in (4.39). In particular, if we require that the points are maxima, or equivalently the second derivative in k_1 and k_2 has a negative sign, we must check one of the two following conditions:

(ii) Maximum conditions for points k_1, k_2

(a) $B_j < 0$ and $\det \mathcal{J} + \mathcal{J}_{22} g(k) \Big|_{k=k_1, k_2} > 0$,

(b) $B_j > 0$ and $\det \mathcal{J} + \mathcal{J}_{22} g(k) \Big|_{k=k_1, k_2} < 0$.

As anticipated we shall consider the case of a self-inhibitory non mobile species, which corresponds to requiring $\mathcal{J}_{22} < 0$. The denominator in (4.39) is then always positive, while $g(k)$ is by definition negative. Accordingly, the kind of stationary points k_1 and k_2 depend on the sign of B_j . In particular, for the condition of maximum (ii), B_j must be negative.

To characterize whether the other stationary points $0, \pi$ are maxima or minima, we

should again turn to evaluating the second derivatives for such choices of k . As $g'(0) = 0$, then equation (4.38) is:

$$\left. \frac{d^2}{dk^2} P_j(k, 0) \right|_{k=0} = \frac{g''(0) (B_j g(0) + C_j)}{(\det \mathcal{J} + \mathcal{J}_{22} g(\pi))^3} = \frac{-2\delta C_j}{(\det \mathcal{J} - 4\delta \mathcal{J}_{22})^3}. \quad (4.40)$$

Therefore $k = 0$ is a maximum, if one of the following conditions is true:

(iii) Maximum condition for $k = 0$

$$(a) \begin{cases} -2\delta C_j < 0 \\ (\det \mathcal{J} - 4\delta \mathcal{J}_{22}) > 0. \end{cases} \quad (b) \begin{cases} -2\delta C_j > 0 \\ (\det \mathcal{J} - 4\delta \mathcal{J}_{22}) < 0. \end{cases}$$

Since by assumption $\mathcal{J}_{22} < 0$, condition **(iii)(b)** cannot be met. This is because the quantity $\det \mathcal{J} - 4\delta \mathcal{J}_{22}$ is positive, as $\det \mathcal{J} > 0$ since we have assumed that $(\hat{\phi}, \hat{\psi})$ is a stationary stable fixed point. The nature of the stationary point $k = 0$ ultimately depends on the sign of C_j . If $C_j > 0$, it is a maximum point, while, if $C_j < 0$, it is a minimum.

Consider now $k = \pi$ and observe that $g'(\pi) = 0$. Equation (4.38) reads:

$$\left. \frac{d^2}{dk^2} P_j(k, 0) \right|_{k=\pi} = \frac{g''(\pi) (B_j g(\pi) + C_j)}{(\det \mathcal{J} + \mathcal{J}_{22} g(\pi))^3} = \frac{2\delta (-4\delta B_j + C_j)}{(\det \mathcal{J} - 4\delta \mathcal{J}_{22})^3}. \quad (4.41)$$

For having a maximum in $k = \pi$ one of the following conditions must be satisfied:

(iv) Maximum condition for $k = \pi$

$$(a) \begin{cases} -4\delta B_j + C_j < 0 \\ (\det \mathcal{J} - 4\delta \mathcal{J}_{22}) > 0. \end{cases} \quad (b) \begin{cases} -4\delta B_j + C_j > 0 \\ (\det \mathcal{J} - 4\delta \mathcal{J}_{22}) < 0. \end{cases}$$

Since $\mathcal{J}_{22} < 0$, the condition **(iii)(b)** is never satisfied: as already remarked, the term $\det \mathcal{J} - 4\delta \mathcal{J}_{22}$ is in fact always positive.

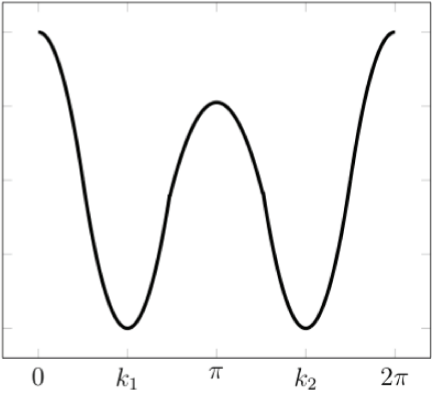
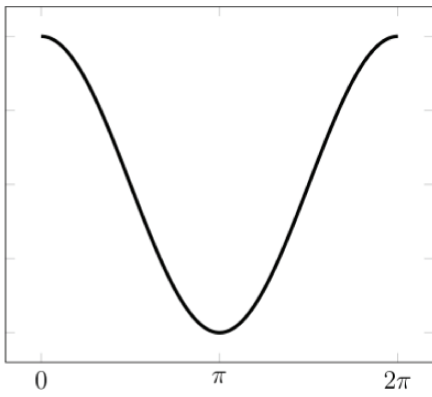
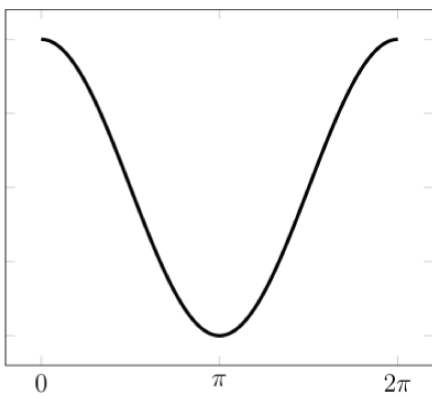
Notice that, if $k = \pi$ is a maximum the values $k = k_1$ and $k = k_2$ are minima. Otherwise if k_1 and k_2 are maxima, $k = \pi$ is a minimum. To show this, let us consider two different cases, respectively $B_j < 0$ and $B_j > 0$.

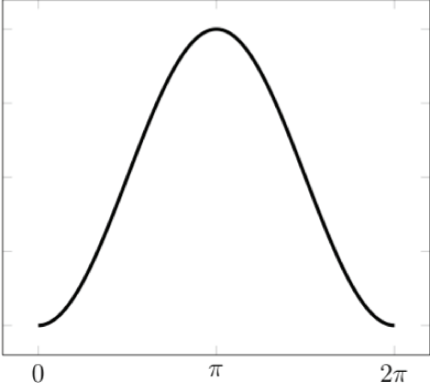
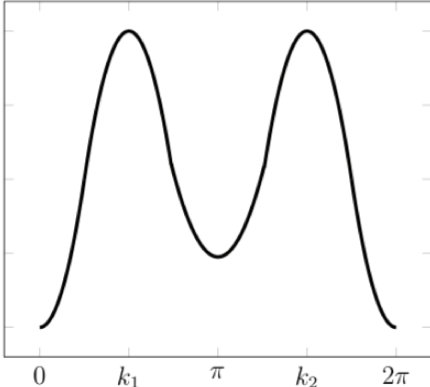
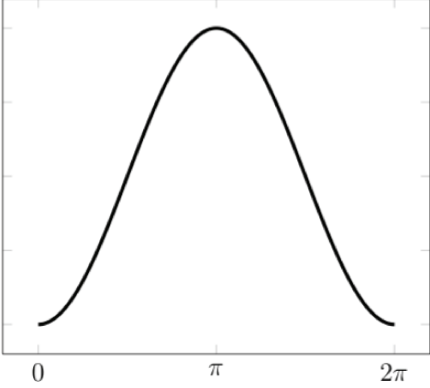
If $B_j < 0$ and, at the same time, condition **(i)** is satisfied, then k_1 e k_2 exist. In this case, the condition **(ii)(a)** guarantees that the stationary points else than π are maxima. Indeed, $B_j < 0$ and $(\det \mathcal{J} + \mathcal{J}_{22} g(k))|_{k=k_1, k_2}$ is positive. The condition for having a maximum in $k = \pi$, namely $-4\delta B_j + C_j < 0$, is in contradiction with **(i)**. If $B_j, C_j < 0$, in fact, we can write $-4\delta B_j + C_j < 0$. Taking into account the signs of the

quantities involved, it results $4\delta|B_j| - |C_j| < 0$, which implies $\delta < \frac{|C_j|}{4|B_j|}$, in disagreement with the condition **(i)**. In conclusion $k = \pi$ is necessarily a minimum.

Let us now turn to considering the case $B_j > 0$. To have the existence of k_1 and k_2 one must impose $C_j > 0$ and $\delta > \frac{C_j}{4B_j}$. Clearly, condition **(ii)** cannot be then satisfied and the two stationary points are minima. A maximum is instead found in $k = \pi$, as dictated by condition **(iv)**(b).

A summary of the above results is given in the Tables annexed below, where the different scenarios are highlighted depending on the sign of the reference quantities. We recall that our results have been derived under the hypothesis of discrete lattice spacing a (set to one in the calculations). Similar Tables can be in principle obtained for the case of a spatially continuum lattice, i.e. when $a \rightarrow 0$ and $g(k) \equiv -\delta k^2$. It can be however shown [59, 60] that the power spectrum of fluctuations scales with an amplitude prefactor proportional to a^d , d being the dimension of the embedding space ($d = 1$, in our case). Hence, in the limit $a \rightarrow 0$, fluctuations fade away and the stochastic patterning is non detectable. However, as remarked in [17], another continuum limit can be performed, starting from the same microscopic discrete formulation. One could in fact imagine to keep patch dimension to a constant, while sending to infinity both ω and the linear size of the physical space which hosts the system under scrutiny. This is indeed the case considered in [56]: working under this alternative scenario, fluctuations, and so the triggered patterns, are persistent also in the continuum limit. The choice of operating with patches of finite size, where microscopic constituents are supposed well mixed, and accounting for the possibility of jumping towards neighbor patches of a finite lattice, proves useful when modeling ecological systems [61], or in cellular biology, the space inside the membrane being partitioned in macro compartments and organelles [62], but also for studying chemical systems as e.g. the device introduced in [63].

$\mathcal{J}_{22} < 0$	$C_j > 0$
$B_j > 0$	<p data-bbox="651 264 1168 318">$\delta \geq \frac{C_j}{4B_j} \quad \exists \quad k_1 \text{ and } k_2 \text{ and are minima.}$</p> <p data-bbox="692 322 1126 353">Maxima are found in $k = 0, \pi, 2\pi$.</p> <div data-bbox="513 421 1040 815">  </div> <p data-bbox="545 904 1273 958">$\delta < \frac{C_j}{4B_j} \quad \nexists \quad k_1 \text{ and } k_2. \quad k = 0 \text{ and } k = 2\pi \text{ are maxima.}$</p> <p data-bbox="715 963 1104 994">A minimum is found in $k = \pi$.</p> <div data-bbox="513 1061 1040 1456">  </div>
$B_j < 0$	<p data-bbox="619 1563 1206 1594">$\nexists \quad k_1 \text{ and } k_2. \quad k = 0 \text{ and } k = 2\pi \text{ are maxima.}$</p> <p data-bbox="715 1608 1104 1639">A minimum is found in $k = \pi$.</p> <div data-bbox="513 1706 1040 2101">  </div>

$\mathcal{J}_{22} < 0$	$C_j < 0$
$B_j > 0$	<p data-bbox="533 275 1098 353">$\nexists k_1$ and k_2. $k = \pi$ is always a maximum. Two minima are found in $k = 0$ and $k = 2\pi$.</p> 
$B_j < 0$	<p data-bbox="395 902 1235 947">$\delta > \frac{C_j}{4B_j} \quad \exists k_1$ and k_2 and are maxima. $k = 0, \pi, 2\pi$ are minima.</p>  <p data-bbox="453 1496 1177 1585">$\delta < \frac{C_j}{4B_j} \quad \nexists k_1$ and k_2. $k = 0$ and $k = 2\pi$ are minima. A maximum is found in $k = \pi$.</p> 

4.5 A simple stochastic reaction–diffusion model

We have so far demonstrated that a stochastic amplification of spatial modes takes place for reaction-diffusion models, defined on a discrete lattice, in which only one species diffuses. Working in a general context, we elaborated on the conditions which lead to such stochastic pattern (termed stochastic Turing patterns in [18]), mediated by demographic noise.

As an application of the results discussed above, we consider a specific stochastic reaction-diffusion model, which can be cast in the form specified by (4.1) and (4.2). We choose in particular:

$$f_1\left(\frac{s_i}{V}, \frac{q_i}{V}\right) = \eta_1 \quad (4.42)$$

$$f_2\left(\frac{s_i}{V}, \frac{q_i}{V}\right) = \eta_2 \left(\frac{s_i}{V}\right)^p + \eta_3 \left(\frac{q_i}{V}\right)^n \quad (4.43)$$

$$g_1\left(\frac{s_i}{V}, \frac{q_i}{V}\right) = \eta_4 \quad (4.44)$$

$$g_2\left(\frac{s_i}{V}, \frac{q_i}{V}\right) = \eta_5 \left(\frac{s_i}{V}\right)^p + \eta_6 \left(\frac{q_i}{V}\right)^n \quad (4.45)$$

to define the microscopic reaction rates implicated in chemical equations (4.1). Here η_i are positive real numbers, while p and n are integers. We will set $p = 4$ and $n = 1$. Note that the proposed model has no specific applied interest: it is solely introduced for demonstrative purposes, aiming at testing the validity of the mathematical analysis developed above.

In the mean-field approximation, one gets:

$$\begin{cases} \frac{\partial \phi_i}{\partial t} = -\eta_2 \phi_i^p - \eta_3 \psi_i^n + \eta_1 + \delta \Delta \phi_i \\ \frac{\partial \psi_i}{\partial t} = -\eta_5 \phi_i^p - \eta_6 \psi_i^n + \eta_4. \end{cases} \quad (4.46)$$

To calculate homogeneous fixed point $(\hat{\phi}, \hat{\psi})$ of system (4.46) one needs to solve the following equations:

$$\begin{cases} -\eta_2 \hat{\phi}^p - \eta_3 \hat{\psi}^n + \eta_1 = 0 \\ -\eta_5 \hat{\phi}^p - \eta_6 \hat{\psi}^n + \eta_4 = 0 \end{cases} \quad (4.47)$$

which immediately yield:

$$\hat{\phi} = \left(\frac{\eta_1\eta_6 - \eta_3\eta_4}{\eta_2\eta_6 - \eta_3\eta_5} \right)^{1/p} \quad (4.48)$$

$$\hat{\psi} = \left(\frac{\eta_2\eta_4 - \eta_1\eta_5}{\eta_2\eta_6 - \eta_3\eta_5} \right)^{1/n}. \quad (4.49)$$

The parameters are to be in turn assigned so that the above fixed point is real and positive, a condition on which we shall return in the following. Furthermore, we require $(\hat{\phi}, \hat{\psi})$ to be a stable fixed point, so to match the theory prescriptions. The trace of the Jacobian matrix \mathcal{J} associated to the homogeneous (a-spatial) version of system (4.46) reads:

$$\text{tr } \mathcal{J} = - \left(\eta_2 p \hat{\phi}^{p-1} + \eta_6 n \hat{\psi}^{n-1} \right). \quad (4.50)$$

The trace is therefore always negative, for any choice of the parameters which returns a physically sound $(\hat{\phi}, \hat{\psi} > 0)$ homogeneous fixed point. For the fixed point to be stable, one should further impose:

$$\det \mathcal{J} = (\eta_2\eta_6 - \eta_3\eta_5) p n \hat{\phi}^{p-1} \hat{\psi}^{n-1} > 0. \quad (4.51)$$

This latter condition translates in:

$$\eta_3 < \left(\frac{\eta_2}{\eta_5} \right) \eta_6 \equiv \gamma_1 \eta_6, \quad (4.52)$$

where we brought into evidence the dependence on η_6 and η_3 , since they will later on act as control parameters. By using the above condition (4.52) into equations (4.48) the condition for positive concentrations $\hat{\phi}, \hat{\psi} > 0$ gives:

$$\eta_2\eta_4 - \eta_1\eta_5 \equiv \gamma_2 > 0 \quad (4.53)$$

$$\eta_3 < \left(\frac{\eta_1}{\eta_4} \right) \eta_6 \equiv \gamma_3 \eta_6. \quad (4.54)$$

The homogeneous fixed point $(\hat{\phi}, \hat{\psi})$ determined above exists and it is stable, provided conditions (4.52) and (4.53) are simultaneously met. Moreover, and as discussed in the first chapter, the spatially extended system (4.46) cannot experience a (deterministic)

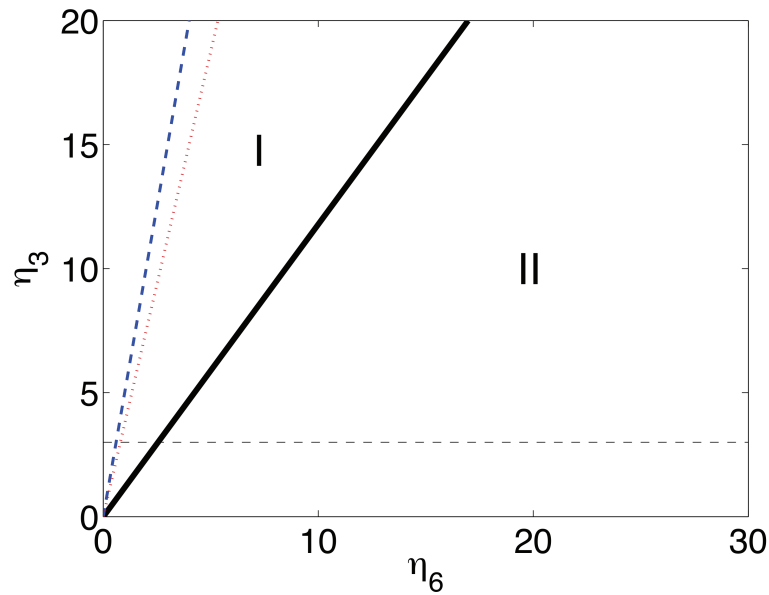


FIGURE 4.1: The plane (η_6, η_3) is partitioned into two regions. In region II, the power spectrum of fluctuations is predicted to display two peaks in, respectively, k_1 and k_2 . These are positions symmetric with respect to π . In region I the power spectrum has instead a maximum in $k = 0$. The parameters are $\eta_1 = 15$; $\eta_2 = 20$; $\eta_4 = 4$; $\eta_5 = 4$; $\delta = 42.9473$. With this choice, $\gamma_1 = 4$; $\gamma_3 = 20 > 0$; $\gamma_3 = 3.75$. The two lines which cross the origin represent respectively the two conditions $\eta_3 = \gamma_1 \eta_6$ (blue) and $\eta_3 = \gamma_3 \eta_6$ (red). Region I is delimited by this latter and the thick solid line which marks the transition to the adjacent region II. The horizontal dashed lines is drawn at $\eta_3 = 3$: the data reported in the following figures (4.2) and (4.3) refer to choices of the parameters that fall on such a line.

Turing instability since $g_\psi = -n\eta_6 \hat{\psi}^{n-1}$ is by definition negative. The homogeneous fixed point is hence a stable, although trivial attractor of the spatial deterministic model.

A different scenario holds instead when the stochastic version of the deterministic model (4.46) is considered. As we will show, it is in fact possible to assign the model parameters so as to generate a power spectrum of the stochastic fluctuations with two maxima for non trivial values of k_1 and k_2 , for $\omega = 0$. These maxima are interpreted as the signature of stochastic Turing patterns.

To this end we fix all parameters to nominal, arbitrarily chosen values, except for η_3 and η_6 which can be tuned. We will then adjust η_3 and η_6 so to match conditions (i) and (ii), as outlined in the preceding section. This results in region II of the parameter plane, as depicted in Figure 4.1. Conversely, in region I the power spectrum of fluctuations is predicted to display an isolated maximum for $k = 0$.

In Figure 4.2(b) we plot a two dimensional view of the theoretical power spectrum for a choice of the parameters (η_6, η_3) which falls in region II. The predicted profile is just displayed in the interval $k \in [0, \pi]$: a peak is present for a value of k smaller than π . A

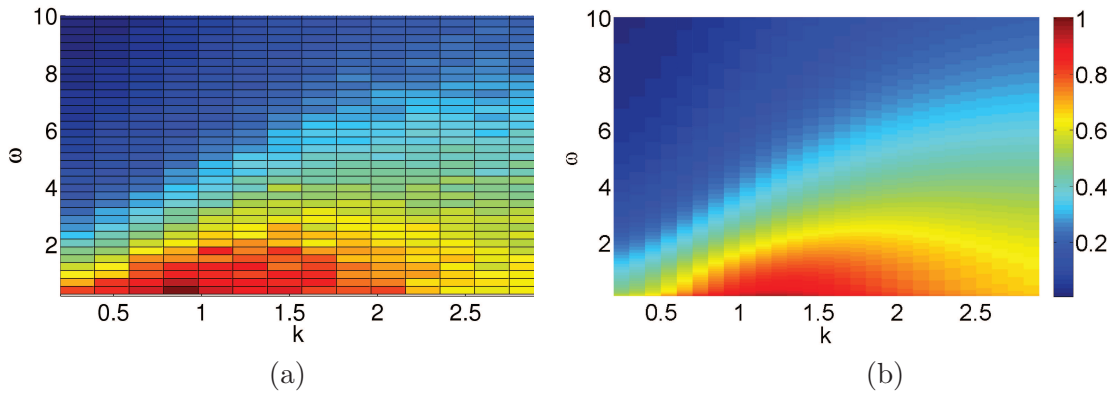


FIGURE 4.2: In panel (a), the numerical power spectrum of the fluctuations for species Z is represented, with an appropriate color code, in the plane (ω, k) , for a choice of the parameters that fall in region I of Figure 4.1. Specifically, we have set $\eta_6 = 25$, $\eta_3 = 3$. The other parameters are set to the values specified in the caption of Figure 4.1. Here $V = 5000$ and $\Omega = 32$. The numerical power spectrum is obtained by averaging over 200 independent realizations based on the Gillespie algorithm. A peak is found in the interval $[0, \pi]$. A symmetric maximum exists in $[\pi, 2\pi]$ (non displayed). In panel (b) the power spectrum calculated analytically is plotted and shown to agree with the numerical result. The power spectra are normalized so to have maximum equal to unit.

The color bar applies to both panels.

second, specular, peak is clearly found for $k > \pi$. The two maxima of the power spectrum occur for $\omega = 0$. They correspond therefore to stationary non homogeneous patterns. To validate the theory predictions we performed direct numerical simulations, by means of the Gillespie algorithm [64]. This is a Monte Carlo based scheme which produces realizations of the stochastic dynamics equivalent to those obtained from the governing master equation. The power spectrum calculated by averaging over a large collection of independent realizations of the stochastic dynamics is depicted in Figure 4.2(a), showing a good agreement with the corresponding theoretical profile. This confirms the validity of the analysis developed above, and summarized in the Tables presented above.

In Figure 4.3, the position of the maxima of the power spectrum of species Z is plotted as a function of the control parameter η_6 , while η_3 is set to the value that corresponds to the dashed horizontal line in Figure 4.1. This results in a bifurcation diagram from zone I to zone II. A similar plot can be obtained for the co-evolving species Y . The solid line stands for the theoretical predictions, which follows the results summarized in the Tables annexed above. A transition from zone I (one isolated peak) to zone II (two symmetric peaks) is predicted to occur at $\eta_6 \simeq 2.5$. The symbols in Figure 4.1 refer to the position of the power spectrum as obtained via direct simulations and confirms the correctness of the theoretical scenario.

A final comment is mandatory at this point. Fluctuations driven patterns are stochastic

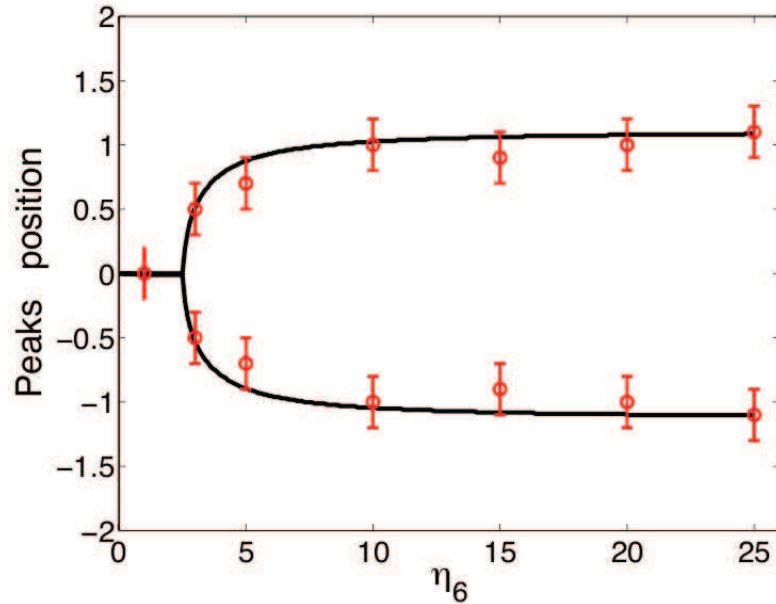


FIGURE 4.3: A bifurcation diagram is displayed, which exemplifies the transition from zone I to zone II. More specifically, the position of the peaks of the power spectrum of species Z is plotted as a function of the control parameter η_6 . Here, $\eta_3 = 3$, a value that corresponds to the horizontal dashed line in Figure 4.2. The solid line stands for the theory prediction, while the symbols refer to direct simulations of the stochastic dynamics. The simulations are averaged over 150 independent realizations. The error in the location of the peak is assumed as twice the spacing of the imposed wavelength mesh.

in nature: as such they are not stationary, unlike their deterministic analogue. Stochastic patterns continuously decay, while they are recreated by the effect of the noise [65]. In general, the noisy nature of the patterns makes them hard to detect by visual inspection. The emergence of a length scale become often clear only via a Fourier analysis. This is for instance the conclusion reached in [66] where stochastic simulations for the Schnakenberg kinetics [67] are carried out just outside the (deterministic) region of Turing order. On the other hand, patterns can possibly become more distinct depending on the simulated model, the dimensionality of the system ($1D$ vs. $2D$) and the structure (lattice vs. network) of the embedding space. For the Levin-Segel model [68] studied in two dimension [17], stochastic patterns are quite visible at the naked eye. Similarly, robust and rather distinct patterns are found when a stochastic reaction model of the Brusselator type [69] is defined on a network topology (see the following Chapter 5 and ref. [19]). Also, quasi-waves patterns found in [56] for a modified version of the Brusselator model with long range couplings, stand out rather clearly from one single realization of the stochastic dynamics. The search for the necessary ingredients that make stochastic pattern accessible at visual inspection, remains however an important and still open question that deserves to be further addressed. As concerns the model here investigated, striped patterns are seen when plotting the density in the space-time

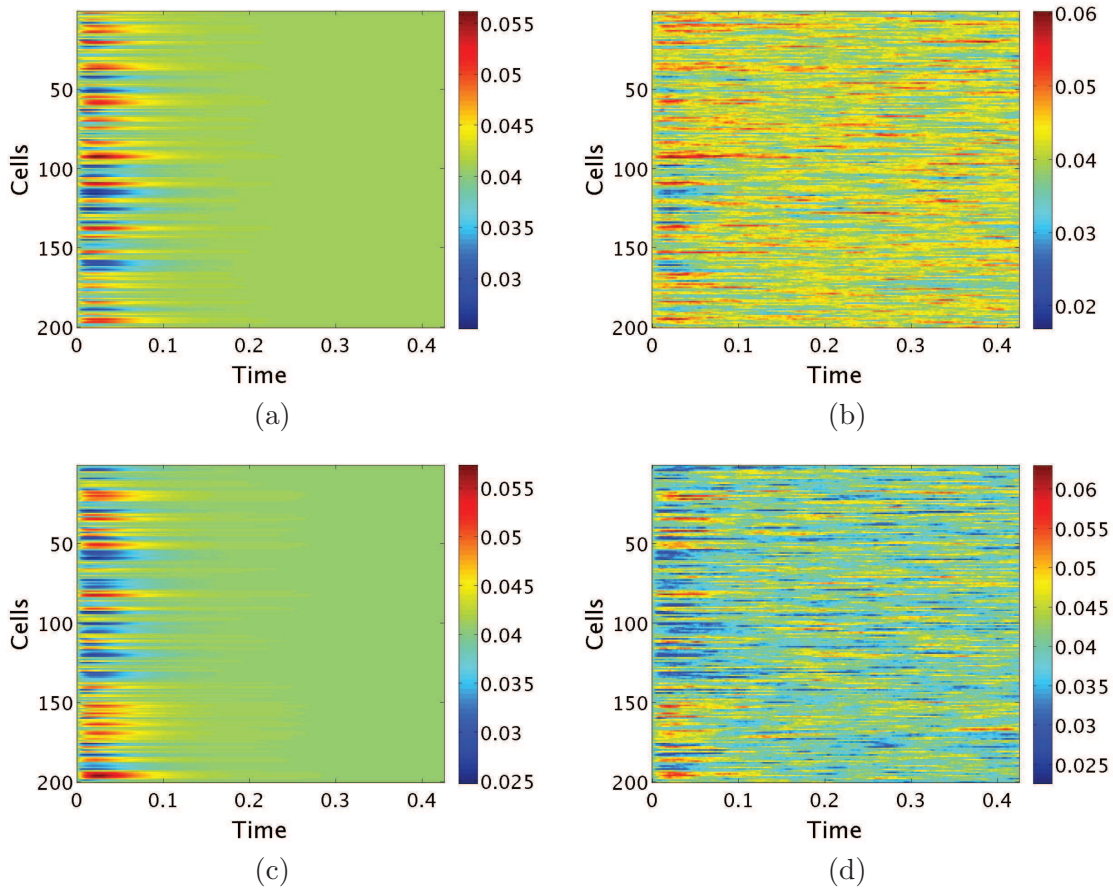


FIGURE 4.4: In panel (a), the time evolution of the mean field concentration of species Y is plotted. Initially, a random perturbation is imposed on the homogeneous fixed point. Fluctuations are rapidly washed out and the system converges to the stable homogenous solution. In panel (b), the result of a stochastic simulation is displayed. The number of stochastic iterations is set so to span the same time window of the deterministic solution depicted in panel (a). Striped horizontal patterns develop, signaling a degree of spatial order which is instead lacking in the corresponding mean-field picture. As explained in the main text, stochastic patterns decay, while being recreated at different locations. The stripes look therefore noisy, although still detectable by eye inspection. Calculating the power spectrum of the individual stochastic realization reported in panel (b) makes it possible to quantify the dominant spatial wavelength, which appears to be consistent with that predicted by the theory. Here $V = 10000$ and $\Omega = 200$. The choice of V has been roughly optimized so to reach the following compromise. V is taken sufficiently large so to mitigate the disruptive effect of noise. On the other hand, it is still moderately small for the finite size corrections to eventually matter. In panel (c) and (d) the same comparison is drawn for a different realization of the initial perturbation and for a distinct stochastic simulation.

plane. The stripes are noisy and intermittent but clearly detectable for an optimal choice of the system size V , see Figure 4.4(b). Notice that the initial fluctuations are instead quickly damped when operating under the mean field approximation. The deterministic system converges in fact to the deputed homogeneous solution, as demonstrated in Figure 4.4(b).

4.6 Conclusion

Reaction-diffusion models are deterministic in nature. They omit the stochastic contributions that need to be included when dealing with finite populations and, in this respect, represent an idealized approach to the modeling of the inspected phenomena. The classical, deterministic theory for the Turing instability requires that at least two species diffuse in a domain in which they are confined: the diffusion potentially leads to an instability in following a perturbation of a stable equilibrium of the homogeneous system. Conversely, if just one species is allowed to diffuse the Turing instability is always precluded, when the system is defined on a continuum support (see discussion in the first chapter). Working on a discrete lattice, Turing patterns can in principle develop, but just for a trivial choice of the most unstable wave number and limited to models that assume the non diffusing species to operate as a self-activator.

Beyond the deterministic viewpoint, the concept of stochastic Turing instability has been introduced in the literature [17, 18]: discrete systems, made of a large though finite number of constitutive entities (or equivalently bound to occupy a finite domain with a given carrying capacity), can generate stochastic order on a macroscopic scale, as follows a resonant mechanism which self-consistently amplifies the intrinsic demographic noise. Building on these ideas, we have considered here a general stochastic reaction-diffusion model, with just one diffusing species, and showed that spatial modes can spontaneously amplify also when the non mobile species has a self-inhibitory capability, i.e. a condition for which deterministic patterns are a priori excluded. General analytical conditions for the existence of the stochastically driven patterns are given. The predictions are tested numerically working with a simplified model that falls in the general class of systems for which the theory has been developed. The quantitative agreement observed between theory and simulations points to the validity of our analysis, which, we believe, could open up novel perspectives to tackle the problem of pattern formation beyond the classical deterministic picture.

Chapter 5

Stochastic patterns on a network

5.1 Introduction

As already remarked, the vast majority of studies devoted to investigating the emergence of Turing patterns use deterministic partial differential equations to model the reactions and diffusion of the constituents, which are hence characterized by continuous spatial distributions. In the first chapter, we discussed the extension of the Turing paradigm to systems defined on complex networks [11]. This is an important step forward [70], which could eventually shed novel light onto the mechanisms that drive self-organization on networks [71–73].

As discussed in the preceding chapter, Turing patterns have also been observed and analyzed in models with a finite number of constituents. In this case reaction-diffusion processes are amenable to individual-based models, which take into account the intrinsic discreteness of the system. Stochastic effects are therefore present, and ultimately stem from the finite size of the interacting populations.

At first sight it might appear surprising that stochastic effects are important in reaction-diffusion systems, which after all consist of a large number of constituents. However, the fluctuations due to the discreteness of these constituents can amplify through resonant effects and so yield macroscopically ordered patterns, both in time [74, 75] and in space [17, 18, 76]. Stochastic Turing patterns [18] (also termed quasi-Turing patterns [17]) can appear in a region of the parameter space for which the homogeneous fixed point is predicted to be stable from a deterministic linear stability analysis. Similarly, stochastic waves [56] have been observed in reaction-diffusion models defined on a regular lattice. Importantly, the effect of fluctuations arising from this discreteness of the populations of elementary constituents can not only be seen in numerical simulations,

but also analytically understood by expanding the governing master equation within the so-called Linear Noise Approximation (LNA) scheme, as we already discussed in Chapter 4.

In this chapter we report analytical progress by carrying out the LNA for systems in which the population is distributed over a set of nodes, which are connected to each other in some way. Each node hosts a large number of individuals, so this is a metapopulation model [77] — a collection of populations allowing some exchange between them. Examples are: in ecology, where individuals reside on patches and may migrate to other patches that are nearby [77]; in island models of evolutionary theory, where individuals carrying certain alleles may migrate to other islands [78]; in epidemiology, where the nodes are cities connected by commuters who carry disease [79] and in reaction kinetics, where the nodes are compartments in which chemical reactions take place [80]. Our aim is to formally extend the analysis of stochastic driven patterns to the relevant setting where the system is defined on a complex network.

More specifically, in the first part of the chapter, we shall consider a stochastic version of the Zhabotinsky model [24], introduced into a static scale-free network. This latter is created via the preferential attachment probability rule [7], as described in Chapter 1. The power spectrum of fluctuations is analytically calculated by developing and systematizing the LNA technique to network-based applications. A localized peak for the power spectrum signals the presence of stochastic travelling waves, a prediction that we confirm with stochastic simulations [64]. The power spectrum is calculated from a generalized Fourier transform, the standard plane waves found in a spatial context being replaced by the eigenvectors of the discrete Laplacian operator defined on the network. To benchmark theory and simulations, we have therefore implemented and tested a numerical routine which handles the generalized Fourier analysis. This is a diagnostic tool that could prove useful beyond the specific case study, by guiding the unbiased search for structured patterns on a network topology [81]. In the second part of the chapter we will turn to consider the Brusselator model modified with the inclusion of a non linear transport terms. The stochastic effects are in this case responsible for the emergence of stationary non homogeneous patterns, reminiscent of the Turing instability.

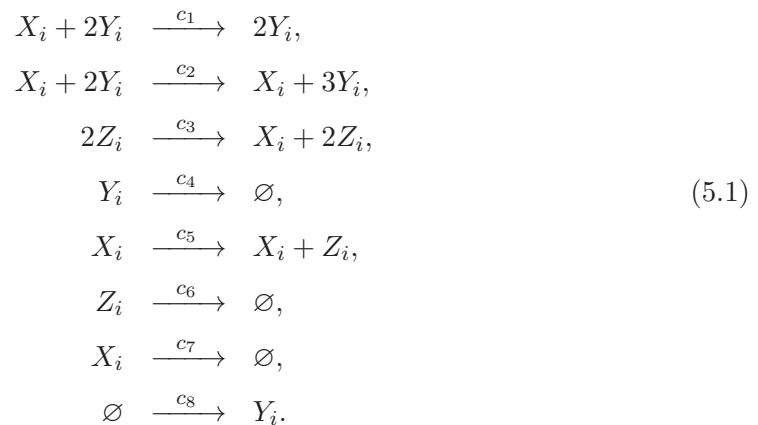
The chapter is organized as follows. In the next section we will introduce the Zhabotinsky model and discuss the basic steps of the LNA analysis on a graph. The linear stability analysis for the model in its deterministic limit is carried out and numerical simulations are performed to show that the deterministic wave manifests itself as a localized peak in the power spectrum, as obtained from the generalized Fourier transform. Then, we derive the power spectrum of fluctuations which points to the existence of travelling waves, seeded by inherent stochasticity, outside the region of deterministic instability.

Stochastic simulations confirm the validity of the theory. In Section 5.3, we consider a modified stochastic Brusselator model which yields stochastic Turing-like patterns. In the final Section we sum up and conclude.

5.2 Stochastic travelling waves case

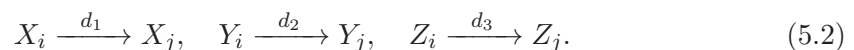
5.2.1 Model definition and the linear noise approximation (LNA)

The reaction scheme that we will investigate was introduced by Zhabotinsky et al. to study travelling waves arising from destabilization of a homogeneous state [24]. The scheme involves molecules of three chemical species: X , Y and Z — that we will also respectively call the first, second and third species. The molecules are placed on the nodes of a network composed of Ω nodes, each of which has a finite volume V . We label a molecule of species X located on the i -th node with X_i ; Y_i and Z_i are similarly defined. The number of molecules of type X_i , Y_i and Z_i are denoted by x_i , y_i and z_i , respectively. The Ω -dimensional vectors: $\mathbf{x} = (x_1, \dots, x_\Omega)$, $\mathbf{y} = (y_1, \dots, y_\Omega)$ and $\mathbf{z} = (z_1, \dots, z_\Omega)$, specify the state of the system. Within each node, the molecules interact through the following reaction scheme:



The reaction rates are denoted by c_1, c_2, \dots, c_8 . As explained in [24] they are all constant except c_7 that is given by $c_7 = c'_7 / (g + \frac{x_i}{V})$, with $g = 10^{-4}$.

The structure of the network is described by the $\Omega \times \Omega$ adjacency matrix, W . This is a symmetric matrix whose elements, W_{ij} , is equal to one if node i is connected to node j , and zero otherwise. The molecules can migrate between two connected nodes as specified by the diffusion reactions:



The constants d_1 , d_2 and d_3 are the diffusion coefficients.

The construction of a stochastic model proceeds by assigning a transition rate $\mathbb{T}(\mathbf{x}', \mathbf{y}', \mathbf{z}' | \mathbf{x}, \mathbf{y}, \mathbf{z})$ to each reaction. They indicate the probability per unit of time to transit from state $(\mathbf{x}, \mathbf{y}, \mathbf{z})$ to state $(\mathbf{x}', \mathbf{y}', \mathbf{z}')$. To lighten the notation, we only write the components of the vectors which refer to molecules that take part in a reaction in the transition rates. Invoking mass action, the transition rates associated with reactions (5.1) read [58]:

$$\begin{aligned}
 \mathbb{T}_1(x_i - 1 | x_i) &= c_1 \frac{x_i y_i^2}{V V^2}, & \mathbb{T}_5(z_i + 1 | z_i) &= c_5 \frac{x_i}{V}, \\
 \mathbb{T}_2(y_i + 1 | y_i) &= c_2 \frac{x_i y_i^2}{V V^2}, & \mathbb{T}_6(z_i - 1 | z_i) &= c_6 \frac{z_i}{V}, \\
 \mathbb{T}_3(x_i + 1 | x_i) &= c_3 \frac{z_i^2}{V^2}, & \mathbb{T}_7(x_i - 1 | x_i) &= c_7 \frac{x_i}{V}, \\
 \mathbb{T}_4(y_i - 1 | y_i) &= c_4 \frac{y_i}{V}, & \mathbb{T}_8(y_i + 1 | y_i) &= c_8.
 \end{aligned} \tag{5.3}$$

In a similar way the transition rates for the diffusion reactions (5.2) are given by:

$$\begin{aligned}
 \mathbb{T}_9(x_i - 1, x_j + 1 | x_i, x_j) &= d_1 \frac{x_i}{V}, \\
 \mathbb{T}_{10}(y_i - 1, y_j + 1 | y_i, y_j) &= d_2 \frac{y_i}{V}, \\
 \mathbb{T}_{11}(z_i - 1, z_j + 1 | z_i, z_j) &= d_3 \frac{z_i}{V}.
 \end{aligned} \tag{5.4}$$

As the dynamics is Markovian, the probability density function (PDF) that the system is in state $(\mathbf{x}, \mathbf{y}, \mathbf{z})$ at time t , $P(\mathbf{x}, \mathbf{y}, \mathbf{z}, t)$, satisfies the master equation:

$$\frac{\partial}{\partial t} P(\mathbf{x}, \mathbf{y}, \mathbf{z}, t) = \sum_{(\mathbf{x}', \mathbf{y}', \mathbf{z}' \neq \mathbf{x}, \mathbf{y}, \mathbf{z})} [\mathbb{T}(\mathbf{x}, \mathbf{y}, \mathbf{z} | \mathbf{x}', \mathbf{y}', \mathbf{z}') P(\mathbf{x}', \mathbf{y}', \mathbf{z}', t) - \mathbb{T}(\mathbf{x}', \mathbf{y}', \mathbf{z}' | \mathbf{x}, \mathbf{y}, \mathbf{z}) P(\mathbf{x}, \mathbf{y}, \mathbf{z}, t)]. \tag{5.5}$$

This is the fundamental equation that governs the dynamics of the system.

The LNA can be applied by carrying out the van Kampen expansion for the master equation [58]. As previously shown this method is used to approximate the master equation (5.5) by a deterministic system of ordinary differential equations — that describes the macroscopic evolution of the concentrations — together with a linear Fokker–Planck equation which characterizes the fluctuations around the macroscopic solution. This begins with changing variables from (x_i, y_i, z_i) to $(\xi_{1,i}, \xi_{2,i}, \xi_{3,i})$, where $i = 1, \dots, \Omega$:

$$\frac{x_i}{V} = \phi_i + \frac{\xi_{1,i}}{\sqrt{V}}, \quad \frac{y_i}{V} = \psi_i + \frac{\xi_{2,i}}{\sqrt{V}}, \quad \frac{z_i}{V} = \eta_i + \frac{\xi_{3,i}}{\sqrt{V}}. \tag{5.6}$$

The functions $\phi_i(t)$, $\psi_i(t)$ and $\eta_i(t)$ describe the concentrations of each chemical species in the deterministic limit, that is, obtained by letting $V \rightarrow \infty$. In this limit the system

is not subject to fluctuations. In the following the indexes i and j refer to the nodes of the network and range from 1 to Ω . The indexes r and s label the chemical species and range from one to three. Finally, the Ω -dimensional vectors, such as \mathbf{x} , \mathbf{y} and \mathbf{z} , are displayed in bold.

Master equations, such as (5.5), can be rewritten by making use of step operators, $\epsilon_{r,i}^\pm$, which represent the creation/destruction of a molecule of species r at node i . For instance, for species X , they act on a general function $f(\mathbf{x}, \mathbf{y}, \mathbf{z})$ by

$$\epsilon_{1,i}^\pm f(\dots, x_i, \dots, \mathbf{y}, \mathbf{z}) = f(\dots, x_i \pm 1, \dots, \mathbf{y}, \mathbf{z}). \quad (5.7)$$

The master equation (5.5) then reads:

$$\begin{aligned} \frac{\partial}{\partial t} P(\mathbf{x}, \mathbf{y}, \mathbf{z}, t) = & \sum_{i=1}^{\Omega} \left[(\epsilon_{1,i}^+ - 1) T_1(x_i - 1 | x_i) + (\epsilon_{2,i}^- - 1) T_2(y_i + 1 | y_i) + (\epsilon_{1,i}^- - 1) T_3(x_i + 1 | x_i) + \right. \\ & (\epsilon_{2,i}^+ - 1) T_4(y_i - 1 | y_i) + (\epsilon_{3,i}^- - 1) T_5(z_i + 1 | z_i) + (\epsilon_{3,i}^+ - 1) T_6(z_i - 1 | z_i) + (\epsilon_{1,i}^+ - 1) T_7(x_i - 1 | x_i) + \\ & (\epsilon_{2,i}^- - 1) T_8(y_i + 1 | y_i) + \sum_{j=1}^{\Omega} W_{ij} [(\epsilon_{1,i}^+ \epsilon_{1,j}^- - 1) T_9(x_i - 1, x_j + 1 | x_i, x_j) + (\epsilon_{2,i}^+ \\ & \left. \epsilon_{2,j}^- - 1) T_{10}(y_i - 1, y_j + 1 | y_i, y_j) + (\epsilon_{3,i}^+ \epsilon_{3,j}^- - 1) T_{11}(z_i - 1, z_j + 1 | z_i, z_j) \right] P(\mathbf{x}, \mathbf{y}, \mathbf{z}, t). \end{aligned} \quad (5.8)$$

We now apply the change of variable (5.6). In the new variables, the step operators admit an expansion in powers of V^{-1} [58]. The LNA corresponds to the truncation of the expansion at second order, namely:

$$\epsilon_{r,i}^\pm \approx 1 \pm \frac{1}{\sqrt{V}} \partial_{\xi_{r,i}} + \frac{1}{2V} \partial_{\xi_{r,i}}^2. \quad (5.9)$$

The left-hand side of Eq. (5.5) can be expressed in terms of the PDF of the new variables, $\Pi(\boldsymbol{\xi}_1, \boldsymbol{\xi}_2, \boldsymbol{\xi}_3, t) = P(\mathbf{x}(\boldsymbol{\phi}(t), \boldsymbol{\xi}_1), \mathbf{y}(\boldsymbol{\psi}(t), \boldsymbol{\xi}_2), \mathbf{z}(\boldsymbol{\eta}(t), \boldsymbol{\xi}_3), t)$. This implies that

$$\frac{\partial \Pi}{\partial t} = \partial_t \Pi - \sqrt{V} (\nabla_{\boldsymbol{\xi}_1} \Pi \cdot \partial_t \boldsymbol{\phi} + \nabla_{\boldsymbol{\xi}_2} \Pi \cdot \partial_t \boldsymbol{\psi} + \nabla_{\boldsymbol{\xi}_3} \Pi \cdot \partial_t \boldsymbol{\eta}). \quad (5.10)$$

In the above equation there are terms which are either $O(1)$ or $O(\sqrt{V})$. By contrast, the right-hand side of Eq. (5.8) contains $O(V^{-1/2})$ and $O(V^{-1})$ terms. They can be balanced by rescaling time by $\tau = t/V$. Collecting together the terms of the same order and setting their sum at each order to zero gives, at the leading order, the deterministic

system (5.11):

$$\begin{aligned}
\dot{\phi}_i &= -c_1\phi_i\psi_i^2 + c_3\eta_i^2 - c'_7\frac{\phi_i}{g + \phi_i} + d_1\sum_{j=1}^{\Omega}\Delta_{ij}\phi_j, \\
\dot{\psi}_i &= c_2\phi_i\psi_i^2 - c_4\psi_i + c_8 + d_2\sum_{j=1}^{\Omega}\Delta_{ij}\psi_j, \\
\dot{\eta}_i &= c_5\phi_i - c_6\eta_i + d_3\sum_{j=1}^{\Omega}\Delta_{ij}\eta_j.
\end{aligned} \tag{5.11}$$

Hereafter, a dot above a symbol indicates the time derivative taken with respect to the rescaled time, $\tau = t/V$. The symbol Δ_{ij} denotes the Laplacian operator:

$$\Delta_{ij} = W_{ij} - k_i\delta_{ij}, \tag{5.12}$$

where k_i is the connectivity of node i , $k_i = \sum_{j=1}^{\Omega} W_{ij}$. This form of the Laplacian operator [82] reflects our specific choice for the microscopic reaction rates (5.4). As previously discussed (see Chapter 1), other choices are possible which would yield modified Laplacians [83]. Working in the context of the proposed formulation, Δ_{ij} is symmetric, a feature of which we shall take advantage of when performing the generalized Fourier analysis described below.

For finite volume V , the system is subject to intrinsic noise; these fluctuations perturb the solutions of the deterministic model (5.11), which describes the dynamics of the model in the limit $V \rightarrow \infty$. Within the LNA, the fluctuations are Gaussian and given by a linear Fokker-Planck equation. Before turning to discuss the role played by stochastic fluctuations, we will start by focusing on the deterministic scenario. We will in particular derive the conditions under which self-organized patterns of the wave type emerge. The next subsection is devoted to this issue.

5.2.2 Pattern formation in the deterministic limit

The analysis of pattern formation for system (5.11) defined on a regular lattice in the continuum limit has been already carried out in [24]. Here, we review some of the results of [24], before moving on to discuss how the network affects the pattern formation. Throughout our analysis we have used a scale-free network generated with the Barabási-Albert preferential attachment algorithm [7], with Ω nodes and mean degree $\langle k \rangle$.

We first establish contact with the notation adopted in [24] by making the following choices: $c_1 = c_3 = m$, $c'_7 = a m$, $c_2 = c_4 = n$, $c_8 = b n$ and $c_5 = c_6 = 1$. As in [24], we fix

some of the parameters: $a = 0.9$, $b = 0.2$ and $d_1 = d_2 = 0$. We also set $d_3 = 0.8$. The parameters (m, n) can be freely adjusted and select different dynamical regimes.

The system of differential equations (5.11) admits three fixed points [24]. One of these corresponds to the extinction of both X and Z species and is always stable. Another one is a saddle. The last one is non-trivial, and its stability depends on the values of (m, n) . It is around this point in the two-dimensional plane defined by m and n that the pattern formation is investigated. The concentrations (ϕ^*, ψ^*, η^*) at the fixed point are independent of (m, n) and can be numerically determined.

Patterns arise when (ϕ^*, ψ^*, η^*) becomes unstable with respect to inhomogeneous perturbations [3]. To look for instabilities, we introduce small deviations from the fixed point, $(\delta\phi_i, \delta\psi_i, \delta\eta_i)$, and linearise system (5.11) around it:

$$\begin{pmatrix} \delta\dot{\phi}_i \\ \delta\dot{\psi}_i \\ \delta\dot{\eta}_i \end{pmatrix} = \sum_{j=1}^{\Omega} \left(\mathcal{M}^{*(NS)} \delta_{ij} + \mathcal{M}^{*(SP)} \Delta_{ij} \right) \cdot \begin{pmatrix} \delta\phi_j \\ \delta\psi_j \\ \delta\eta_j \end{pmatrix}. \quad (5.13)$$

The explicit expressions for the matrices $\mathcal{M}^{*(NS)}$ and $\mathcal{M}^{*(SP)}$ are given below (the label NS stands for “non-spatial” and SP for “spatial”).

$$\begin{aligned} \mathcal{M}_{11}^{*(NS)} &= -c_1 \psi^{*2} - \frac{gc'_7}{(g + \phi^*)^2}, & \mathcal{M}_{23}^{*(NS)} &= \mathcal{M}_{32}^{*(NS)} = 0, \\ \mathcal{M}_{12}^{*(NS)} &= -2c_1 \phi^* \psi^*, & \mathcal{M}_{31}^{*(NS)} &= c_5, \\ \mathcal{M}_{13}^{*(NS)} &= 2c_3 \eta^*, & \mathcal{M}_{33}^{*(NS)} &= -c_6, \\ \mathcal{M}_{21}^{*(NS)} &= c_2 \psi^{*2}, & \mathcal{M}_{rs}^{*(SP)} &= d_r \delta_{rs}. \\ \mathcal{M}_{22}^{*(NS)} &= 2c_2 \phi^* \psi^* - c_4, \end{aligned} \quad (5.14)$$

For a regular lattice, the Fourier transform is usually employed to solve the above linear equations. This analysis needs to be adapted in the case of a system defined on a network. To this end we follow the approach of [11, 19] and start by defining the eigenvalues and eigenvectors of the matrix Δ :

$$\sum_{j=1}^{\Omega} \Delta_{ij} v_j^{(\alpha)} = \Lambda^{(\alpha)} v_i^{(\alpha)}, \quad \alpha = 1, \dots, \Omega. \quad (5.15)$$

Since the Laplacian is symmetric, the eigenvalues $\Lambda^{(\alpha)}$ are real and the eigenvectors $v^{(\alpha)}$ form an orthonormal basis. It can actually be proven that for a case of a Barabási-Albert network the $\Lambda^{(\alpha)}$ are negative and non-degenerate [11, 19]. We can now define a transform based on the eigenvectors $v^{(\alpha)}$ which takes the role that the Fourier transform took on for a regular lattice. This leads to the following transforms which will be used

throughout the remainder of the paper:

$$\begin{aligned} f_j(\tau) &= \frac{1}{2\pi} \int_{-\infty}^{\infty} d\lambda \sum_{\alpha=1}^{\Omega} \tilde{f}_{\alpha}(\lambda) v_j^{(\alpha)} e^{\lambda\tau}, \\ \tilde{f}_{\alpha}(\lambda) &= \int_0^{\infty} d\tau \sum_{j=1}^{\Omega} f_j(\tau) v_j^{(\alpha)} e^{-\lambda\tau}, \end{aligned} \quad (5.16)$$

where $\lambda \in \mathbb{C}$ and $f_j(\tau)$ is any function of the nodes and of time. This is a standard Fourier transform in time, but with the spatial modes replaced by the eigenvectors of the network Laplacian. If the network is a regular lattice, the transform (5.16) reduces to a classic Fourier transform for discrete space. From now on the index α is used to label the variable conjugate to the nodes. Using this definition and setting $\lambda = -i\omega$, one can define the power spectrum as $P(\omega, \Lambda^{(\alpha)}) = |\tilde{f}_{\alpha}(\omega)|^2$.

Applying the transform (5.16) to Eq. (5.13) yields the following linear equation:

$$\lambda \begin{pmatrix} \delta\phi_{\alpha} \\ \delta\psi_{\alpha} \\ \delta\eta_{\alpha} \end{pmatrix} = \left(\mathcal{M}^{*(NS)} + \mathcal{M}^{*(SP)} \Lambda^{(\alpha)} \right) \cdot \begin{pmatrix} \delta\phi_{\alpha} \\ \delta\psi_{\alpha} \\ \delta\eta_{\alpha} \end{pmatrix}, \quad (5.17)$$

that is now decoupled in the nodes and in time and thus readily solvable. The matrix $\mathcal{M}^{*(NS)} + \mathcal{M}^{*(SP)} \Lambda^{(\alpha)}$ for a given α , is a 3×3 matrix whose eigenvalues characterize the response of system (5.11) to external perturbations. The eigenvalue with the largest real part will be denoted by $\lambda^{\max}(\Lambda^{(\alpha)})$. If $\text{Re}[\lambda^{\max}(\Lambda^{(\alpha)})] > 0$ the fixed point is unstable and the system exhibits a pattern whose spatial properties are encoded by $\Lambda^{(\alpha)}$. This is the analog of the wavelength for a spatial pattern in a system defined on a regular lattice; it is customarily written $\Lambda^{(\alpha)} \equiv -k^2$ in this case. When the imaginary part of the eigenvalue, $\text{Im}[\lambda^{\max}(\Lambda^{(\alpha)})]$, is different from zero, the pattern oscillates in time [3]. A system unstable for $\Lambda^{(\alpha)} \neq 0$ and $\text{Im}[\lambda^{\max}(\Lambda^{(\alpha)})] \neq 0$ is said to undergo a wave-instability (see Chapter 1) and the emerging patterns consist of travelling waves.

In Fig. 5.1, left panel, the domain of instability is shown as a shaded region in the plane (m, n) . The fixed point (ϕ^*, ψ^*, η^*) is stable for fixed n when $m > m_c$. At $m = m_c$ a wave instability sets in and travelling waves are found to occur for $m < m_c$. The real and imaginary parts of the eigenvalues λ^{\max} are depicted in the right panel, as a function of $-\Lambda^{(\alpha)}$, for two choices of the parameters (m, n) , for which the system is respectively stable and unstable. The circles in the left panel of Fig. 5.1 indicate these two choices.

Since the system is defined on a network, the emerging patterns present two main differences as compared to those obtained for the case of conventional reaction-diffusion

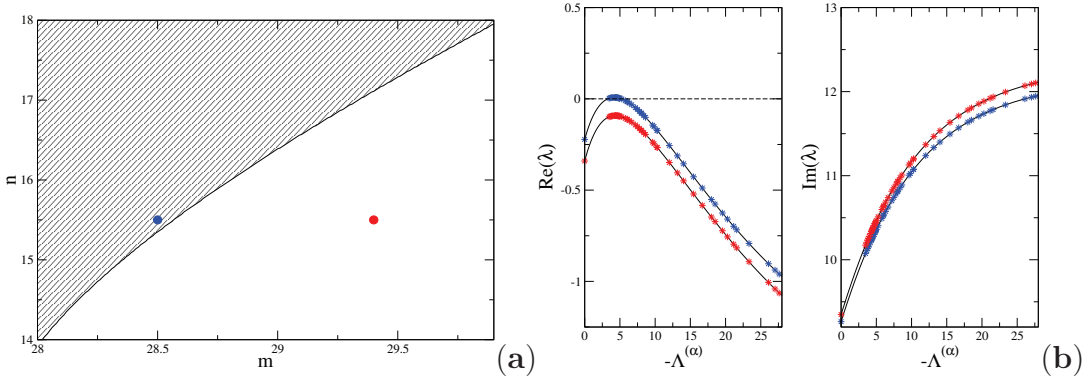


FIGURE 5.1: (a) The shaded region (left) delineates the wave instability domain in the (m, n) plane for the Zhabotinsky model with $a = 0.9$, $b = 0.2$, $d_1 = d_2 = 0$ and $d_3 = 0.8$. The blue circle falls inside of the region of wave instability and is at the point $(28.5, 15.5)$. The red circle is outside the ordered region and is at the point $(29.4, 15.5)$. (b) Real and imaginary parts (right) of λ^{\max} are plotted as a function of both the discrete modes $-\Lambda^{(\alpha)}$ of the network Laplacian (symbols) and their spatial analogs $-k^2$ (solid line). The parameters used are $(m, n) = (28.5, 15.5)$, (blue, upper curves) and $(m, n) = (29.4, 15.5)$, (red, lower curves) and correspond respectively to the two points identified in panel (a). The scale-free network employed in this analysis has 50 nodes with a mean degree $\langle k \rangle = 10$. The fixed point of the system is found to be $(\phi^* \approx 1.1308, \psi^* \approx 0.5787, \eta^* \approx 1.1308)$.

models defined on the continuum. First, only some of the wavenumbers, $\Lambda^{(\alpha)}$, are allowed. This is due to the fact that the solutions of Eq. (5.15) form a discrete set; such a feature also occurs for systems defined on periodic lattices. In this latter case however, the wavenumbers are equally spaced and proportional to the lattice spacing. By contrast, for systems defined on a complex network, there is no clear periodic structure and the wavenumbers are clustered or irregularly distributed, as displayed in panel (b) of Fig. 5.1. The second unusual trait has to do with the shape of the patterns. In a reaction-diffusion system defined on a regular lattice, each point of the lattice has a concentration which assumes a value significantly different from that characterising the homogeneous fixed point. However, for a network, only a fraction of nodes have concentrations which are significantly different from that of the homogeneous fixed point. The fraction that are differentiated in this way depends on the connectivity of the nodes and on the ratio of the diffusion coefficients [11]. This feature cannot be simply understood from linear stability analysis, as it relates to the localization of the Laplacian eigenvectors in large networks, a property that has been recently investigated in this context in [84].

In Fig. 5.2 the power spectrum of the concentration $\phi_i(\tau)$ is plotted for a choice of the parameters that correspond to the leftmost circle (blue) in Fig. 5.1(a). A peak is displayed for $(\omega, \Lambda^{(\alpha)}) \simeq (10, -5)$, in complete agreement with the predictions of the linear stability analysis. Similar results are obtained for the other concentrations $\psi_i(\tau)$ and $\eta_i(\tau)$. Thus, the generalized Fourier algorithm based on Eqs.(5.16) can be effectively employed to resolve complex patterns that develop on networks. This is a valuable tool

which, we believe, could prove useful for the many applications where the dynamics on a network is well known to be central, from neuroscience to epidemics.

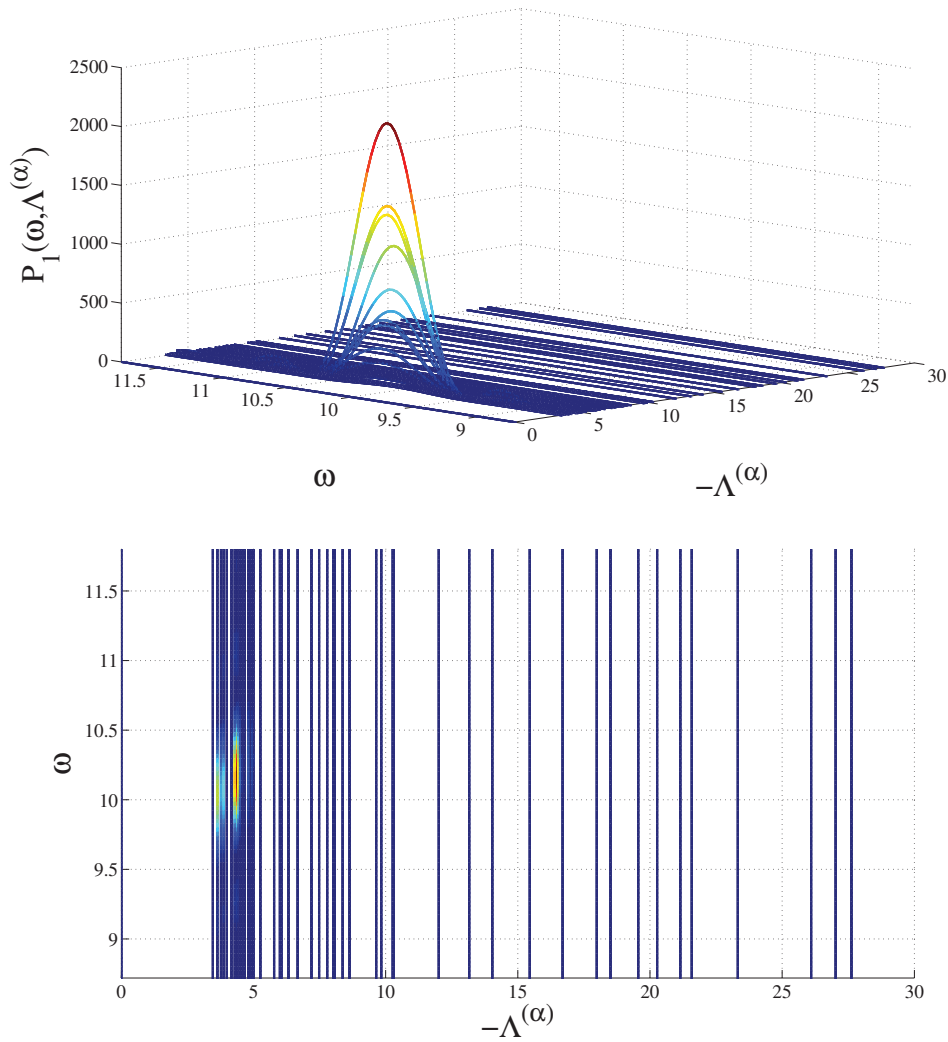


FIGURE 5.2: Upper panel: power spectrum of the concentration $\phi_i(t)$, for a choice of the parameters that corresponds to the unstable configuration of figure 5.1(a) (blue circle). The power spectrum is constructed from the generalized Fourier transform (5.16), using as an input the numerical solution of the deterministic equations (5.11). A peak is seen for $(\omega, \Lambda^{(\alpha)}) \simeq (10, -5)$, confirming the validity of the linear stability analysis and revealing the presence of a travelling wave in the time series. Lower panel: a two-dimensional projection of the power spectrum is displayed. Recall that the power spectrum is defined over a discrete, non-uniform support in $\Lambda^{(\alpha)}$.

The next subsection is entirely dedicated to the study of stochastic patterns, aiming at generalizing the deterministic picture of Fig. 5.1. By applying the LNA, we will demonstrate that stochastic waves exist in a region of the parameter space for which the deterministic analysis predicts a stable homogeneous fixed point. The presence of stochastically driven patterns will be revealed by an analytical calculation of the power

spectra of fluctuations. The theoretical predictions will then be validated by reconstructing the power spectrum from the stochastic time series. Properties of the patterns that in the deterministic picture depend on the eigenvectors, such as localization, will not be addressed in the present work.

5.2.3 Power spectra of fluctuations and stochastic patterns

While in the deterministic limit a study of the eigenvalues reveals the range of parameter values for which patterns are expected to occur, this prediction is not conclusive for systems that are subject to noise. Simulations of the master equation have shown that patterns arise even for parameter values for which the underlying fixed point is stable, provided that the system is sufficiently close to an instability. The corresponding patterns have been called stochastic patterns [18] or quasi-patterns [17]. The LNA allows one to gain analytical insight into the mechanism that yields such patterns [17, 18, 59, 60]. The method has been extended in [19] to the case of a reaction-diffusion system on a network. Here we shall develop the method further and provide the first evidence for the spontaneous emergence of *stochastic waves* (or *quasi-waves*) on a network.

The role of fluctuations can be quantified by use of the van Kampen system-size expansion, which is equivalent to assuming the LNA. The quantity $1/\sqrt{V}$ acts as the small parameter in the perturbative expansion: at the leading order, the macroscopic deterministic equations (5.11) are recovered. At the next-to-leading order one obtains the Fokker-Planck equation (5.18) for the distribution of stochastic fluctuations:

$$\partial_\tau \Pi = \sum_{i=1}^{\Omega} \left(- \sum_{r=1}^3 \partial_{\xi_{r,i}} (\mathcal{M}_{r,i} \Pi) + \frac{1}{2} \sum_{r,s=1}^3 \sum_{j=1}^{\Omega} \partial_{\xi_{s,i}} \partial_{\xi_{r,j}} (\mathcal{B}_{rs,ij} \Pi) \right). \quad (5.18)$$

Equation (5.18) is linear as the matrices \mathcal{M} and \mathcal{B} do not depend on ξ_r , with $r = 1, 2, 3$. However, they do depend on the trajectory $\phi(\tau)$, $\psi(\tau)$, $\eta(\tau)$ that should be chosen beforehand among the solutions of (5.11).

The form of the matrices \mathcal{M} and \mathcal{B} follow from the expansion of the transition rates (5.3) and (5.4). For illustrative purposes, here we shall discuss only the first of the transition rates (5.4), T_9 , explicitly. The contribution to matrix \mathcal{B} associated with this term, labeled $\mathcal{B}^{(9)}$, is found to be

$$\mathcal{B}_{rs,ij}^{(9)} = d_1 \delta_{rs,11} (2k_i \phi_i - W_{ij} (\phi_i + \phi_j)). \quad (5.19)$$

Clearly, the only non-zero entry is for $r = s = 1$, since the rate T_9 involves only the X species. The other diffusion rates, T_{10} and T_{11} , yield similar contributions for

respectively $r = s = 2$ and $r = s = 3$, with diffusion coefficients and concentrations corresponding to the diffusing species. The contributions arising from the transition rates for the reactions (5.3) follow in a similar fashion.

In most applications, the main point of interest is to study the fluctuations around a fixed point. This is certainly our case, as we aim to characterize the pattern that originates from a small perturbation of the fixed point (ϕ^*, ψ^*, η^*) . We therefore substitute $\phi_i(\tau) = \phi^*$, $\psi_i(\tau) = \psi^*$ and $\eta_i(\tau) = \eta^*$ and label by \mathcal{M}^* and \mathcal{B}^* the matrices evaluated at the fixed point.

From the form of the reaction rates it is clear that the following decompositions hold [19]:

$$\begin{aligned}\mathcal{M}^*_{sr,ij} &= \mathcal{M}^{*(NS)}_{sr}\delta_{ij} + \mathcal{M}^{*(SP)}_{sr}\Delta_{ij}, \\ \mathcal{B}^*_{sr,ij} &= \mathcal{B}^{*(NS)}_{sr}\delta_{ij} + \mathcal{B}^{*(SP)}_{sr}\Delta_{ij}.\end{aligned}\quad (5.20)$$

The non-spatial part (NS) refers to the transition rates (5.3), whereas the spatial contribution (SP) refers to the transition rates (5.4). Note that the matrix \mathcal{M}^* above is exactly the same used in eq. (5.13).

We end by giving the elements of the matrix \mathcal{B}^* .

$$\begin{aligned}\mathcal{B}^{*(NS)}_{11} &= c_1\phi^*\psi^{*2} + c_3\eta^{*2} + c'_7\frac{\phi^*}{g + \phi^*}, & \mathcal{B}^{*(SP)}_{11} &= -2d_1\phi^*, \\ \mathcal{B}^{*(NS)}_{22} &= c_8 + c_2\phi^*\psi^{*2} + c_4\psi^*, & \mathcal{B}^{*(SP)}_{22} &= -2d_2\psi^*, \\ \mathcal{B}^{*(NS)}_{33} &= c_5\phi^* + c_6\eta^*, & \mathcal{B}^{*(SP)}_{33} &= -2d_3\eta^*, \\ \mathcal{B}^{*(NS)}_{rs} &= 0, \quad \text{with } r \neq s, & \mathcal{B}^{*(SP)}_{rs} &= 0, \quad \text{with } r \neq s.\end{aligned}\quad (5.21)$$

To quantify the impact of the stochastic components of the dynamics, the power spectrum of fluctuations is utilized. It is defined as:

$$P_r(\omega, \Lambda^{(\alpha)}) = \langle \tilde{\xi}_{r,\alpha}^c(\omega) \tilde{\xi}_{r,\alpha}(\omega) \rangle = \langle |\tilde{\xi}_{r,\alpha}(\omega)|^2 \rangle, \quad (5.22)$$

where $\tilde{\xi}_{r,\alpha}^c(\omega)$ is the complex conjugate of $\tilde{\xi}_{r,\alpha}(\omega)$, which is given by transforming $\xi_{r,i}(\tau)$ via the generalized transform (5.16). The average $\langle \cdot \rangle$ is performed over many realizations of the stochastic dynamics. The Fokker-Planck equation (5.18), with the matrices evaluated at the fixed point, describes fluctuations about the fixed point, and is equivalent to the Langevin equation [58]:

$$\begin{aligned}\frac{d\xi_{r,i}}{d\tau} &= \sum_{s=1}^3 \sum_{j=1}^{\Omega} \mathcal{M}^*_{rs,ij} \xi_{s,j} + \chi_{r,i} \\ &= \sum_{s=1}^3 \sum_{j=1}^{\Omega} \left(\mathcal{M}^{*(NS)}_{rs} \delta_{ij} + \mathcal{M}^{*(SP)}_{rs} \Delta_{ij} \right) \xi_{s,j} + \chi_{r,i}.\end{aligned}\quad (5.23)$$

The Gaussian white noises $\chi_{r,i}$ have zero mean and correlator:

$$\langle \chi_{r,i}(\tau) \chi_{s,j}(\tau') \rangle = \mathcal{B}_{rs,ij} \delta(\tau - \tau'). \quad (5.24)$$

Equation (5.23) generalises (5.13) to include stochastic fluctuations. In solving Eq. (5.23), we again make use of the transforms (5.16) with $\lambda = -i\omega$. We express the $\xi_{r,i}$ and the associated noise in terms of their transformed analogs. Collecting each term, except the noise, to the left-hand side of the equation yields:

$$\left(-i\omega \mathcal{I} - \mathcal{M}^{*(NS)} - \mathcal{M}^{*(SP)} \Lambda^{(\alpha)} \right) \cdot \begin{pmatrix} \tilde{\xi}_{1,\alpha} \\ \tilde{\xi}_{2,\alpha} \\ \tilde{\xi}_{3,\alpha} \end{pmatrix} = \begin{pmatrix} \tilde{\chi}_{1,\alpha} \\ \tilde{\chi}_{2,\alpha} \\ \tilde{\chi}_{3,\alpha} \end{pmatrix}, \quad (5.25)$$

where \mathcal{I} is the 3×3 identity matrix. By introducing $\mathcal{F}^{(\alpha)} = -i\omega \mathcal{I} - \mathcal{M}^{*(NS)} - \mathcal{M}^{*(SP)} \Lambda^{(\alpha)}$ the solution of Eq. (5.25) may be written as:

$$\tilde{\xi}_{r,\alpha} = \sum_{s=1}^3 \mathcal{F}_{rs}^{-1} \tilde{\chi}_{s,\alpha}, \quad (5.26)$$

where we have omitted the α index on \mathcal{F} for clarity. We now insert Eq. (5.26) into Eq. (5.22) to obtain an expression for the power spectra:

$$P_r(\omega, \Lambda^{(\alpha)}) = \sum_{s,l=1}^3 \mathcal{F}_{rl}^{-1} \langle \tilde{\chi}_{l,\alpha} \tilde{\chi}_{s,\alpha}^c \rangle \mathcal{F}_{sr}^{-1\dagger}. \quad (5.27)$$

The symbol \dagger signifies the adjoint operator, here equivalent to the conjugate transpose operator. We now need to express $\langle \tilde{\chi}_{l,\alpha} \tilde{\chi}_{s,\alpha}^c \rangle$ in terms of known quantities. We begin by transforming Eq. (5.24) using the inverse transform (5.16), which leads to

$$\langle \tilde{\chi}_{l,\alpha} \tilde{\chi}_{s,\alpha}^c \rangle = 2\pi \sum_{i,j=1}^{\Omega} v_i^{(\alpha)} v_j^{(\alpha)} \mathcal{B}_{ls,ij}^*. \quad (5.28)$$

The dependence on the Laplacian eigenvectors can be eliminated using the fact that they are orthonormal and complete:

$$\sum_{i=1}^{\Omega} v_i^{(\alpha)} v_i^{(\alpha')} = \delta_{\alpha\alpha'}, \quad \sum_{\alpha=1}^{\Omega} v_i^{(\alpha)} v_j^{(\alpha)} = \delta_{ij}. \quad (5.29)$$

To do so, we substitute the decomposition (5.20) into Eq. (5.28), then use the above properties to arrive at:

$$\langle \tilde{\chi}_{l,\alpha} \tilde{\chi}_{s,\alpha}^c \rangle = 2\pi \left(\mathcal{B}_{ls}^{*(NS)} + \mathcal{B}_{ls}^{*(SP)} \Lambda^{(\alpha)} \right). \quad (5.30)$$

The right-hand side of Eq. (5.30) is known through expressions (5.21), and so $\langle \tilde{\chi}_{l,\alpha} \tilde{\chi}_{s,\alpha}^c \rangle$ can be found. By substituting Eq. (5.28) into Eq. (5.27) we arrive at the final formula for the power spectra:

$$\begin{aligned} P_r(\omega, \Lambda^{(\alpha)}) &= \sum_{s,l=1}^3 \mathcal{F}_{rl}^{-1} \left(\mathcal{B}_{ls}^{*(NS)} + \mathcal{B}_{ls}^{*(SP)} \Lambda^{(\alpha)} \right) \mathcal{F}_{sr}^{-1\dagger} \\ &= \left(\mathcal{F}^{-1} \left(\mathcal{B}^{*(NS)} + \mathcal{B}^{*(SP)} \Lambda^{(\alpha)} \right) \mathcal{F}^{-1\dagger} \right)_{rr}. \end{aligned} \quad (5.31)$$

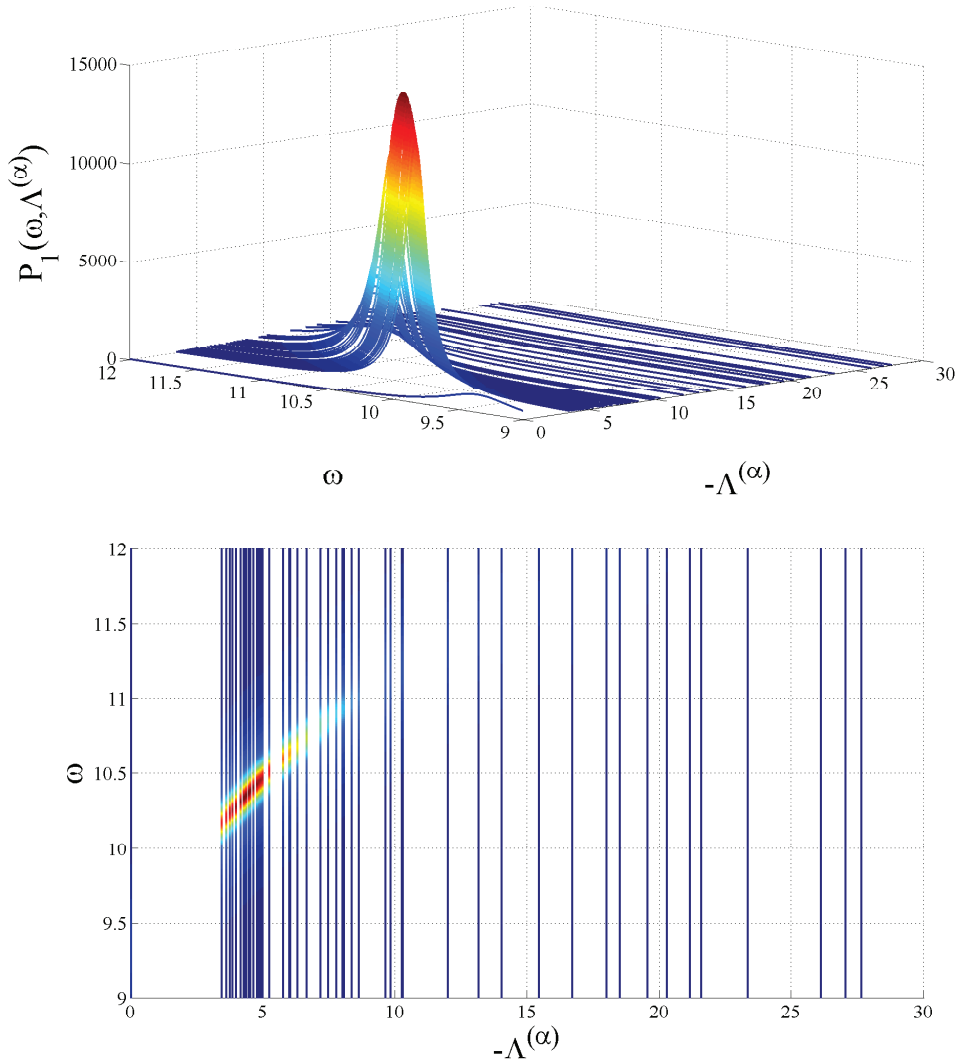


FIGURE 5.3: Upper panel: analytical power spectrum of the fluctuations, plotted as a function of the continuum frequency ω and the discrete wavelength Λ_α . The parameters (m, n) are chosen so as to fall outside the region of deterministic order, i.e. as indicated by the rightmost circle (red) of Fig. 5.1(a). The other parameters are set to the values specified in the caption of Fig. 5.1. Lower panel: a two-dimensional projection of the power spectrum is displayed.

Once the parameters of the model have been assigned, it is therefore possible to calculate the power spectrum of fluctuations and look for signatures of emerging self-organized structures. In Fig. 5.3 the analytical power spectrum for species X is plotted for a choice of parameters that corresponds to the rightmost circle in Fig. 5.1 (a), namely outside the region for which the deterministic waves occur. As can be seen, the power spectrum of fluctuations is characterized by a localized peak for $(\omega_M, \Lambda_M^{(\alpha)})$. Therefore, species $r = 1$ oscillates with an angular frequency ω_M and, at the same time, displays a pattern at wavelength $\Lambda_M^{(\alpha)}$. Stochastic waves, or quasi waves, are hence predicted to occur, in a region of the parameter plane for which the homogeneous fixed point is stable, according to the deterministic picture. In other words, stochastic corrections,

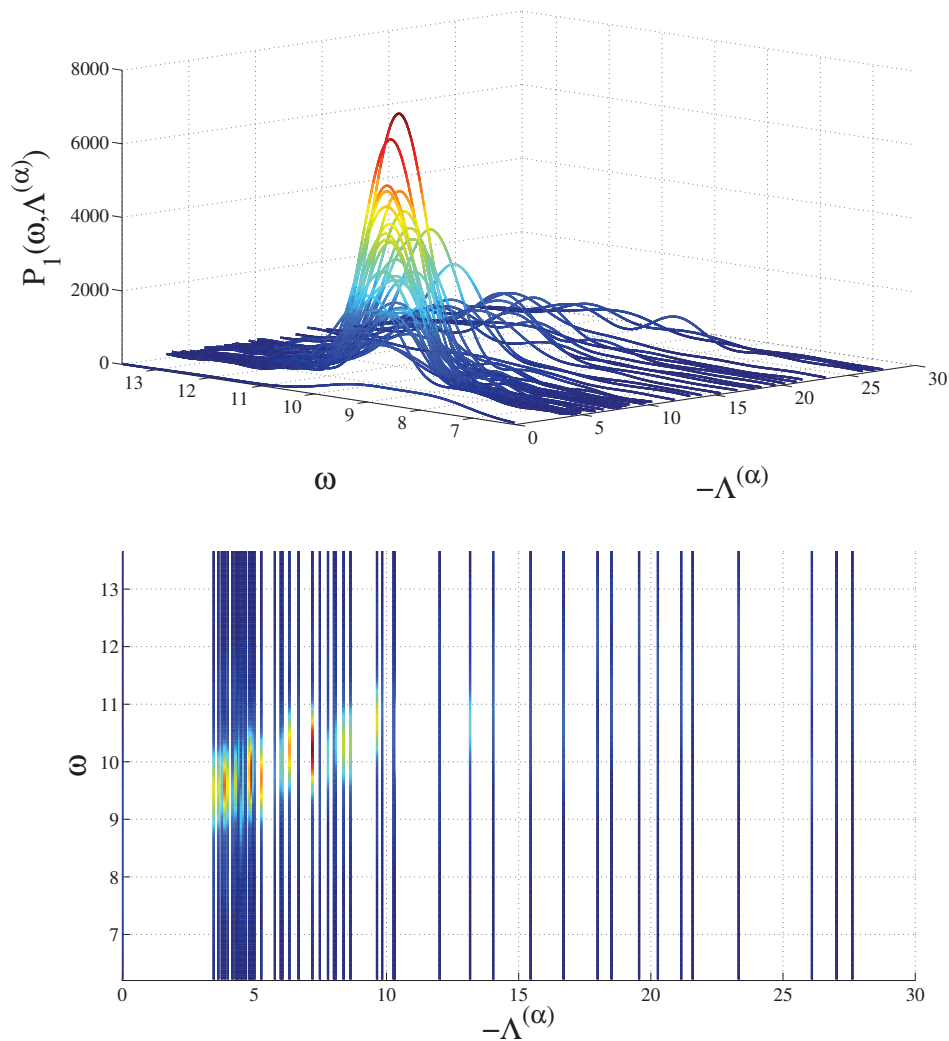


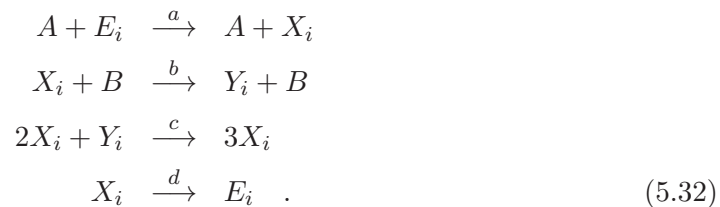
FIGURE 5.4: Upper panel: numerical power spectrum of the fluctuations obtained by simulating the stochastic dynamics via the Gillespie algorithm. The power spectrum is calculated by using the generalized Fourier transform (5.16) and by averaging over 40 independent realizations. The parameters are the same as in Fig. 5.3. Here $V = 10^4$. Lower panel: two-dimensional projection of the power spectrum.

stemming from finite size, and, as such, endogenous to the system under scrutiny, can eventually produce macroscopically ordered structures.

To test the correctness of the theoretical prediction we carried out stochastic simulations of the processes (5.1) and (5.2) using the Gillespie algorithm [64] described in the Appendix A. The numerical power spectrum is reconstructed by applying the generalized transform (5.16) to the time series, and averaging over independent realizations of the stochastic dynamics. The result is shown in Fig. 5.4 and is seen to agree with the theoretically-predicted spectrum. The location of the maximum is captured by the theory, as well as the characteristic shape of the profile. In the remaining part of this chapter we will apply a similar analysis to a modified version of the classical Brusselator model.

5.3 Stochastic Turing-like patterns

In this section, we will consider a stochastic version of the Brusselator model [4] which will be placed on top of an heterogeneous network of Ω nodes. More concretely, two species, respectively X_i and Y_i are assigned to the generic node i , and therein react according to the following chemical reactions [18]:



The symbol E_i stands for an empty case and formally amounts to imposing a finite carrying capacity in each node of the network. This complication is introduced as in the spirit of [85] to model the transport process under crowded conditions. More precisely, we assume that each node can host a maximum number N of molecules (or agents), including the vacancies¹. Let us denote by n_i and m_i the total number of elements belonging to species X and Y in the node i . The corresponding number of empties total hence in $N - n_i - m_i$. The parameters a , b , c and d in Eqs. (5.32) are the reaction rates, while the species A and B are enzymatic activators whose concentrations are supposed to remain constant during the dynamics. In addition to the above activator-inhibitor rules, we assume that the molecules can migrate between neighbour nodes as dictated

¹For a discussion of the role played by finite carrying capacity we refer to [56, 59, 74, 85]. The forthcoming analysis can be repeated by relaxing such an assumption, and yielding qualitative equivalent results.

by the following reactions:



where μ and δ are the diffusion coefficients characteristic of the two species, and the subscript j denotes the generic node connected to i , via the network structure. Similar equations governs the diffusion from node j towards node i . This condition, might sound artificial, but, as we will see later, it is imposed to obtain a symmetric non linear operator for the transport process. To complete the notation we introduce the Ω -dimensional vectors $\mathbf{n} = (n_1, \dots, n_i, \dots, n_\Omega)$ and $\mathbf{m} = (m_1, \dots, m_i, \dots, m_\Omega)$ that unequivocally identify the state of the system. Under the Markov hypothesis, the probability $P(\mathbf{n}, \mathbf{m}, t)$ of seeing the system at time t in state (\mathbf{n}, \mathbf{m}) obeys to the master equation

$$\begin{aligned} \frac{\partial}{\partial t} P(\mathbf{n}, \mathbf{m}, t) = & \sum_{i=1}^{\Omega} \left\{ (\epsilon_{n_i}^- - 1) T(n_i + 1, m_i | n_i, m_i) + (\epsilon_{n_i}^+ - 1) T(n_i - 1, m_i | n_i, m_i) \right. \\ & + (\epsilon_{n_i}^- \epsilon_{m_i}^+ - 1) T(n_i + 1, m_i - 1 | n_i, m_i) + (\epsilon_{n_i}^+ \epsilon_{m_i}^- - 1) T(n_i - 1, m_i + 1 | n_i, m_i) \\ & + \sum_{j=1}^{\Omega} W_{i,j} \left[(\epsilon_{n_i}^+ \epsilon_{n_j}^- - 1) T(n_i - 1, n_j + 1 | n_i, n_j) + (\epsilon_{n_j}^+ \epsilon_{n_i}^- - 1) T(n_j - 1, n_i + 1 | n_i, n_j) \right. \\ & \left. \left. + (\epsilon_{m_i}^+ \epsilon_{m_j}^- - 1) T(m_i - 1, m_j + 1 | m_i, m_j) + (\epsilon_{m_j}^+ \epsilon_{m_i}^- - 1) T(m_j - 1, m_i + 1 | m_i, m_j) \right] \right\} P(\mathbf{n}, \mathbf{m}, t) \end{aligned} \quad (5.34)$$

where use has been made of the step operators $\epsilon_{n_i}^{\pm} f(\dots, n_i, \dots, \mathbf{m}) = f(\dots, n_i \pm 1, \dots, \mathbf{m})$ and $\epsilon_{m_i}^{\pm} f(\mathbf{n}, \dots, m_i, \dots) = f(\mathbf{n}, \dots, m_i \pm 1, \dots)$, $f(\cdot, \cdot)$ being any generic function of the state variables. As usual, the $\Omega \times \Omega$ integers $W_{i,j}$ represent the entries of the symmetric adjacency matrix \mathbf{W} , which characterizes the topology of the network. $W_{i,j}$ is equal to 1 if nodes i and j are connected, and 0 otherwise. The transition rates $T(\mathbf{n}', \mathbf{m}' | \mathbf{n}, \mathbf{m})$ link the initial state (\mathbf{n}, \mathbf{m}) to another state $(\mathbf{n}', \mathbf{m}')$, compatible with the former, and are given by

$$\begin{aligned} T(n_i + 1, m_i | n_i, m_i) &= \frac{a}{\Omega} \frac{N - n_i - m_i}{N} \\ T(n_i - 1, m_i | n_i, m_i) &= \frac{d}{\Omega} \frac{n_i}{N} \\ T(n_i + 1, m_i - 1 | n_i, m_i) &= \frac{c}{\Omega} \frac{n_i^2 m_i}{N^3} \\ T(n_i - 1, m_i + 1 | n_i, m_i) &= \frac{b}{\Omega} \frac{n_i}{N} \\ T(n_i - 1, n_j + 1 | n_i, n_j) &= \frac{\mu}{\Omega} \frac{n_i}{N} \frac{N - n_j - m_j}{N} \left(\frac{1}{k_i} + \frac{1}{k_j} \right) \\ T(m_i - 1, m_j + 1 | m_i, m_j) &= \frac{\delta}{\Omega} \frac{m_i}{N} \frac{N - n_j - m_j}{N} \left(\frac{1}{k_i} + \frac{1}{k_j} \right). \end{aligned}$$

where k_i is the degree of the i -th node. Note the factor $(1/k_i + 1/k_j)$ present in the migration transition rates. In this problem we assume that the transition probability associated to the migration event scales with the connectivity of the departure node. The artificial symmetrization which yields the term $(1/k_i + 1/k_j)$ is obtained if we assume that the move can be initiated by either the physical particle or the virtual vacancy. For more details about alternative formulation of the Laplacian operator, the reader should refer to Appendix A.

To progress in the analysis we again resort to the van Kampen ansatz [58, 86]: $n_i/N = \phi_i + \xi_{1i}/\sqrt{N}$ and $m_i = \psi_i + \xi_{2i}/\sqrt{N}$. ϕ_i and ψ_i are the mean-field concentrations respectively associated to the interacting species X and Y . ξ_{1i} and ξ_{2i} are stochastic fluctuations that originate from finite size corrections, normalized by the scaling factor $1/\sqrt{N}$, as dictated by the central limit theorem [58]. Notice that in this case N is a conserved (large) quantity and can be employed in the definition of the perturbative parameter. In practice $1/\sqrt{N}$ replace $1/\sqrt{V}$ in the analysis carried out in the preceding section. For moderately large system sizes N , the $1/\sqrt{N}$ factor is small and paves the way to the van Kampen system size expansion. At the leading order of the perturbative analysis, the mean-field equations for the deterministic variables are recovered and, for the specific problem here investigated, read:

$$\begin{aligned} \frac{d}{d\tau}\phi_i &= f(\phi_i, \psi_i) + 2\mu \left[\sum_{j=1}^{\Omega} \Delta_{ij}\phi_j + \phi_i \sum_{j=1}^{\Omega} \Delta_{ij}\psi_j - \psi_i \sum_{j=1}^{\Omega} \Delta_{ij}\phi_j \right] \\ \frac{d}{d\tau}\psi_i &= g(\phi_i, \psi_i) + 2\delta \left[\sum_{j=1}^{\Omega} \Delta_{ij}\psi_j + \phi_i \sum_{j=1}^{\Omega} \Delta_{ij}\phi_j - \phi_i \sum_{j=1}^{\Omega} \Delta_{ij}\psi_j \right] \end{aligned} \quad (5.35)$$

where, generalizing the heuristic derivation of [11], we have introduced a new discrete Laplacian $\Delta_{ij} = \tilde{W}_{ij} - \tilde{k}_i\delta_{ij}$ where now $\tilde{k}_i = \sum_{j=1}^{\Omega} \tilde{W}_{ij}$ and $\tilde{W}_{ij} = (1/k_i + 1/k_j)W_{i,j}$. The reaction terms are respectively $f = -(b+d)\phi_i + c\phi_i^2\psi_i + a(1 - \phi_i - \psi_i)$ and $g = b\phi_i - c\phi_i^2\psi_i$. τ is the rescaled time $t/(N\Omega)$. Cross diffusion terms appear in the obtained deterministic equations, because of the finite carrying capacity, imposed at the level of the single node [85]. By relaxing such an assumption [56], conventional diffusion operators are instead recovered as described in the Appendix A. Similarly, the finite carrying capacity assumption reflects in the reaction contribution $a(1 - \phi_i - \psi_i)$ that replaces the usual constant term a in the standard Brusselator equations [18]. Although interesting per se, this modification does not play any substantial role in the forthcoming development: equivalent conclusions can be drawn when working in the diluted setting, i.e. away from jamming or crowding conditions that inspire the physical request for a limited capacity to be explicitly accommodated on each individual node.

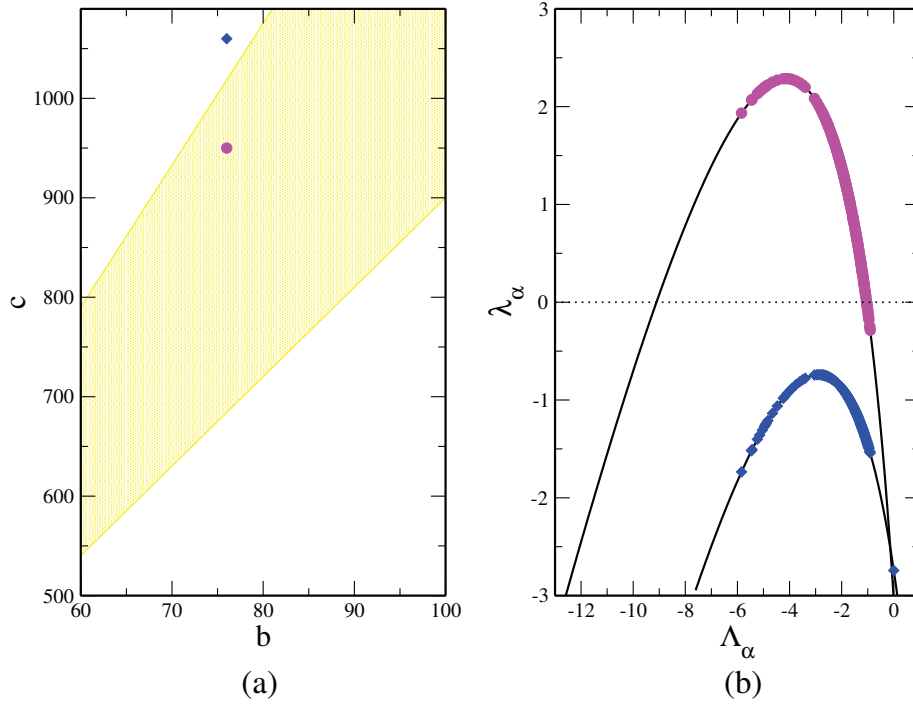


FIGURE 5.5: The darkened region (yellow) in panel (a) delineates the Turing instability domain in the (b, c) plane for the Brusselator model with $a = d = 1$, $\mu = 1$ and $\delta = 15$. The (magenta) point belongs to the Turing instability region and corresponds to $b = 76$ and $c = 950$. The (blue) diamond falls outside the region of Turing order and is positioned at $(76, 1060)$. In panel (b) the dispersion relation (5.37) is plotted as a function of both the discrete eigenvalues of the network Laplacian (symbols) and their real analogues $-k^2$ (solid line). Circles (magenta) refer to $(b, c) = (76, 950)$, while diamonds (blue) to $(b, c) = (76, 1060)$. In the analysis we assumed a scale-free network made of $\Omega = 200$ nodes and mean degree $\langle k \rangle = 20$. The network has been generated according to the Barabási-Albert algorithm [7].

To look for mean-field Turing instability, one needs to introduce a small perturbation to the homogeneous equilibrium point $(\phi^*, \psi^*) = ((a + \sqrt{a^2 - 4ab(a+d)/c})/2/(a+d), b/c/\phi^*)$ of the deterministic system (5.35) and carry out a linear stability analysis. In formulae, $(\phi_i, \psi_i) = (\phi^* + \delta\phi_i, \psi^* + \delta\psi_i)$. It is straightforward to show that the perturbations obey to

$$\begin{aligned} \delta\dot{\phi}_i &= f_\phi\delta\phi_i + f_\psi\delta\psi_i + \mu \left[(1 - \psi^*) \sum_{j=1} \Delta_{ij}\delta\phi_j + \phi^* \sum_{j=1} \Delta_{ij}\delta\psi_j \right] \\ \delta\dot{\psi}_i &= g_\phi\delta\phi_i + g_\psi\delta\psi_i + \delta \left[(1 - \phi^*) \sum_{j=1} \Delta_{ij}\delta\psi_j + \psi^* \sum_{j=1} \Delta_{ij}\delta\phi_j \right], \end{aligned}$$

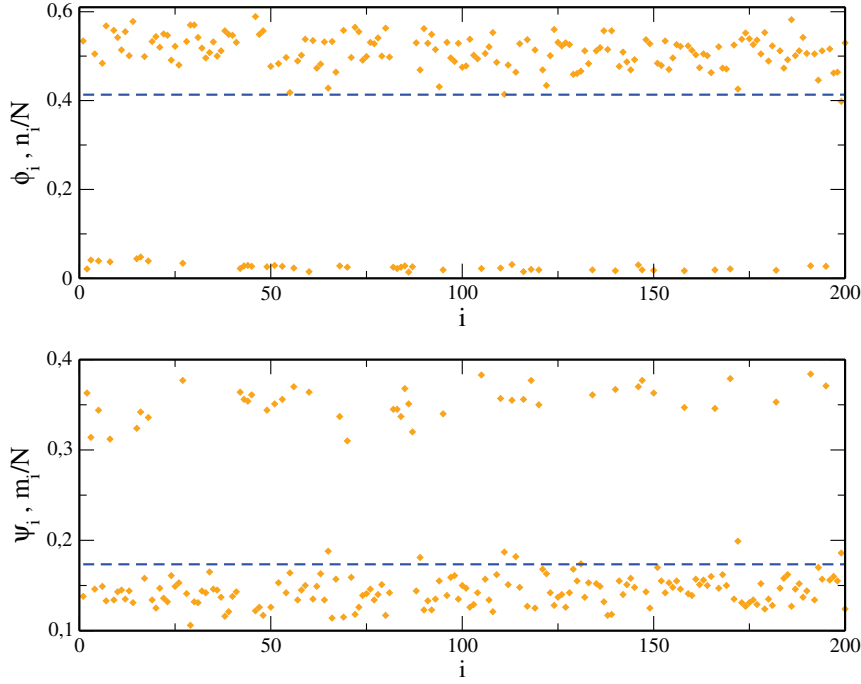


FIGURE 5.6: Simulations of the stochastic chemical model (5.32)-(5.33) outside the region of Turing order, $a = d = 1$, $b = 76$, $c = 1060$, $\mu = 1$, $\delta = 15$. Here $N = 1000$. The late time concentrations per node n_i/N (resp. m_i/N) are plotted in the upper panel (resp. lower) panel, as a function of the node index i . The (orange) diamonds are obtained from one realization of the stochastic Gillespie algorithm [64]. The network is generated as described in the caption of Fig. 5.5. The stochastic dynamics yields the emergence of two distinct activator-rich and activator-poor groups, while the deterministic dynamics is attracted towards the stable (and trivial) homogeneous fixed point, dashed (blue) horizontal line.

under the linear approximation. To exploit the linearity of the resulting equations for the perturbation amounts, we find it convenient to expand $\delta\phi_i$ and $\delta\psi_i$ as:

$$\delta\phi_i = \sum_{\alpha=1}^{\Omega} c_{\alpha} e^{\lambda_{\alpha}\tau} v_i^{(\alpha)} \quad \delta\psi_i = \sum_{\alpha=1}^{\Omega} c_{\alpha} \beta_{\alpha} e^{\lambda_{\alpha}\tau} v_i^{(\alpha)} \quad (5.36)$$

where $\mathbf{v}^{(\alpha)} = (v_1^{(\alpha)}, \dots, v_{\Omega}^{(\alpha)})$ stand for the eigenvectors of the Laplacian operator corresponding to the eigenvalue Λ_{α} ².

By inserting Eqs. (5.36) into the linearized differential equation for the perturbations $\delta\phi_i$ and $\delta\psi_i$, one obtains the usual characteristic equation for λ_{α} , which can be here cast

²The Laplacian operator $\Delta_{i,j}$ is defined by the real and symmetric matrix $\Delta_{ij} = \tilde{W}_{ij} - \tilde{k}_i \delta_{ij}$. So, the eigenvalues are real and non-positive. The eigenvectors are orthonormalized so to match the condition $\sum_i v_i^{(\alpha)} v_i^{(\beta)} = \delta_{\alpha,\beta}$.

in the form:

$$\det \begin{pmatrix} f_\phi + \mu(1 - \psi^*)\Lambda_\alpha - \lambda_\alpha & f_\psi + \mu\phi^*\Lambda_\alpha \\ g_\phi + \delta\psi^*\Lambda_\alpha & g_\psi + \delta(1 - \phi^*)\Lambda_\alpha - \lambda_\alpha \end{pmatrix} = 0 \quad (5.37)$$

where $f_q = \partial f / \partial q$ and $g_q = \partial g / \partial q$ for $q = \phi, \psi$.

The Turing instability occurs, and the perturbation gets thus amplified, if $\lambda_\alpha(\Lambda_\alpha)$ is positive for some value of Λ_α . In Fig. 5.5(b), the dispersion relation is plotted for two distinct choices of the parameters (see legend). Symbols refer to the discrete linear growth rates λ_α , as function of the corresponding Laplacian eigenvalues Λ_α . The solid line represents the homologous dispersion relations, as obtained working within the continuous representation ($\Lambda_\alpha \rightarrow -k^2$). The upper curve (panel (b) of Fig. 5.5, circles) signals the presence of an instability. A significant fraction of the discrete rates λ_α is in fact positive. Conversely, the other profile (diamonds) is obtained for a choice of the chemical parameters that yields linear stability. By tuning the parameters, and evaluating the corresponding dispersion relation, one can eventually single out in a reference parameter space the region deputed to the instability. This is done in Fig. 5.5(a) working in the plan (b, c) : the region of Turing instability, as predicted by the deterministic analysis, is filled with a uniform colour (yellow). The (blue) diamond falls outside the region of Turing order and points to the parameters employed in depicting the stable dispersion curve in panel (b). Similarly, the circle (magenta) refers to the unstable profile. In this latter case, performing a direct integration of the mean-field equations (5.35) one observes the spontaneous differentiation in activator-rich and activator-poor groups, as discussed in [11]. A stochastic simulation can be also carried out, using an *ad hoc* implementation of the Gillespie Monte Carlo scheme [64]. Finite size fluctuations materialize in a modest perturbation ($\propto 1/\sqrt{N}$) of the idealized mean-field dynamics.

Substantially different, is instead the scenario that is eventually recovered when comparing the simulations outside the region deputed to Turing instability. Setting the parameters $(b = 76, c = 1076)$ to the values $(b = 76, c = 1060)$ that correspond to the diamond (blue) of Fig. 5.5(a), the deterministic simulations always converge to the homogeneous fixed point, the concentrations of the species being therefore identical on each node of the network. At variance, a fragmentation into distinct groups is clearly observed in the stochastic simulations. The late time evolution of the stochastic system, as compared to the corresponding (trivial) deterministic solution, is displayed in Fig. 5.6. As for the case of continuous media, the endogenous stochastic noise is amplified and drives the formation of spatially extended, self-organized patterns outside the region of

classical Turing order. Following [18], we call these self-organized, asymptotically stable configurations, *Stochastic Turing patterns* on a network.

To gain analytic insight into the above mechanism, one can return to the van Kampen perturbative analysis and consider the next to leading approximation. One obtains a system of Langevin equations [18, 74] for the fluctuations ξ_{si} , $s = 1, 2$:

$$\frac{d\xi_{si}}{d\tau} = \sum_{rj} \mathcal{M}_{sr,ij} \xi_{rj} + \eta_{si}(\tau) \quad (5.38)$$

where η_{si} is a Gaussian noise with zero mean and correlator given by $\langle \eta_{s,i}(\tau) \eta_{r,j}(\tau') \rangle = \mathcal{B}_{sr,ij} \delta_{\tau\tau'}$. The explicit form of the matrices \mathcal{M} and \mathcal{B} is given as below:

$$\begin{aligned} \mathcal{M}_{11}^{*(NS)} &= -a - b - d + 2c\phi^*\psi^*, & \mathcal{M}_{11}^{*(SP)} &= 2\mu(1 - \psi^*), \\ \mathcal{M}_{12}^{*(NS)} &= -a + c\phi^{*2}, & \mathcal{M}_{12}^{*(SP)} &= 2\mu\phi^*, \\ \mathcal{M}_{21}^{*(NS)} &= b - 2c\phi^*\psi^*, & \mathcal{M}_{21}^{*(SP)} &= 2\delta\psi^*, \\ \mathcal{M}_{22}^{*(NS)} &= -c\phi^{*2}, & \mathcal{M}_{22}^{*(SP)} &= 2\delta(1 - \phi^*), \end{aligned} \quad (5.39)$$

and

$$\begin{aligned} \mathcal{B}_{11}^{*(NS)} &= a(1 - \phi^* - \psi^*) + \phi^*(b + c\phi^*\psi^* + d), & \mathcal{B}_{11}^{*(SP)} &= 4\mu\phi^*(1 - \phi^* - \psi^*), \\ \mathcal{B}_{12}^{*(NS)} &= \mathcal{B}_{21}^{*(NS)} = -\phi^*(b + c\phi^*\psi^*), & \mathcal{B}_{12}^{*(SP)} &= \mathcal{B}_{21}^{*(NS)} = 0, \\ \mathcal{B}_{22}^{*(NS)} &= \phi^*(b + c\phi^*\psi^*), & \mathcal{B}_{22}^{*(SP)} &= 4\delta\psi^*(1 - \phi^* - \psi^*). \end{aligned} \quad (5.40)$$

Employing the transformation (5.16), one can hence find an analytical expression of the power spectrum of fluctuations of species $s = 1, 2$, $P_s(\omega, \Lambda_\alpha) = \langle |\tilde{\xi}_s|^2 \rangle$, in completely analogy with what it was done in the previous model.

In Fig. 5.7 the power spectrum of species X , is plotted in the plane $\omega = 0$, as a function of Λ_α , for the parameters selection that corresponds to the diamond in Fig. (5.5), i.e. outside the region of deterministic Turing instability. Symbols are obtained by sampling the power spectrum over the discrete Laplacian eigenvalues Λ_α . The solid line stands for the power spectrum calculated in the continuous limit when the discrete Λ_α is replaced with its real counterpart $\rightarrow -k^2$. A clear peak is displayed ³, a finding that explains in turn the outcome of the stochastic based simulations reported in Fig. 5.6, proving on a formal ground that stochastic Turing patterns do exist on a network topology.

³Similar conclusions hold for species Y , the power spectrum.

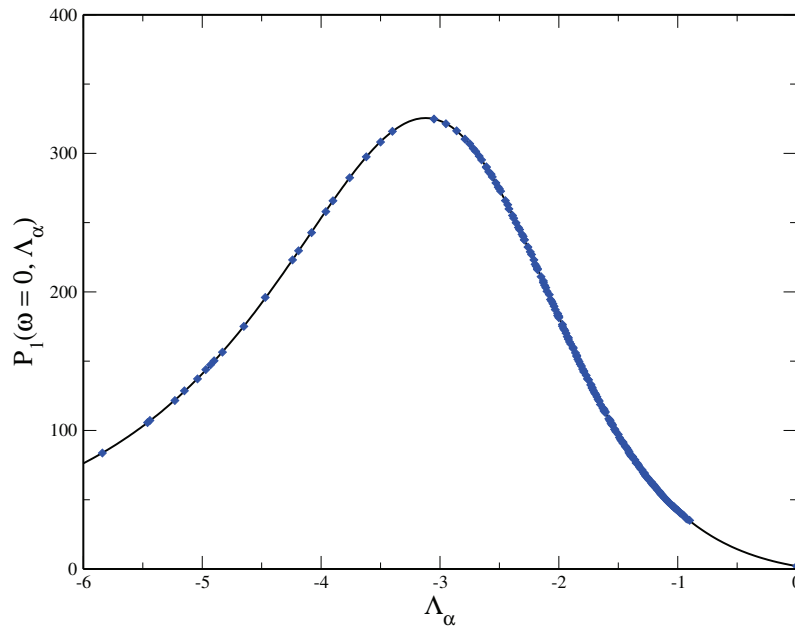


FIGURE 5.7: Power Spectrum of fluctuations for species X as a function of Λ_α , $\omega = 0$ (symbols). The solid line is the power spectrum calculated for a continuum media, i.e. when Λ_α is replaced by $-k^2$, where k denotes the wavenumber of the plane wave mode. The curve refers to $a = d = 1$, $b = 76$, $c = 1060$, $\mu = 1$, $\delta = 15$, a choice of parameters that correspond to operate outside the region of Turing instability (diamond in 5.5(a)).

The network is constructed as specified in the caption of Fig. 5.5.

5.4 Conclusions

Pattern formation has been extensively studied in the literature and with reference to a wide variety of problems. Typically, the concentrations of the species involved are assumed to obey partial differential equations. The conditions under which an instability occurs follow from standard linear stability analysis around a stable homogeneous fixed point. Recently, the emergence of steady state inhomogeneous patterns has been also studied for deterministic reaction-diffusion models defined on a network, generalizing the concept of a Turing instability to this important new area of investigation.

Deterministic models represent, however, an idealized approach to the phenomenon being investigated: they omit stochastic fluctuations that need to be included when dealing with finite populations of interacting elements. Finite size corrections result in intrinsic stochastic perturbations which undergo amplification, and, through a resonant mechanism, eventually yield self-organized patterns.

In this chapter, we have developed the theory of stochastic patterns for reaction-diffusion systems defined on a network. The analysis is based on a systematic and general application of the linear noise approximation scheme. Stochastic travelling waves and stochastic Turing patterns are predicted to exist, and numerically observed in a region

of the parameter plane for which the deterministic partial differential equations converge to a stable homogeneous solution. The analysis is carried out for two specific systems, the stochastic analog of the Zhabotinsky [24] and the Brusselator [4] models. The techniques discussed are however general, and can be readily adapted to any reaction-diffusion model defined on a network. To benchmark theory and simulations we have also developed, and successfully tested, a numerical algorithm that performs the generalized Fourier transform, employed in the analytical derivation. This transform decomposes the signal along the eigenvectors of the discrete Laplacian operator, tailoring the analysis to the network under consideration, and so allowing the spectral properties of the emerging patterns to be fully characterized.

Conclusions

In this thesis we have studied the problem of pattern formation on complex networks, a topic of paramount importance with applications in different disciplinary contexts. Starting from a prototypical reaction-diffusion model, two main directions of investigation have been explored: on the one side, we have examined the system in its deterministic limit, where partial differential equations are assumed to govern the coupled evolution of the concentrations of the interacting species. Then, in the second part of the thesis, we have turned to considering a stochastic approach to the scrutinized problem. Working in this context, finite size effects, stemming from the inherent discreteness of the populations, are explicitly taken in account. Both in the deterministic and in the stochastic settings, the species are assumed to populate a complex graph, which ultimately provide the spatial backbone to the inspected model. Diffusion is allowed between neighbouring nodes, as designated by the associated adjacency matrix.

According to the deterministic formulation, a small perturbation of a homogeneous fixed point can spontaneously amplify in a reaction-diffusion system, as follow a symmetry breaking instability and eventually yield asymptotically stable non homogeneous patterns. These are the Turing patterns. Travelling waves can also developed as follows an analogous dynamical instability. Recently, in a seminal paper [11], Nakao and Mikhailov investigated the effects of the embedding complex graph structure on the Turing instability in nonlinear diffusive systems, so paving the way for novel discoveries in an area of widespread interest. Building on their approach, we have here extended the analysis to account for the rather peculiar setting where the system is hosted on a directed network [12]. Due to the structure of the network Laplacian, the dispersion relation has both real and imaginary parts, at variance with the conventional case for a symmetric network. The homogeneous fixed point of the system can consequently turn unstable due to the topology of the network, resulting in a new class of instabilities which cannot be induced on undirected graphs. Results from a linear stability analysis allow the instability region to be analytically traced. Numerical simulations show that the instability can lead to travelling waves, or quasi-stationary patterns, depending on the characteristics of the

underlying graph. The results here presented could impact on the diverse range of disciplines where directed networks are found, such as neuroscience, computer networks and traffic systems.

Another scenario where topology matters is that of multi-layered networks, also known as multiplex networks. Multiplex provide an idealized mathematical setting to elaborate on the degree of mutual interference between networks that participate to a shared dynamical process. Multiplex have been for instance invoked when modeling complex structure like the brain, internet or even social networks [13–15]. Working in this context, we have shown that the emergence of patterns on a multiplex can be triggered by a constructive interference between layers [16]. It can be in fact proven that patterns can emerge for a reaction-diffusion system defined on a multiplex, also when the Turing-like instability is prevented to occur on each single layer taken separately. In other cases inter-layer diffusion can have a destructive influence on the process of pattern formation, so disrupting those regular collective motifs which are instead predicted to self-assemble in the limit of decoupled layers.

Beyond the deterministic scenario, single individual effects can also impact the process of pattern formation. Stochastic fluctuations, originating from finite size populations, can in fact significantly modify the mean-field predictions and seed the emergence of regular macroscopic patterns, in time and space, outside the region of deterministic instability [18, 56]. In the last two chapters of the thesis, we have analysed in some details the dynamics of (stochastic) reaction-diffusion models defined on a complex network [19–21]. To gain insight into the role of fluctuations and eventually work out the conditions for the emergence of stochastic patterns, we have chosen to operate under the Linear Noise Approximation (LNA) scheme. Simulations via Gillespie algorithm were performed to test the analytical results and analyzed via a generalized Fourier transform which is defined using the eigenvectors of the discrete graph Laplacian. Travelling waves, as well as stationary patterns, reminiscent of the Turing instability, can develop as mediated by the discreteness of the stochastic medium. Interestingly, stochastic patterns can also set in for reaction-diffusion systems where the activator is solely allowed to diffuse. This is a remarkable observation, that we have here cast on rigorous ground and which marks a significant difference with the conventional deterministic theory of pattern formation.

In conclusion, in this thesis we aimed at contributing to the multi-faceted studies on pattern formation. To this end we chose to deal with reaction-diffusion models defined on complex networks. Interestingly, and as a general remark, the topology of the hosting support plays an important role which couples non trivially with other purely dynamical aspects accommodated for within the models. The thesis work was directed so to partially

resolve this intriguing interplay, following a direction of investigation that will hopefully finds applications in those fields where the concept of networks often recurs.

Appendix A

A.1 Stochastic processes

In the second part of this thesis we have focused on *stochastic processes*, systems which evolve probabilistically in time. Here we review a selection of key concepts that relate to this important topic.

A.1.1 Basic definitions

Let us start by labelling with $X(t)$ a time-dependent random variable. Assume $X(t)$ takes values x_1, x_2, x_3, \dots etc., at times t_1, t_2, t_3, \dots and hypothesise that a joint probability density $p(x_1, t_1; x_2, t_2; x_3, t_3; \dots)$ exists, which describes completely the system. The set of all the x_i , called *samples* or *realizations of the processes*, constitutes the *ensemble* of all possible values that the stochastic process $X(t)$ can take. If the trajectory of a stochastic process $x_i(t)$ crosses all the values of the ensemble for long but finite time intervals, then the system is said to be *ergodic*. Another important property of stochastic processes is the stationarity. Let first define the n -th moment of the stochastic processes as:

$$\langle X(t_1)X(t_2) \dots X(t_n) \rangle = \int_S x_1 x_2, \dots, x_n p(x_1, t_1; x_2, t_2, \dots, x_n, t_n) dx_1 dx_2, \dots, dx_n$$

where with S we denote the samples set. The 1-th moment $\langle X(t) \rangle$ is therefore the *mean* (or expected value) of the distribution at a given time t . A stochastic process is said to be *stationary* when all its moments are invariant under any translation in time, namely:

$$\langle X(t_1 + \tau)X(t_2 + \tau) \dots X(t_n + \tau) \rangle = \langle X(t_1)X(t_2) \dots X(t_n) \rangle, \quad (\text{A.1})$$

for all t_1, t_2, \dots, t_n and for a general τ . In particular, we have, that $\langle X \rangle$ is independent of time and the *autocorrelation function* $\eta(t_1, t_2)$, defined as $\eta(t_1, t_2) = \langle X(t_1)X(t_2) \rangle$, depends only on $|t_1 - t_2|$.

Before we introduce the class of stochastic processes that we will deal with in this thesis, let us define the conditional probability $P(x_2, t_2|x_1, t_1)$ as the probability of event x_2 at time t_2 given that the event x_1 has occurred at an earlier time t_1 , ($t_2 > t_1$). This latter quantity satisfies the relation

$$P(x_2, t_2|x_1, t_1) = \frac{P(x_1, t_1; x_2, t_2)}{P(x_1, t_1)}. \quad (\text{A.2})$$

A.1.2 Markov processes

A *Markov* process has the property that for any set of n successive times (i.e. $t_1 < t_2 < \dots < t_n$) one has

$$P(x_n, t_n|x_1, t_1; x_2, t_2; \dots x_{n-1}, t_{n-1}) = P(x_n, t_n|x_{n-1}, t_{n-1}). \quad (\text{A.3})$$

The conditional probability depends solely on the value x_{n-1} at time t_{n-1} and does not keep track of the preceding instants. For this reason systems whose dynamics can be described as Markov processes are called *memory-less* systems. The right hand side in Eq. (A.3) is called *transition probability* and, when it is stationary, it is often denoted as $T_\tau(x_n|x_{n-1})$ with $\tau = t_n - t_{n-1}$.

As we will see a Markov process is fully determined by the two functions $P(x_1, t_1)$ and $P(x_2, t_2|x_1, t_1)$, since the whole hierarchy of moments can be constructed from them. Indeed, taking $t_1 < t_2 < t_3$ and making use of Eq. (A.2),

$$\begin{aligned} P(x_1, t_1; x_2, t_2; x_3, t_3) &= P(x_3, t_3|x_1, t_1; x_2, t_2)P(x_1, t_1; x_2, t_2) \\ &= P(x_3, t_3|x_2, t_2)P(x_2, t_2|x_1, t_1)P(x_1, t_1). \end{aligned} \quad (\text{A.4})$$

By iterating recursively this reasoning one can eventually characterize all $P(x_1, t_1; x_2, t_2; \dots; x_n, t_n)$. This property makes Markov processes very useful in applications.

A.1.3 Master equation

Here, we introduce the Master equation which describes the stochastic dynamics that governs a stochastic system. It is the pivot of most of the work developed in the second part of the thesis.

Integrating eq. (A.4) over x_2 and then dividing both sides by $P(x_1, t_1)$ one obtains

$$P(x_3, t_3|x_1, t_1) = \int P(x_3, t_3|x_2, t_2)P(x_2, t_2|x_1, t_1)dx_2 \quad (\text{A.5})$$

This is called the *Chapman-Kolmogorov equation* and it must be obeyed by the transition probability of any Markov process. It will serve as a prelude for the Master equation.

At this point let define the *transition probability for unit time* or *transition rate* from state x_1 to state x_2 as

$$T(x_2|x_1) = \lim_{\tau \rightarrow 0} T_\tau(x_2|x_1), \quad x_2 \neq x_1. \quad (\text{A.6})$$

Since for $t_1 = t_2$

$$P(x_2, t_2|x_1, t_1) = \delta_{x_1, x_2},$$

we can expand the transition probability $T_\tau(x_2|x_1)$ around t_1 for a small τ

$$T_\tau(x_2|x_1) = \delta_{x_1, x_2} + T(x_2|x_1)\tau + \mathcal{O}(\tau^2).$$

On the other hand from the normalization condition $\int T_\tau(x_2|x_1)dx_2 = 1$ we have that the coefficient associated to the delta function should be corrected as follows

$$\overline{T}_\tau(x_2|x_1) = (1 - \alpha\tau) \delta_{x_1, x_2} + T(x_2|x_1)\tau + \mathcal{O}(\tau^2).$$

The coefficient $1 - \alpha\tau$ is the probability that no transition takes place during τ ; hence

$$\alpha(x_1) = \int T(x_2|x_1)dx_2 \quad (\text{A.7})$$

which also follows immediately from the assumption made above. Now insert the expression for T_τ in the Chapman-Kolmogorov equation (A.5)

$$T_{\tau+\tau'}(x_3|x_1) = (1 - \alpha(x_3)\tau') T_\tau(x_3|x_1) + \tau' \int T(x_3|x_2)T_\tau(x_2|x_1)\tau.$$

Dividing by τ' and then taking the limit for $\tau' \rightarrow \infty$, one obtains

$$\frac{\partial}{\partial \tau} T_\tau(x_3|x_1) = \int [T(x_3|x_2)T_\tau(x_2|x_1) - T(x_2|x_3)T_\tau(x_3|x_1)] dx_2$$

the differential form of the Chapman-Kolmogorov equation, widely known like the *master equation*. It is usually written in a more intuitive and simpler form as:

$$\frac{\partial}{\partial t} P(x, t) = \int [T(x|x')P(x', t) - T(x'|x)P(x, t)] dx'. \quad (\text{A.8})$$

If the samples space S is a discrete collection of states each labelled with the index n , the equation reduces to

$$\frac{\partial}{\partial t} P_n(t) = \sum_n [T_{nn'}P_{n'}(t) - T_{n'n}P_n(t)] \quad (\text{A.9})$$

The master equation describes the *gain and loss* of the probabilities of different states n . The first term on the right hand side measures in fact the gain of state n due to the transition from other allowed states n' , and the second term is the loss due to transitions from n towards distinct target states.

In general, it is not possible to solve Eqs. (A.8,A.9) in a closed analytical form. To gain analytical insight one can therefore proceed with approximated techniques as the Kramers-Moyal or van Kampen expansion [58, 86]. At the first order of the van Kampen system size expansion one obtains for instance the so called mean-field (deterministic) representation of the scrutinized process. Typically, this is a reaction-diffusion system of the type considered in the main body of the thesis. The next-to-leading order in the expansion yields a complete characterization of the fluctuations in terms of the Fokker-Planck equation whose structure reflects the underlying stochastic process.

A.2 Random walk graph Laplacian

Let us here discuss the alternative formulation of the Laplacian operator to which we alluded in Chapter 5 and which descends from a stochastic microscopic formulation of the random walk on a network. A *random walk* is a path across a network created by taking repeated random steps. Starting at some specified initial node i , at each step of the walk we choose uniformly at random between k_i links attached to the current node, perform the move along the chosen link (ij) to the node j at its other end, and repeat the procedure again. If no restrictions are imposed, random walks are normally allowed to go along edges more than once and also visit nodes more than once. If the coupling matrix \mathbf{W} does not coincide with the adjacency matrix \mathbf{A} than the probability of chosen the link (ij) should be weighted by w_{ij} .

Consider a random walk that starts at a specified vertex and takes n random steps. Let $P_i(t_n)$ be the probability that the walk is at vertex i at the step n . If the walk is at vertex j at the step $n - 1$, the probability of taking a step along any particular one of the k_j edges (weighted if necessary, so $k_j = \sum_{l=1}^{\Omega} W_{jl}$) attached to j is $1/k_j$, so on an undirected network $P_i(t_n)$ is given by

$$P_i(t_n) = \sum_{j=1}^{\Omega} \frac{W_{ij}}{k_j} P_j(t_{n-1}).$$

Furthermore, a continuity equation must be satisfied locally; so one must require that

$$\begin{aligned} P_i(t_n) - P_i(t_{n-1}) &= \sum_{j=1}^{\Omega} \frac{W_{ij}}{k_j} P_j(t_{n-1}) - \sum_{j=1}^{\Omega} \frac{W_{ji}}{k_i} P_i(t_{n-1}) \\ &= \sum_{j=1}^{\Omega} \left(\frac{W_{ij}}{k_j} - \delta_{ij} \right) P_j(t_{n-1}). \end{aligned}$$

Taking the limit for infinitesimal time between successive jumps we get explicitly the usual master equation as in eq. (A.9)

$$\frac{\partial P_i(t)}{\partial t} = \sum_{j=1}^{\Omega} \tilde{\Delta}_{ij} P_j(t) \quad (\text{A.10})$$

with the only difference that now the Laplacian matrix takes the form $\tilde{\Delta} = \Delta \mathbf{K}^{-1}$ where $(\Delta)_{ij} = W_{ij} - k_i \delta_{ij}$ and the diagonal matrix \mathbf{K} , such that $\text{diag}(\mathbf{K})_i = k_i$.

This transport operator is different from the one mainly used in this thesis, with the exclusion of the last part of Chapter 5. In fact, its spectrum is locally scaled with a factor k_i . It is still possible to prove that the eigenvalues of the above operator are real as it happens for the other operator defined in the main body of the thesis. From the definition above one obtains that $\tilde{\Delta}$ can be related to a symmetric matrix \mathbf{S} by the following similarity transformation $\mathbf{S} = \mathbf{T} \tilde{\Delta} \mathbf{T}^{-1}$ where \mathbf{T} is the diagonal matrix $\text{diag}(\mathbf{T})_i = 1/\sqrt{k_i}$. Thus, in conclusion $\tilde{\Delta}$ and \mathbf{S} will have the same eigenvalue spectrum.

Let us notice that both $\tilde{\Delta}$ and Δ are used in the literature devoted to studying the process of diffusion on networks [11, 19, 82, 83].

Bibliography

- [1] A. M. Turing. The chemical basis of morphogenesis. *Phil. Trans. R. Soc. Lond. B*, 237:37–72, 1952.
- [2] J.D. Murray. *Mathematical Biology*. Springer, second edition, 1991.
- [3] M. Cross and H. Greenside. *Pattern Formation and Dynamics in Nonequilibrium Systems*. Cambridge University Press, Cambridge, 2009.
- [4] I. Prigogine and R. Lefever. Symmetry breaking instabilities in dissipative systems. ii. *J.Chem. Phys.*, 48:1695–1700, 1968.
- [5] V. Castets, E. Dulos, J. Boissonade, and P. Kepper. Experimental evidence of a sustained standing turing-type nonequilibrium chemical pattern. *Phys. Rev. Lett.*, 64:2953–2956, 1990.
- [6] Q. Ouyang and H. L. Swinney. Transition from a uniform state to hexagonal and striped turing patterns. *Nature*, 352:610–612, 1991.
- [7] A.L. Barabási and R. Albert. Emergence of scaling in random networks. *Science*, 286:509–512, 1999.
- [8] M. E. J. Newman. The structure and function of complex networks. *SIAM Review*, 45:167–256, 2003.
- [9] D. J. Watts and S. H. Strogatz. Collective dynamics of 'small-world' networks. *Nature*, 393:440–442, 1998.
- [10] H. G. Othmer and L. E. Scriven. Nonlinear aspects of dynamic pattern in cellular networks. *J. Theor. Biol.*, 43:83–112, 1974.
- [11] H. Nakao and A. S. Mikhailov. Turing patterns in network-organized activator-inhibitor systems. *Nature Physics*, 6:544–550, 2010.
- [12] M. Asllani, J. D. Challenger, F. S. Pavone, L. Sacconi, and D. Fanelli. The theory of pattern formation on directed networks. *Nature Communications*, 5:4517, 2014.

-
- [13] S. Gomez, A. Diaz-Guilera, J. Gomez-Gardeñes, C. J. Perez-Vicente, Y. Moreno, and A. Arenas. Diffusion dynamics on multiplex networks. *Phys. Rev. Lett.*, 110:028701, 2013.
- [14] P. J. Mucha, T. Richardson, K. Macon, M. A. Porter, and J. P. Onnela. Community structure in time-dependent, multiscale, and multiplex networks. *Science*, 328(5980):876–878, 2010.
- [15] G. Bianconi. Statistical mechanics of multiplex networks: Entropy and overlap. *Phys. Rev. E*, 87:062806, 2013.
- [16] M. Asllani, D. M. Busiello, T. Carletti, D. Fanelli, and G. Planchon. Turing patterns in multiplex networks. *Phys. Rev. E*, 90(4):042814, 2014.
- [17] T. Butler and N. Goldenfeld. Robust ecological pattern formation induced by demographic noise. *Phys. Rev. E*, 80:030902(R), 2009.
- [18] T. Biancalani, D. Fanelli, and F. Di Patti. Stochastic turing patterns in the brusselator model. *Phys. Rev. E*, 81:046215, 2010.
- [19] M. Asllani, F. Di Patti, and D. Fanelli. Stochastic turing patterns on a network. *Phys. Rev. E*, 86:046105, 2012.
- [20] M. Asllani, T. Biancalani, D. Fanelli, and A. McKane. The linear noise approximation for reaction-diffusion systems on networks. *Europ. Phys. J.*, 86:476, 2013.
- [21] L. Cantini, C. Cianci, D. Fanelli, E. Massi, L. Barletti, and M. Asllani. Stochastic amplification of spatial modes in a system with one diffusing species. *J. of Math. Bio.*, 2013.
- [22] B. Ermentrout and M. Lewis. Pattern formation in systems with one spatially distributed species. *Bull. of Math. Biol.*, 59(3):533–549, 1997.
- [23] B.P. Belousov. A periodic reaction and its mechanism in collection of short papers on radiation medicine for 1985. *Med. Publ. Moschow*, 1959.
- [24] A. M. Zhabotinsky, M. Dolnik, and I. R. Epstein. Pattern formation arising from wave instability in a simple reaction-diffusion system. *J. Chem. Phys.*, 103:10306, 1995.
- [25] J. Gomez-Gardenes, I. Reinares, A. Arenas, and L. M. Floria. Evolution of cooperation in multiplex networks. *Scientific Reports*, 2:620, 2012.
- [26] P. Erdős and A. Rényi. On random graphs I. *Publ. Math. Debrecen*, 6:290–297, 1959.

- [27] E. N. Gilbert. Random graphs. *Annals of Mathematical Statistics*, 30:1141–1144, 1959.
- [28] M. E. J. Newman and D. J. Watts. Scaling and percolation in the small-world network model. *Phys. Rev. E*, 60:7332–7342, 1999.
- [29] W. John, M. Dusi, and K. Claffy. Estimating routing symmetry on single links by passive flow measurements. *Tech. rep., ACM 1st International Workshop on TRaffic Analysis and Classification (TRAC)*, 2010.
- [30] E. R. Kandel, J. H. Schwartz, and T. M. Jessell. *Principles of neural science*. McGraw-Hill, fourth edition, 2000.
- [31] O. Sporns, G. Tononi, and R. Kötter. The human connectome: A structural description of the human brain. *PloS Comp. Biol.*, 1:e42, 2010.
- [32] <http://www.humanconnectomeproject.org/>.
- [33] J. W. Lichtman and W. Denk. The big and the small: Challenges of imaging the brain’s circuits. *Science*, 334:618, 2011.
- [34] R. Olfati-Saber and R.M. Murray. Consensus problems in networks of agents with switching topology and time-delays. *IEEE Transactions on Automatic Control*, 49(9):1520–1533, 2004.
- [35] A. Banerjee and J. Jost. On the spectrum of the normalized graph laplacian. *Linear algebra and its applications*, 428 (11-12):3015–3022, 2008.
- [36] P. D’Odorico L. Ridolfi, C. Camporeale and F. Laio. Transient growth induces unexpected deterministic spatial patterns in the turing process. *Europhys. Lett.*, 95:18003, 2011.
- [37] H. E. Bell. Gerschgorin’s theorem and the zeros of polynomials. *Amer. Math. Monthly*, 72:292–295, 1965.
- [38] C.N. Angstmann, I.C. Donnelly, and B.I. Henry. Pattern formation on networks with reactions: A continuous-time random-walk approach. *Phys. Rev. E*, 87:032804, 2013.
- [39] O. Sporns, D. R. Chialvo, M. Kaiser, and C. C. Hilgetag. Organization, development and function of complex brain networks. *Trends Cogn. Sci.*, 8(9):418–425, 2004.
- [40] W. Singer S. Yu, D. Huang and D. Nikolić. A small world of neuronal synchrony. *Cerebral Cortex*, 18(12):2891–2901, 2008.

-
- [41] R. FitzHugh. Mathematical models of threshold phenomena in the nerve membrane. *Bull. Math. Biophys.*, 17:257–278 B, 1955.
- [42] R. FitzHugh. Impulses and physiological states in theoretical models of nerve membranes. *Biophys. J.*, 1:445–466, 1961.
- [43] J. Nagumo, S. Arimoto, and S. Yoshizawa. An active pulse transmission line simulating nerve axon. *Proc. IRE.*, 278:2061–2070, 1962.
- [44] R. G. Morris and M. Barthelemy. Transport on coupled spatial networks. *Phys. Rev. Lett.*, 109:128703, 2012.
- [45] V. Nicosia, G. Bianconi, V. Latora, and M. Barthelemy. Non-linear growth and condensation in multiplex networks. *Phys. Rev. Lett.*, 111:058701, 2013.
- [46] M. Kurant and P. Thiran. Layered complex networks. *Phys. Rev. Lett.*, 96:138701, 2006.
- [47] S. R. Zou, T. Zhou, A. F. Liu, X. L. Xu, and D.R. He. *Phys. Rev. A*, 374:4406, 2010.
- [48] E. Bullmore and O. Sporns. The economy of brain network organization. *Nat. Rev. Neurosci.*, 10:186, 2009.
- [49] S. Wasserman and K. Faust. *Social Network Analysis: Methods and Applications*, volume 8. Cambridge University Press, 1994.
- [50] G. Golub and Ch. F. Van Loan. *Matrix computations*. Johns Hopkins University Press, 1996.
- [51] M.I. Friswell. The derivatives of repeated eigenvalues and their associated eigenvectors. *Transaction of the ASME*, 118:390–397, 1996.
- [52] N. P. Van Der AA, H. G. Ter Morsche, and R. R. M. Mattheij. Computation of eigenvalue and eigenvector derivatives for a general complex-valued eigensystem. *Electronic J. of Linear Algebra*, 16:300–314, 2007.
- [53] B. Wu, Z. Xu, and A. Li. *Commun in Numer. Meth. in Engng*, 23:241–251, 2007.
- [54] D.Fanelli, C. Cianci, and F. Di Patti. Turing instabilities in reaction diffusion systems with cross diffusion. *Eur. Phys. J. B*, 86:142, 2013.
- [55] T. E. Woolley, R. E. Baker, E. A. Gaffney, and P. K. Maini. Stochastic reaction and diffusion on growing domains: understanding the breakdown of robust pattern formation. *Phys. Rev. E*, 84:046216, 2011.

-
- [56] T. Biancalani, T. Galla, and A. J. McKane. Stochastic waves in a brusselator model with nonlocal interaction. *Phys. Rev. E*, 84:026201, 2011.
- [57] R. A. Satnoianu, M. Menzinger, and P.K. Maini. Turing instabilities in general systems. *J. Math. Biol.*, 41:493–512, 2000.
- [58] N. G. van Kampen. *Stochastic preocesses in Physics and Chemistry*. North Holland, Amsterdam, 1992.
- [59] C. A. Lugo and A. J. McKane. Quasicycles in a spatial predator–prey model. *Phys. Rev. E*, 78:051911, 2008.
- [60] P. de Anna, F. Di Patti, D. Fanelli, A. J. McKane, and T. Dauxois. Spatial model of autocatalytic reactions. *Phys. Rev. E*, 81:056110, 2010.
- [61] A. J. Black and A. J. McKane. Stochastic formulation of ecological models and their applications. *Trends in Ecology and Evolution*, 27(6):337–345, 2012.
- [62] H. Lodish. *Molecular Cell Biology*. W. H. Freeman and Company Editor, 2002.
- [63] M. S. Paoletti, C. R. Nugent, and T.H. Solomon. Stochastic formulation of ecological models and their applications. *Phys. Rev. Lett.*, 96:124101, 2006.
- [64] D. T. Gillespie. A general method for numerically simulating the stochastic time evolution of coupled chemical reactions. *J. Comp. Phys.*, 22:403–434, 1976.
- [65] A. J. McKane, T. Biancalani, and T. Rogers. Stochastic pattern formation and spontaneous polarisation: the linear noise approximation and beyond. *Bull. Math. Biol.*, 2013.
- [66] L. J. Shumacher, T. E. Woolley, and R. E. Baker. Stochastic pattern formation and spontaneous polarisation: the linear noise approximation and beyond. *Phys. Rev. E*, 87:042719, 2013.
- [67] J. Schnakenberg. Simple chemical reaction systems with limit cycle behaviour. *J. Theor. Biol.*, 81 (3):389–400, 1979.
- [68] S. Levin. The problem of pattern and scale in ecology: the robert h. macarthur award lecture. *Ecology*, 73:1943, 1992.
- [69] I. Prigogine and R. Lefever. Symmetry breaking instabilities in dissipative systems. ii. *J. Chem. Phys.*, 48:1695, 1968.
- [70] R Pastor-Satorras and A. Vespignani. Complex networks: Patterns of complexity. *Nature Physics*, 6:480–481, 2010.

-
- [71] V. Colizza, A. Barrat, M. Barthelemy, and A. Vespignani. The role of the airline transportation network in the prediction and predictability of global epidemics. *Proc. Natl Acad. Sci. USA*, 103:2015, 2006.
- [72] R. Pastor-Satorras and A. Vespignani. Epidemic spreading in scale-free networks. *Phys. Rev. Lett.*, 86:3200, 2001.
- [73] V. Colizza, R. Pastor-Satorras, and A. Vespignani. Reaction-diffusion processes and metapopulation models in heterogeneous networks. *Nature Physics*, 3:276, 2007.
- [74] A. J. McKane and T. J. Newman. Predator-prey cycles from resonant amplification of demographic stochasticity. *Phys. Rev. Lett*, 94:218102, 2005.
- [75] T. Dauxois, F. Di Patti, D. Fanelli, and A. J. McKane. Enhanced stochastic oscillations in autocatalytic reactions. *Phys. Rev. E*, 79:036112, 2009.
- [76] T. E. Woolley, R. E. Baker, G. E. A. Gaffney, and P. K. Maini. Stochastic reaction and diffusion on growing domains: Understanding the breakdown of robust pattern formation. *Phys. Rev. E*, 84:046216, 2011.
- [77] I. Hanski. *Metapopulation Ecology*. Oxford University Press, Oxford, 1999.
- [78] T. Maruyama. *Stochastic Problems in Population Genetics*. Lectures in Biomathematics 17, (Springer), Berlin, 1977.
- [79] G. Rozhnova, A. Nunes, and A. J. McKane. Stochastic oscillations in models of epidemics on a network of cities. *Phys. Rev. E*, 84:051919, 2011.
- [80] J. D. Challenger and A. J. McKane. Synchronization of stochastic oscillators in biochemical systems. *Phys. Rev. E*, 88:012107, 2013.
- [81] N. E. Kouvaris, H. Kori, and A. S. Mikhailov. Traveling and pinned fronts in bistable reaction-diffusion systems on networks. *PLoS ONE*, 7:e45029, 2012.
- [82] R. Burioni, S. Chibbaro, D. Vergni, and A. Vulpiani. Reaction spreading on graphs. *Phys. Rev. E*, 86:055101(R), 2012.
- [83] I. Simonsen, K. A. Eriksen, S. Maslov, and K. Sneppen. Diffusion on complex networks: a way to probe their large-scale topological structures. *Physica A*, 336:163, 2004.
- [84] P. N. McGraw and M. Menzinger. Laplacian spectra as a diagnostic tool for network structure and dynamics. *Phys. Rev. E*, 77:031102, 2008.
- [85] D. Fanelli and A. J. McKane. Diffusion in a crowded environment. *Phys. Rev. E*, 82:021113, 2010.
- [86] C. W. Gardiner. *Handbook of Stochastic Methods*. Springer, second edition, 1985.